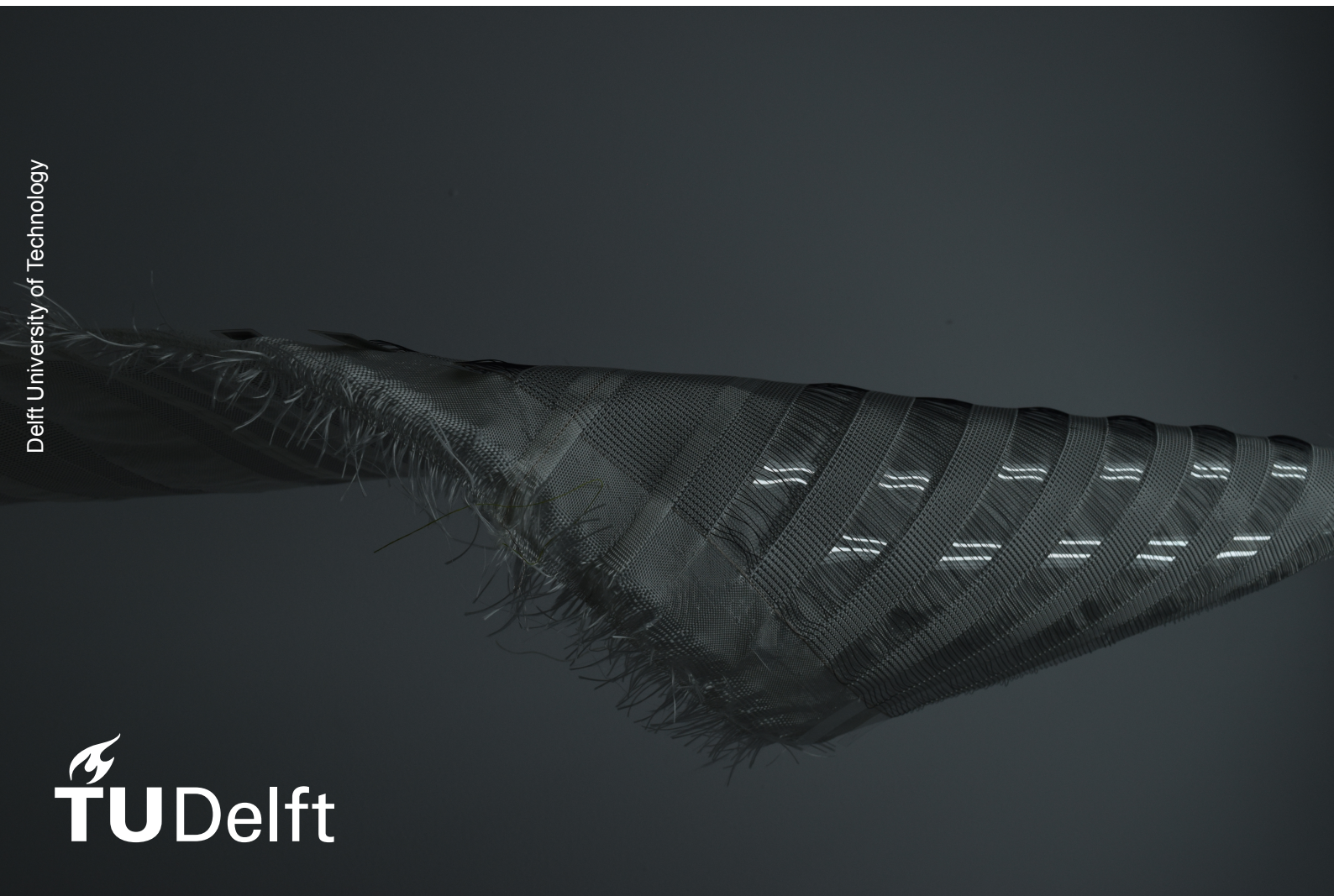# Structural Solar Textile

Design & Analysis of Woven Solar Cell-Integrated Textile For Textile Architecture Application

Ahmed Bakrelsedik Mohamed Ahmed

Delft University of Technology

TUDelft

Structural Solar Textile

Design & Analysis of Woven Solar Cell-Integrated Textile For Textile Architecture Application

by

Ahmed Bakrelsedik Mohamed Ahmed

to obtain the degree of Master of Science in Civil Engineering,
Building Engineering track
at Delft University of Technology.

Student number: 5002982
Thesis committee: Dr. Ir. H.R. Schipper,   TU Delft (Chair)
                     Dr. Ir. M. Popescu,   TU Delft (Supervisor)
                     Dr. Ir. F.A. Veer,   TU Delft
                     Ir. R. Houtman,   Tentech B.V.

This thesis is confidential and cannot be made public until May 31, 2024.

Page intentionally left blank

Summary

In the endeavor to diminish the carbon footprint induced by the civil engineering and construction industry, more resources are now being allocated towards the transition to renewable energy solutions. One of the lucrative and most consistently researched solutions is the integration of solar cells technology in building architecture. The advancements in solar cell technology, especially in the photovoltaics realm, have facilitated the induction of solar energy-harnessing techniques into construction material. The work presented herein looks into expanding further the usage of solar cells in civil engineering applications.

In this research, the question of whether flexible solar films can be integrated into woven textiles for the load-bearing applications of textile architecture is addressed. The main aim is to achieve a functional integrated fabric capable of withstanding a characteristic tensile load of 3000 N/5cm without compromising the solar film's performance; this value is considered a lower boundary needed for practical architectural applications. Key knowledge from the fields of textile architecture, photovoltaics, and fabrics engineering were extracted to facilitate the design and verification. Laboratory tests were fundamentally used to understand the fabric's failure behaviors and the solar film's electro-mechanical performance.

Results demonstrated a maximum strength of 2200 N/5cm was possible, and so the fabric configuration proved insufficient to meet the strength benchmark; however, the failure behavior indicates that a higher strength is achievable if the failure zones are reinforced. Further development of the fabric requires the electric connections design and their strength to be investigated.

Acknowledgements

Contents

Glossary

Terms

Term	Definition
Compensation	Reduction in size of a cutting pattern, such that during installation the panel elongates to achieve an initial nominal prestress.
Electric Power	The product of current and voltage.
Ends	The number of warp yarns in a fabric.
Fabric	Cloth produced by weaving or knitting yarns.
Fiber	A long and thin strand of thread.
Float	The loose length of a yarn between two consecutive intersection points.
Gauge Length	The distance between the clamps of a tensile loading machine.
Initial Length	The length of the specimen after the application of an initial prestress.
I-V curve	Graph representing the relationship between current and voltage.
Module	Multiple solar cells connected together in a circuit.
Picks	The number of weft yarns in a fabric.
Photodoping	The change in conductive characteristics of semiconductors (or other materials) under the influence of light.
Seam	A connection of two or more pieces of membrane material.
Source meter	An electronic instrument capable of precisely measuring voltage and current either individually or simultaneously.
Substrate	A material which provides the surface on which another material is deposited or inscribed.
Warp	The yarn which is placed longitudinally in a weaving loom.
Weave	The interlacement between yarns to create a fabric.
Weft/Fill	The yarn placed in the transverse direction in a loom that is perpendicular to the warp.
Yarn	A long continuous length of interlocked fibers.

Abbreviations

Abbreviation	Definition
ASCA	Organic photovoltaics manufacturer
FF	Fill Factor
FPV	Flexible Photovoltaic
I_{MPP}	Current at maximum power point
I_{SC}	Short-circuit current
MPP	Maximum Power Point
MPPT	Maximum Power Point Tracking
OPV	Organic Photovoltaic
PES	Polyethersulfone
PET	Polyethylene terephthalate
P_{MPP}	Power at maximum power point
SF	Solar Film
STC	Standard Testing Conditions
TPU	Thermoplastic Polyurethane
V_{OC}	Open-circuit voltage

Symbols

Symbol	Definition	Unit
I_{MPP}	Current at maximum power point	[A or mA]
I_{SC}	Short-circuit current	[A or mA]
P_{MPP}	Power at maximum power point	[Watts or W]
V_{MPP}	Voltage at maximum power point	[v]
V_{OC}	Open-circuit voltage	[v]
η	Efficiency	[%]

1

Introduction

1.1. Rationale

Tensile/textile structures have been part of architecture for decades, captivating spectators and engineers alike with the various intricate free form shapes. Whether it be woven, knitted, or non-woven fabric, the end result is majorly a lightweight and aesthetically pleasing structure as typically seen in stadiums, temporary event structures, tents, canopies, and shading systems. Recent studies and developments, however, have seen more innovative utilization of architectural textiles where fabrics serve multiple purposes rather than a purely shading one.

Textile membranes have garnered a strong reputation for their application in facade elements, a natural consequence given their inherent lightweight, flexible, and possibly translucent properties. But perhaps the most prominent and attractive practical feature of using textiles in facades is the versatility of integration with the building's exterior envelope to meet desired performance requirements; they could be used as a stand-alone primary facade (**Figure 1.1**), where textiles become the main barrier between indoor and outdoor environments, or applied as a second skin layer either partially (**Figure 1.2**) or fully (**Figure 1.3**), to offer a variety of functions from sun shading, wind protection, wa-

Figure 1.1: Al bayt Stadium, Qatar. [1]

ter and acoustic proofing to climate regulation. And so, regardless of the structure's life cycle stage, the structure's performance can be altered via a wide range of customizable textile materials with varying performances as well as aesthetic qualities. Less traditional approaches of integrating textiles with structural glass facades are also possible where open-mesh textiles are embedded within the glass glazing for sun shading and enhancing the glass's load-bearing capacity, or even designed to be the interior curtains behind the glass facade for blast-resistance [5].

Figure 1.2: Sedus Stoll AG, Dogern, Germany. [47]

Figure 1.3: Double-skin textile facade - Rijkwaterstaat building, Utrecht, The Netherlands. [61]

1

A rather new domain in which architectural textiles are gaining prominence is the refurbishment and preservation of archaeological and cultural heritage areas; it is deemed crucial in the preservation of archaeological sites to protect the unearthed findings while limiting any disturbance to the site [62]. Membrane structures present a solid option capable of spanning large column-free areas with minimal impact on the nearby environment that is both mobile and fast in construction. The highly customizable fabric can be specifically designed to provide protection against natural deteriorating agents (i.e. humidity, rain, ultraviolet light, etc.) specific to a certain region or ambient atmosphere. Additionally, fabrics could be a retrofitting solution to improve the energy efficiency of archaeological excavation sites and heritage buildings with minimal demand on the load bearing structure made possible by their lightweight nature [62]. For cultural heritage buildings in specific, technical textiles supplied with monitoring devices could even be applied externally, or internally for less invasive measures, to continuously monitor the structural integrity of those aging structures. However, this is a rather futuristic application than what textiles are currently used for in buildings of heritage value; usually they are used to replace a lost portion of the building, to create room for integrating new functions, or to emphasize the temporal difference between old and new [62].

Figure 1.4: Terrace houses, Ephesus, Turkey. [30] **Figure 1.5:** Thierstein Ruins, Germany. [56]

Investigating innovative potential textile applications, Heinzelmann et. al demonstrated how textile structures could possibly be designed to incorporate green roofs for indoor climate regulation, silica aerogel for maximizing light transmittance and insulation, or algae cultures for energy production and illumination [19]. In addition to climate control, a green roof textile serves to improve air quality, reduce the urban heat island effect, and offers soundproofing qualities to the structure. The application of silica aerogel in translucent textile membranes also offers an inherent means of cutting the energy demand while simultaneously providing high light transmission. An even higher added value could be achieved via integrating algae into textiles since not only do these photosynthetic organisms convert CO_2 and waste water into oxygen and clean water, but they are also capable of energy production that is possible to collect and store. In all three cases, the extent of the added benefits mentioned is proportional to the area used which makes textile architecture a valid option for such integration.
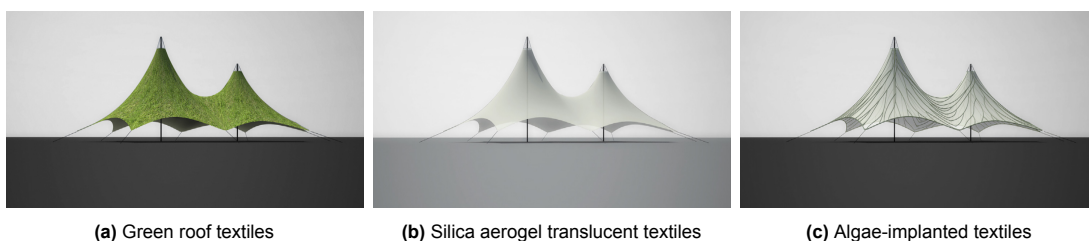
(a) Green roof textiles   **(b)** Silica aerogel translucent textiles   **(c)** Algae-implanted textiles

Figure 1.6: Impression of innovative multi-purpose architecture textiles. [19]

Along the same thought process aimed at achieving highly efficient and sustainable tensile structures, integrating energy generation techniques became relevantly appealing especially solar energy-harnessing methods. The advancements in solar cell technology gave rise to flexible and lightweight versions of photovoltaics capable of integration with various objects including architecture textiles. This was demonstrated by several realized projects in which flexible solar cells were mechanically combined,

printed, or laminated on top of ETFE and coated fabric structures [27]. Flexible photovoltaic panels are capable of following a fabric structure's convoluted curvature, emphasizing on the large areas susceptible to solar radiation to gather more energy; however, they are most commonly seen combined with translucent ETFE foils in small-scale shading structures due to the inherent sunlight-exposed function these structures possess. Amongst the three textile-to-photovoltaic integration techniques, mechanical combination and lamination are the most used in practice as opposed to printing which is not widely available and still needs to address scalability as well as temporal degradation concerns. The resulting fabric is thus monotonous in design where darker coloured PV patches are visible and in some cases the wiring connecting the cells is also seen crossing the fabric. For architecture textiles application, these issues render the fabric less appealing and hinders the adoption of PV techniques by architects or designers who prefer more design freedom as well as less invasiveness. Woven fabrics present a convenient solution for accommodating solar cells in regards to the aforementioned drawbacks.

The idea of integrating flexible solar cells into woven textiles is not uncommon. It has been and continues to be explored in the fields of wearable electronics and electronic textiles, or E-textiles. Initially, energy storage textiles which relied on batteries and rechargeable gadgets were created to meet the surge in energy demand following the growing use of wearable electronics; nevertheless, they lacked aesthetics, durability, and comfortability [45]. Here is where energy-harvesting textiles, also labeled smart textiles, were developed as a complementary solution or a novel alternative capable of generating energy derived from kinetic energy caused by motion, thermal energy from the human body's temperature, wind energy, and solar energy [45]. Woven textiles pose a unique substrate for solar cell integration owing to their mechanical sturdiness which allows them to host thin PV layers, otherwise incapable of handling stresses on their own. They also offer endless possibilities in terms of weaving designs and textures which translate to infinite permutations of aesthetic, mechanical, and building-physics properties. More importantly, they allow for multiple strategies to create integrated solar textiles through printing and/or imbibing of solar cells after the weaving process or by including solar cell fiber, yarn, or tape within the weaving process [24]. In turn, woven fabrics are less likely to have the aesthetic design compromised by the solar cells and are better fit for scalability.

To conclude, architectural textiles and membranes are no longer thought of as merely aesthetic sun shade coverings but as a versatile and structural building component that can be utilized in various current and novel domains such as in facades and in the preservation of archeological/cultural heritage sites, respectively. Also when used for stand-alone conventional spatial coverings, textile materials can be efficiently designed to offer unconventional benefits especially with regards to energy production to meet the ever-growing energy demand. The latest developments in solar cell technology further solidify its position as the leading renewable energy technology [8] and hence, is continuously investigated for the integration with textiles; however, the current integration trend relies on techniques that create monotonous designs which limit the application scope and discourages designers from making use of this technology. A promising alternative can be found in combining woven textiles with flexible photovoltaics to create a stable and scalable solar textile. Considering the possibility to customize both the weave and the solar cell shape and/or dimensions to attain different properties along with the possibility to adopt parametric design tools, this technique becomes more intriguing to investigate towards practical implementation.

1.2. Research Description

In this research, an attempt is made at merging woven textiles with encapsulated flexible solar cell tape to reach a configuration that can perform structurally while generating energy. The effect of weave structures, fabric coating, and yarn properties are investigated along with a study of the flexible photovoltaics (FPV) options, principles, and important properties. Viability of current mechanical testing and assessment criteria of architectural fabrics is also inspected for possible limitations in the case of an integrated solar fabric.

The technical design of the research is outlined in this section including a breakdown of the formulated research question, objectives, scope and methods, and finally, a synopsis of the possible challenges is given. Chapter 2 presents a literature review of key knowledge in textile architecture, material testing, flexible solar cell technology, and integration techniques followed by an analysis of

the woven fabric structure and the most influential design parameters for the design of technical woven fabrics in chapter 3. In chapter 4, a fabric design is proposed and the reasoning underlying parametric choices is provided. All the relevant testing undertaken are explained and analyzed in depth in the 5th chapter and the results are discussed. The concluding chapter answers the research question and provides final conclusions on the results and methodology followed in addition to recommendations for further future developments.

1.2.1. Research Question

"Can a structural solar textile be created using flexible solar film integrated in woven textile for architectural application?"

The main research question explores the feasibility of achieving a structural membrane capable of harnessing solar energy based specifically on the solar film integration method during the weaving process. This question is further divided into the following sub-questions to address individual aspects required for the fabric development:

Q1. What is the design approach to integration in terms of materials used, thin solar film type, the fabrics layout and dimensions?

Multiple flexible solar cell options with different material compositions exist that are capable of textile integration, yet only a few exhibit the stability and efficiency needed for a solar textile application. A suitable version of a thin photovoltaic cell should not only perform mechanically and electrically but also cause the least nuisance to the adjacent fabric dimensions. Thus, exploring this question aims to provide a description of the materials used and the reasoning behind the choices in addition to how the different components interact together in a solar film-to-weave configuration.

Q2. What is the optimal weaving pattern to accommodate solar cells for application in architecture from tensile strength and weaving practicality perspectives?

When a fabric coating is not present, one of the main strength influencing parameters is the weaving pattern; it influences the mechanical behavior such as the tensile, shear, and tearing strengths as well as the acoustic and light-transmission properties. Finding the optimal weaving pattern mainly pertains to the tensile strength and the weaving practicality.

Q3. How to test the fabric composite for strength and stiffness?

The current testing norms are meant to test coherent fabrics in which solar cells are not a constituent fabric component, and so alterations to the testing guidelines will have to be made to accurately represent the combined-fabric's behavior.

Q4. What is the tensile bearing capacity of the integrated solar textile?

Identifying the maximum tensile load the fabric can withstand is crucial for structural performance. It is therefore necessary to benchmark the tensile strength obtained with the designed fabric's configuration.

Q5. How does the solar cell tape behave electro-mechanically?

By examining the stress-strain behavior of the solar film in addition to the load at which the solar conductivity is compromised, a better design decision can be made regarding the extent of its contribution to the overall fabric's strength, and the appropriate stress-relief mechanisms required.

1.2.2. Objectives

The following pre-set objectives are put forth to define what a solar textile is and serve as both, guiding criteria to the design process and benchmarking criteria for the final assessment of whether the main research question have been answered:

• A sufficient tensile strength for textile architecture applications in both warp and weft directions corresponding to a Type I fabric (i.e., 3000 N/5cm), which is the lowest strength threshold for a practical architectural textile.

- A 50% solar film to fabric area proportion; this requirement guarantees equilibrium between the energy generation potential and the tensile strength of the fabric especially if scaling takes place.
- An energy yield of approximately 20 watts per m^2 of fabric under STC.

1.2.3. Scope, Limitations, & Methods

This research aims to compose a modular architectural fabric unit with energy generation functionality that can be woven using standard weaving machinery and to verify its tensile capacity and elongation behavior. Solar cell films based on organic photovoltaic technology are used for energy collection due to their stable format as well as their ability to function under low irradiance (i.e. under shading). However, the tape's dimensions are fixed to allow for the insertion into a weaving loom during the weaving process and hence, the impact of varying tape dimensions on the tensile strength of the fabric or on the energy output is not taken into account. The design of the electrical connections are also not within this work's scope; nevertheless, the effect of varying the weave pattern and yarn properties on the fabric's tensile strength and more importantly, on the implanted solar film behavior will be investigated. Other properties such as fire retardancy, water-retardancy, and ultraviolet-light transmission are also taken into account within the design, yet not included within the testing and verification due to the complexity of performing standardized tests on the final fabric.

The research approach can be characterized as quantitative with more depth towards practical application. Knowledge from the textile and photovoltaic fields will be exploited to guide the lab testing which will be extensively used to address the objectives.

1.2.4. Challenges

Presence of different components in the fabric design poses several challenges which thwart achieving a congruent fabric; firstly, solar cells cannot handle stresses in the same manner textiles could. They tend to lose their efficiency at a much lower stress or strain than those needed for the fabric to break. Similarly, any electrical connection linking the solar cells together runs the risk of a loss of function due to the discrepancy in strength between itself and the adjacent components. Predicting the mechanical behavior of the fabric is yet another challenge given the unorthodox configuration and the large number of variables that can impact the fabric's mechanical properties. Furthermore, the unconventional configuration of the fabric further complicates the testing procedure, requiring specific adjustments to the testing standards available.

2

Literature Review

2.1. Textile Architecture

Textiles have always served a vital purpose in the architecture domain evident in the early small-scale tent and conical dwellings for shelter and in the later large-scale structures encompassing temporary and permanent functions. It was through classical Roman architecture that textiles were first introduced as military tents as well as temporary retractable shading roof elements, building on the sail construction knowledge transferred from maritime technology; the Colosseum in Rome (AD 70-82) employed a foldable textile roof, or velarium, to cover the amphitheater for sunlight protection during the day while possibly opening up for improved airflow at night [25]. The advent of mechanical spinning brought up by the industrial revolution in the late 18th century allowed for larger textile constructions that are fast and portable, and hence widened the textile's field of applications to include transportable circus tents, temporary hospitals, and acoustic membranes. Prior to that period, textile materials relied on natural fibers which lacked the durability and resilience against deterioration to be considered a reliable building component. That is why rubber was used for coating the fabrics shortly after [49].

Textile architecture is now a term coined to refer to a multitude of fabric materials and constructions that are used in the same domain. In the following sections, current textile architecture materials and key principles of the design of such structures will be investigated.

2.1.1. Materials For Fabric Structures

In textile structures, membrane or fabric materials are load-bearing components which require the strength to transfer tensile forces and the ability to undergo shear deformation inorder to achieve a doubly-curved geometry [17]. Durability is yet another critical material factor to consider especially when considering the sustainability aspect. After all, these structures are designed to interact with the outside environment dictating the need to withstand adverse scathing elements from rain/snow and ultraviolet radiation to micro-organism attack and fires. Fabrics made solely from natural fibers such as cotton, wool, linen, or silk are vulnerable to these factors thus, more prone to failure compared to their synthetic counterparts which offer stronger, more resilient, and efficient alternatives.

Textile fabrics, in general, fall into one of three categories depending on their production tech-

Fibers: raw material used to create textiles. Through spinning or twisting processes, yarns are formed.

Yarns: intermediate component formed from natural or synthetic fibers that are interlaced, interlooped, or bonded together to form fabrics.

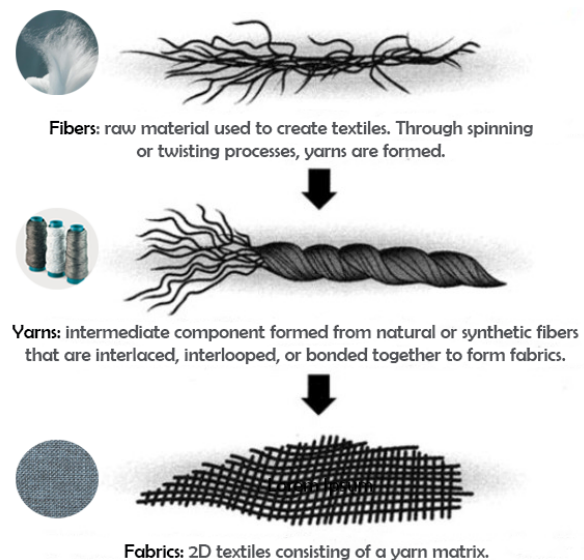**Fabrics:** 2D textiles consisting of a yarn matrix.

Figure 2.1: Fabrics construction process. [34]

6

nique: yarn-based fabrics, fiber-based fabrics, or combined fabrics [15]. Yarn-based fabrics refer to woven and knit constructions made from spun or monofilament yarns while fiber-direct fabrics (also known as nonwovens) are those constructed from fibers without the need to form yarns first. Combined fabrics are multi-layered fabrics that are made from yarn-based or fiber-based fabrics, and these include quilted, laminated, and coated fabrics. Although textile architecture makes use of fabrics from all three categories, combined fabrics in the form of coated fabrics remain the most used. The following sections will discuss the architecture textile materials used in practice, elaborating more on the constituent elements at the yarn and fabric levels along with the types of coating.

Yarns

Fibers are the fundamental building blocks of any fabric that are either naturally occurring or man-made. Through extrusion spinning of melted materials and twisting processes fibers are transformed into yarns, or threads, which are interlaced or interlooped to form fabrics. Yarns are typically defined by [17]:

a) Number of filaments.
b) Linear density or count.
c) Filament diameter.
d) Number and direction of twists per meter.
e) Finishing treatment.

Synthetic fibers are also known as filaments and in theory, can be of infinite length whereas natural fibers are restricted in length. A single yarn is mostly a fibrous composition of hundreds of fibers or filaments bound together, but when a yarn is composed of one single fiber, it is referred to as monofilament; this is normally made via extrusion of melted polymeric solution in diameters of 100-2000 μm [55]. Therefore, yarns can be broadly categorized into three main categories: (1) Staple yarns, manufactured from natural or broken synthetic fibers, (2) Filament yarns, and (3) Composite yarns [55]. The number of filaments and their diameters within a yarn are two necessary parameters to characterize a yarn since not only does this information physically describe the yarn but also reflect its mechanical properties. For instance, an increase in the number of filaments and filament diameter stipulates an increase in tensile strength and porosity, respectively.
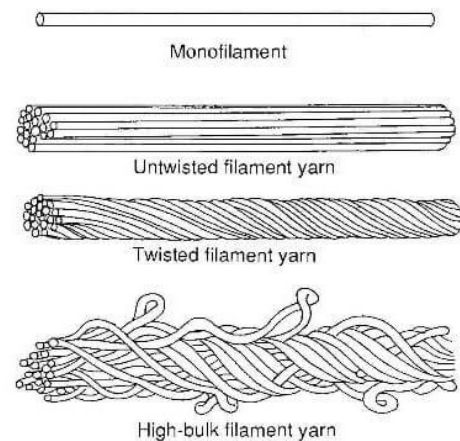

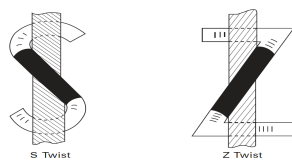**Figure 2.2:** Structural geometry of filament yarns. [54]

Figure 2.3: Twist direction [7]
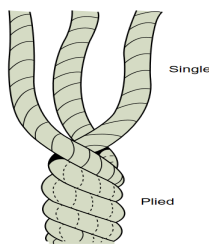
Figure 2.4: Plying process [55]

Another characterizing parameter exclusive to textiles is the linear density or "count" which is indicative of the fineness of a yarn. Due to the difficulty in achieving a constant and stable cross-sectional area along the yarn's length, the diameter cannot be used to indicate the fineness. The linear density is thus used for convenience and is measured in tex (= g/1000m) or dtex (= g/10,000m). Yarns spun from fibers normally undergo twisting inorder to stabilize them around their central axis which is not the case for flat, or untwisted filament yarns, nevertheless twisting makes the yarns easier to handle. Twisting also creates forces within the yarn that holds the fibers together and increases the angle of fibers with respect to the yarn axis which, in turn, influences the stress-strain relationship of the yarn, the moisture absorption, durability, handle, and appearance [55]. There is however an optimum value to the amount of strength increase twisting can provide to the yarn beyond which the strength decreases. Twisting may take the form of an S-twist or a Z-twist depending on the twist direction. An S-twist is one where the fibers are oriented along the diagonal line present in the letter "S", or in other words, in

the direction of a negative slope. Likewise for a Z-twist, the fibers are oriented along the diagonal line in the letter "Z", or in the direction of a positive slope. The direction of twists does not necessarily influence the yarn properties, however, it becomes important for stability when plying multiple yarns is needed (see **Figure 2.4**). Specifying the yarn twist and direction is therefore necessary for yarn definition. Furthermore, finishing treatments could be applied to the yarns to enhance certain properties like aesthetics, permeability, or surface adhesion, especially when a coating is to be used, and so the type of treatment used becomes a characterizing attribute for yarn.
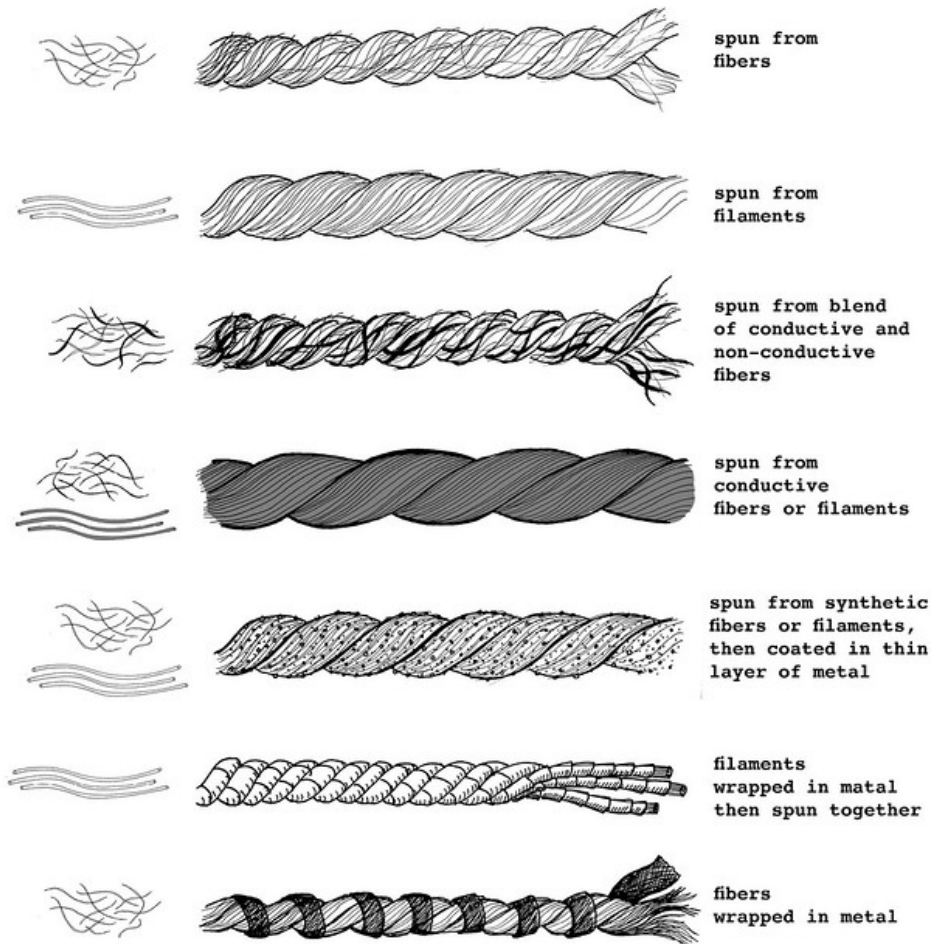
Figure 2.5: Staple yarn, Filament yarn, and various conductive yarns constructions, used dominantly in electronic & smart textiles. [21]

(a) Staple spun yarn
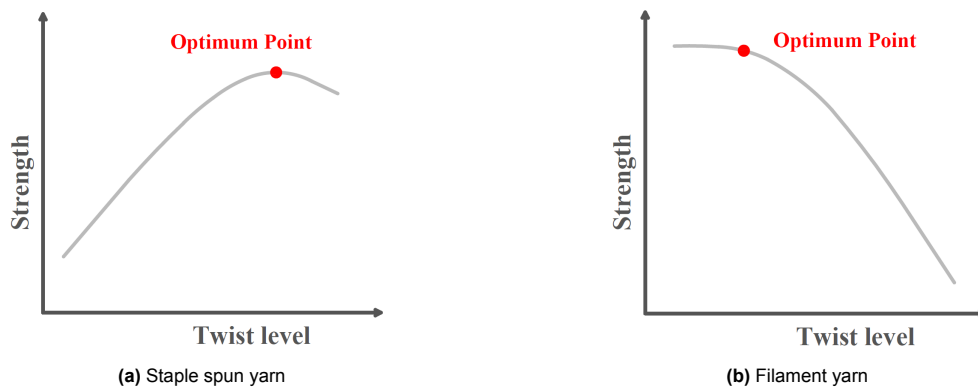
(b) Filament yarn

Figure 2.6: Strength vs.Twist level for staple spun yarns and filament yarns.

In terms of material, yarns used in architecture textiles are predominantly polymeric with the exception of glass and a few natural materials like cotton. Cotton is highly resistant to UV light, however, since it is an organic material, it is biodegradable with fleeting durability that limits its use to a maximum of four to five years. Polyamide (or Nylon) yarns are also used to a limited extent; even though they possess high strength, stiffness, and tenacity among their polymeric peers, they tend to elongate excessively and swell when exposed to moisture which renders them unsuitable for outside use. Polyester (PES), on the other hand, is one of the most widely accepted textile materials that is sometimes recognised through its PET (Polyethylene Terephthalate) format. Polyester yarns can exhibit higher tensile strength and elastic modulus depending on the degree of crystallization and orientation of the macromolecular chains during the cooling process, resulting in a higher tenacity of at least 0.7 N/tex [17]. Due to the lack of pigmentation and their organic nature, polyester yarns are sensitive to UV light and hydrolysis, respectively [17]. This means they are susceptible to aging causing their mechanical properties to deteriorate over time. Another yarn material extensively used in architectural fabrics is glass via filaments as minute as 3 microns in diameter. Fiberglass demonstrates a low creep behavior as well as a brittle failure behavior where high tensile strength is achieved at low elastic strains. Aging does not thwart the mechanical behavior of glass yarns, especially that they are UV and weather resistant; nevertheless, moisture is detrimental to their tensile strength. Fluoropolymer yarns such as those from PTFE or PVDF present unique properties not characteristic to either PES or glass yarns. Although their low strength and stiffness pose a limitation to their performance, they are very flexible with high bending capacity. They are also highly translucent and possess self-cleaning properties which make them frequently used in retractable roof applications.

Special fiber materials with exceptional strengths and low densities exist but are rarely used in the architectural textile context due to their high cost. Aramid fiber, commercially known as Kevlar, possesses very high strengths of upto 2700 N/mm^2 and is resistant to abrasion in addition to chemical and thermal degradation. Aramid yarns are typically seen in antiballistic applications such as tactical clothes. Similarly, carbon fibers and liquid crystal polymers (LCP) have very high strengths that can exceed 3000 N/mm^2. LCPs, or Vectran, lack UV resistance, yet they are resistant to flame, creep, abrasion, and chemical reaction and are therefore utilized in abundance in aerospace applications.

Table 2.1: Properties of commonly used fibers. [20] [50]

Material	Density (g/cm^3)	Tensile Strength (N/mm^2)	TensileStrain %	Elasticity (N/mm^2)
Cotton	1.5-1.54	350-700	6-15	4500-9000
Polyamid 6.6 (nylon)	1.14	Up to 1000	15-20	5000-6000
Polyester Fiber	1.38-1.41	1000-1300	10-18	10,000-15,000
Fiberglass	2.55	Up to 3500	2.0-3.5	70,000-90,000
Aramid Fiber (Kevlar)	1.45	Up to 2700	2-4	130,000-150,000
Liquid Crystal Polymer (LCP)	1.4	Up to 3200	2.9-4.3	75,000-103,000
Polytetrafluorethylene (PTFE)	2.1-2.3	160-380	13-32	700-4000
Carbon Fibers	1.7-2.0	2000-3000	<1	200,000-500,000

Fabrics

Architecture textiles are in essence either coated woven fabrics or extruded plastic foils hence the term "membranes" is used to refer to them collectively. Typical coated fabric is composed of a plain weave or 2/2 basket weave acting as the reinforcement compressed between two layers of coatings applied both on top and at the bottom. Each layer of coating is further subdivided into three layers: a prime coating, a top coat, and a surface sealing/paint (**Figure 2.8**). In this configuration, the properties of the woven base fabric and its constituent yarns dictate the strength and the elastic behavior of the membrane material whereas the coating determines its durability and stability [11]. The prime coat functions as a proofing layer against rainwater and humidity as well as protection against ultraviolet light and abrasive agents in the atmosphere. It also stabilizes the fabric geometry and provides the material which, when combined with a suitable top coat, allows for the application of welded seams to join the fabric panels. In addition to improving the weldability, top coats offer a shielding layer of

protection to the prime coating.

(a) Coated fabric: plain weave (left) & panama weave (right).

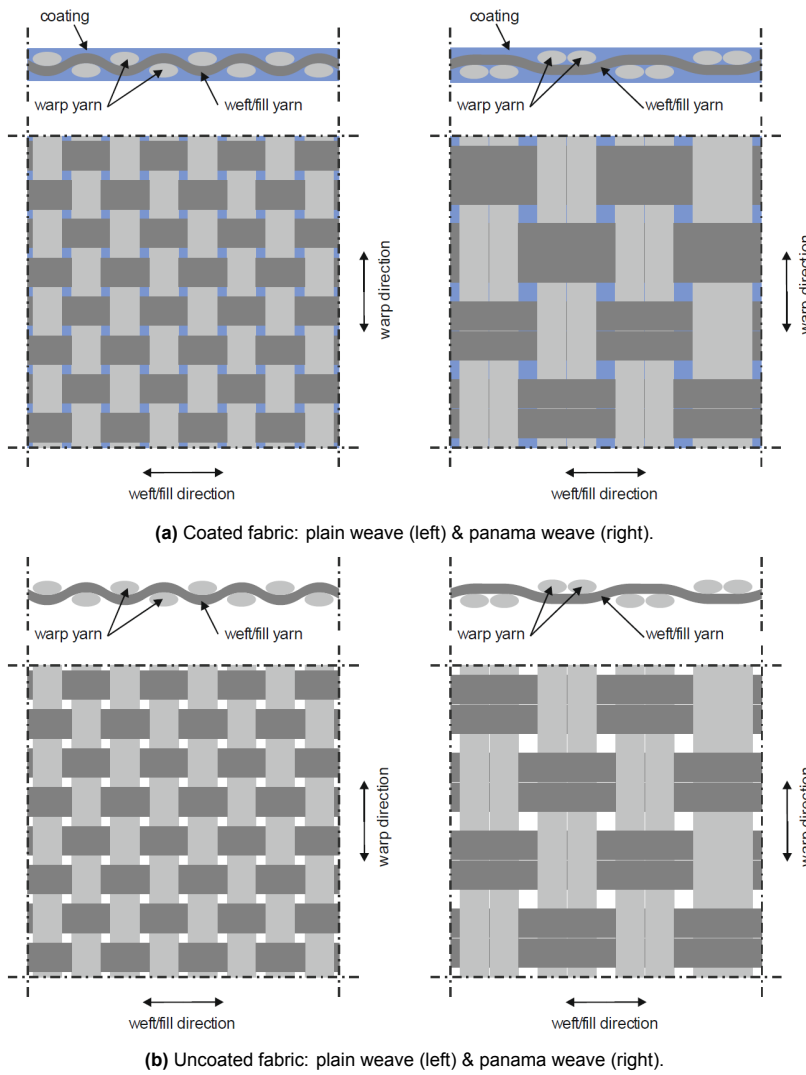**(b)** Uncoated fabric: plain weave (left) & panama weave (right).

Figure 2.7: Most common architectural fabrics' weave structures. [53]
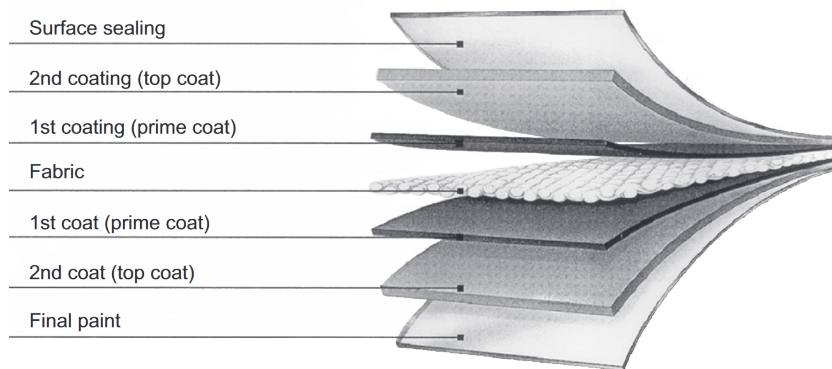


Figure 2.8: Composition of a coated fabric [11]

A wide variety of fabrics are possible depending on the yarn material and prime coating combinations, yet the most commonly used in practice remain the PVC coated polyester fabrics, PTFE coated

glass fabrics, silicon coated glass fabrics, and PTFE coated PTFE fabrics. As for foils, ETFE is by far the most utilized non-fibrous building envelope. To better understand their performance and real-life applications, each of these variants will be discussed further:

I. *PVC coated polyester fabrics*

Polyester fabrics coated with polyvinyl chloride (PVC) are one of the two most employed textile fabric composites, reaching strengths as high as 10,000 N/5cm. The membrane is translucent with limited transparency percentages of approximately 15%. Additives in the form of plasticizers and UV-stabilizers can be added to the PVC coating to enhance the fire-retardancy and UV light protection properties. PVC-coated meshes are applicable in temperatures between -30°C & 70°C and with a PVDF topcoat, could achieve a lifespan of more than 20 years which makes them suitable for temporary as well as permanent applications.
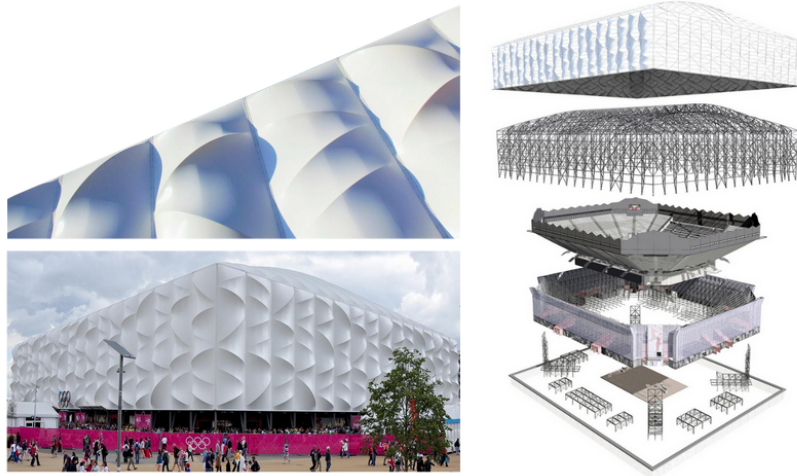
Figure 2.9: PES/PVC fabric used in the London basketball stadium, summer olympics 2012. [37]

II. *PTFE coated glass fabrics*

Mainly used for permanent structures, PTFE-coated glass fabric is the second most utilized textile fabric. It is the most durable textile membrane material able to withstand temperatures from -73°C to +232°C with a lifespan exceeding 25 years. Since glass yarns are vulnerable to moisture, using PTFE coating, which is inherently moisture-resistant, becomes necessary for the functioning of the fabric. PTFE-coated meshes are also chemically inert, UV resistant, fire-retardant, and mildly affected by creep which makes the fabric defy ageing; however, the glass fibers present cause stiffness in the fabric composite that makes folding difficult. Thus, the fabric composite is neither used for temporary nor retractable roof structures.

Figure 2.10: PTFE/Glassfiber fabric-Pompidou Center, Metz. [41]

III. *Silicone coated glass fabrics*

This version of coated glass fabrics is more flexible compared to its PTFE counterpart. Its major advantage, however, is its high visible light transmission that enables highly translucent fabrics.

Initially, the seams connecting the Si-coated mesh panels lacked strength to transfer the necessary forces which limited the scale of implementation, obstructing the acceptance of this composite fabric; nevertheless, the emergence of seaming through vulcanisation rendered the seaming problem obsolete. Another drawback that hindered using this membrane material is that silicon as a material exhibits an electrostatic behavior that tends to collect debris on its surface, but a solution was developed via a nonstick topcoat layer [20].

Figure 2.11: Si/Glassfiber fabric-Zenith Music Hall, Strasbourg. [64]

IV. *PTFE coated PTFE fabrics*

PTFE fabrics offer both coated and uncoated textile versions that can be applied as is, yet the uncoated form demonstrates higher tensile strength values (> 10,000 N/5cm) relative to the coated form (4000 N/5cm). Similar to all other PTFE materials, the fluoropolymer-coated PTFE fabrics are immune to UV rays, combustion, and biodegradability. They also feature high tear-resistance, flexibility and translucencies up to 40%, all of which are valuable qualities for retractable roofing or movable shading application.
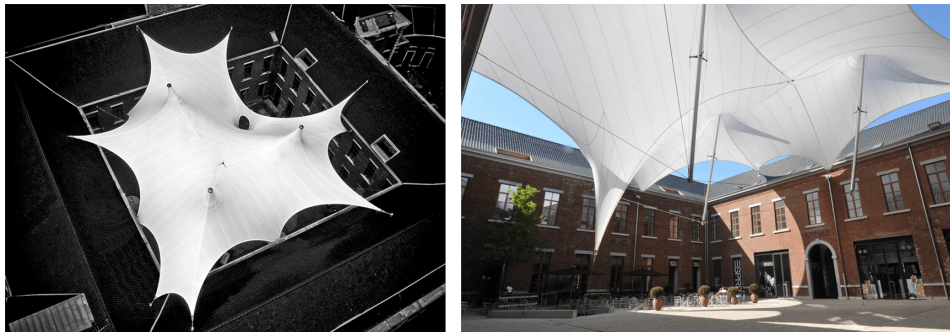
Figure 2.12: PTFE/PTFE fabric-Julianus shopping in Tongeren, Belgium. [59]

V. *ETFE foils*

ETFE membranes are one of the most frequently used textile architecture materials with thicknesses ranging from 50 µm to 350 µm, usually seen in multi-layered air cushion envelopes, but, more recently, single layer foils were deployed as well. Their favorable low mass property comes at the expense of acoustic insulation and thermal resistance properties for which the air gap compensates for. Furthermore, they are flame retardant, chemically inert, self-cleaning, and weather-resistant; their most outstanding properties, however, are their high light transmission and durability. The former reaches up to 95% which surpasses clear glass with lesser embodied energy during manufacturing while the latter is estimated at more than 30 years under normal conditions and up to 50 years as demonstrated by lab experience [31].

From a mechanical performance point of view, ETFE film is a highly elastic homogeneous material.

Despite its low tensile strength, it strains to a large extent which makes it susceptible to creep effects influenced by the stress level, temperature, and load duration.

Figure 2.13: ETFE foil cushions-The Eden Project, Cornwall. [14]

Other fabrics are available that are used to a lesser extent or for special projects only. Cotton fabric, for instance, is used specifically for tent structures but is sprayed with silicon and its fibers blended with polyester beforehand to improve the deteriorating durability characteristic of natural fibers. Aramid fabric coated with PVC, PTFE, or silicon is another less popular membrane form that offers unrivaled strengths of 24,500 N/5cm at 5-6% strains; it is mainly valuable when high tensile stresses are expected. PVDF fabric is yet another membrane material that shares most of the optical and resistance properties of ETFE foils but in woven yarn format, possibly implemented without coating.

Table 2.2: Comparison between tensile membrane fabrics. [17] [23]

Property	PVC coated polyester fabrics	PTFE coated glass fabrics	Silicone coated glass fabrics	PTFE coated PTFE fabrics
Tensile strength warp/weft (kN/m)	115/102	124/100	107/105	84/80
Fabric weight (g/m^2)	1200 (type 3)	1200 (type 3)	1100	830
Trapezoidal tear warp/weft (N)	800/950	400/400	960/700	925/925
Visible light transmission (%)	10-15	10-20	25-30	19-38
Flexibility/crease recovery	high	low	high	high
Fire reaction	M2 (NFP 92 503) B1 (DIN 4102)	M1 (NFP 92 503) B1/A2 (DIN 4102)	A (ASTM E-108) B1 (DIN 4102)	B1 (DIN 4102)
Seaming	by high-frequency welding	thermally	vulcanisation	high-frequency welding
Life span	>15-20	>25	>25	>25

Table 2.3: Mechanical properties of commonly used fabrics. [20]

Fabric/coating	Weight (g/m^2) DIN 55352	Tensile strength warp/weft (N/50mm) DIN 53354	Tensile strain warp/weft (%) DIN 53345	Tear strength (N) DIN 53363
Cotton-polyester/—	350	1700/1000	35/18	60
	520	2500/2000	38/20	80
Polyester/PVC				
Type I	750	3000/3000	15/20	300/300
Type II	900	4200/4000	15/20	500/500
Type III	1100	5800/5400	15/25	850/800
Type IV	1300	7500/6500	15/30	1200/1200
Type V	1450	10,000/9000	20/30	1800/1800
Fibreglass/PTFE	800	3500/3500		300/300
	900	5000/4500		350/350
	1200	7000/6000		500/500
	1500	8000/7000		500/500
Fibreglass/Si	350	2000/2000		
	1156	5000/5000		
Aramid/PVC	750	7500/7500	5/6	500/500
	1050	8000/6500	5/6	600/600
	2020	24,500/24,500	5/6	4450/4450
PTFE/—	320	2000/2050		365/330
PTFE/—	530	4000/3700		669/550
PTFE/PVDF	1080	4000/4000		798/752
PVDF/PVDF	200	1400/1300		
	260	1600/1500		
ETFE foil Thickness		N/mm^2 (DIN 53455)		
50 µm	87.5	64/56	450/500	450/450
80 µm	140	58/54	500/600	450/450
100 µm	175	58/57	550/600	430/440
150 µm	262.5	58/57	600/650	450/430
200 µm	350	52/52	600/600	430/430
250 µm	437.5	>40/>40	>300/>300	>300/>300
300 µm	450	>40/>40	>300/>300	>300/>300
350 µm	525	>40/>40	>300/>300	>300/>300

2.1.2. Weaving & Knitting

In the field of textiles, weaving and knitting are two established processes able to turn 1D yarns into 2D fabrics. The two methods share the same ultimate purpose of creating traditional or function-focused fabrics, yet they are fundamentally different in their constructions and their final fabrics properties. Woven fabrics are the dominant type among the two as they demonstrate high dimensional stability, durability, and versatility; this allows them to meet different performance criteria through the permutations of parameters including density, fabric cover, and the combinations of yarn and/or fiber types. A woven structure is built up of two sets of yarns (i.e. warp & weft) interlaced perpendicular to each other. The yarns running along the length of the fabric are called warp ends while those inserted along the width of the fabric are called weft picks or fillings. The way the warp ends and the weft picks interlace is referred to as the fabric construction or weave pattern which is the most critical influencing factor to the fabric's performance [15]. Three basic weave patterns, namely Plain, Twill, and Satin, are

considered the parent patterns from which the majority of other patterns are derived.

(a-1) Plain weave

(a-2) Unbalanced
(rib) plain weave

(a-3) 2/2 Basket
plain weave

(b-1) Twill weave
(warp-face/right-handed)

(b-2) Twill weave
(warp-face/left-handed)

(c-1) Satin weave
(warp-faced)
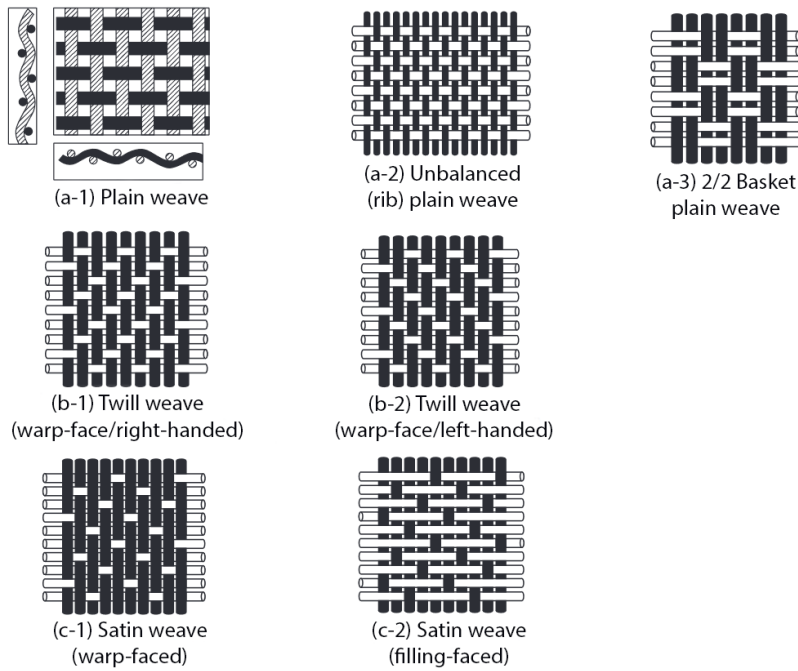
(c-2) Satin weave
(filling-faced)

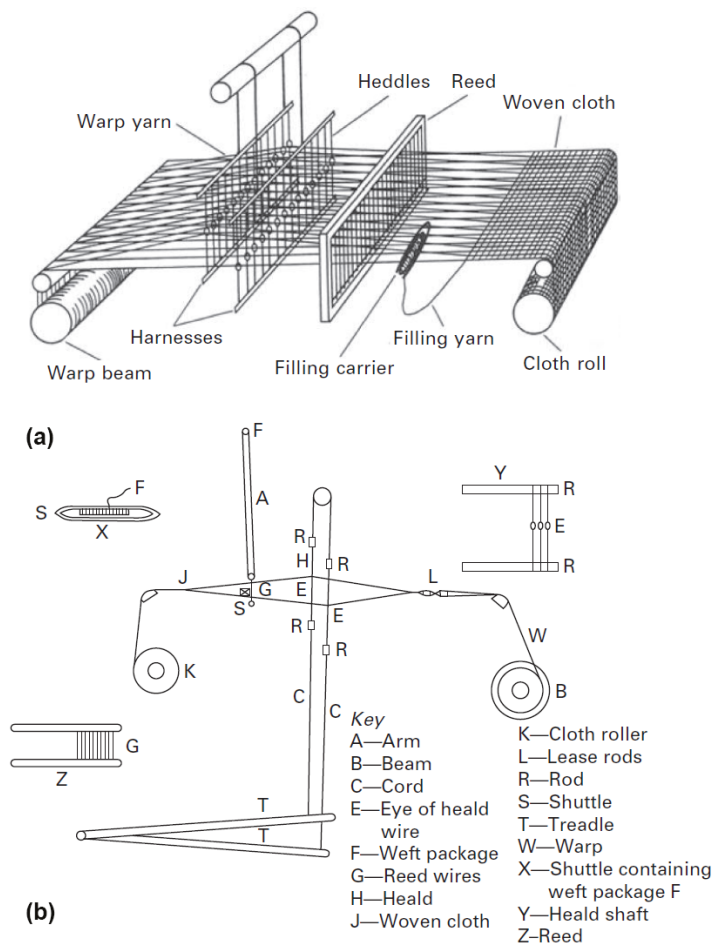**Figure 2.14:** Basic weave constructions. [15]

Figure 2.15: (a) Table loom components **(b)** basic hand loom with treadles schematics. [18]

The weaving process is the same regardless of the type of loom used whether it be a table loom, a hand loom, or a power loom. Initially, the warp beam is prepared by transferring the warp yarns from a cone to the beam through a process of unwinding, winding, and cutting such that the warp yarns are completely wrapped around the beam with the warp ends loose. All warp yarn ends are then drawn through the eyes of the heddles/heald wires in the shafts after which they are passed through the dents of the reed. The reed, which consists of parallel strips of steel wires with gaps (or dents) in between, keeps the warp yarns evenly separated and held parallel as they pass through the dents. The whole operation of inserting every warp yarn through the heddles and the reed is called drawing-in. Once this is accomplished, the beam is installed at the back of the loom and the warp ends are attached to the cloth roll. The loom performs three primary mechanisms: shedding, picking, and beat-up to enable the interlacement of the weft yarns. Shedding is the separation of the warp threads into two layers by lifting some of the heald shafts while lowering others, thus creating an opening known as shed. A minimum of two shafts are required to form a shed, but when more than two shafts are used, the weave structure dictates which shafts are lifted and which are lowered. Picking is the subsequent mechanism where a shuttle carrying the weft yarn passes through the shed. When the shuttle reaches the other side of the loom, the shed is closed by reversing the position of the lifted and lowered shafts. Finally, the beat-up takes place where the reed pushes against the inserted weft yarn towards the edge of the already woven cloth, at a point labeled "fell of the cloth", and then returns to its original position. All the three mechanisms constitute one revolution of the loom and are continuously repeated as the weaving continues.
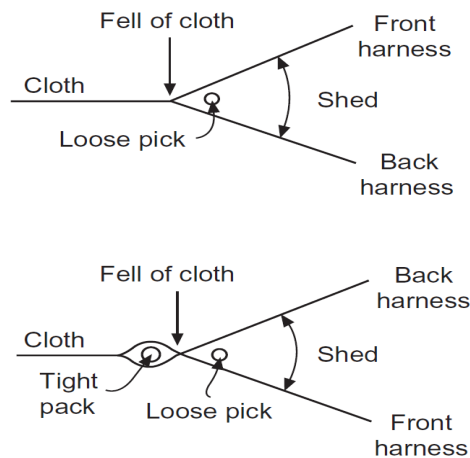
Figure 2.16: Fell of the cloth. [18]

Knitting, on the other hand, is produced by interlocking continuous yarns into loops. The two basic types of knits are weft and warp knits. Similar to weaving, the warp direction is along the fabric length while the weft direction is along the fabric width. Weft knit fabric is a construction in which the traversing yarn creates a row of loops crosswise (i.e. Course) whereas warp knit fabric is one in which the traversing yarn creates a column of loops lengthwise (i.e. Wale) (**Figure 2.17**).
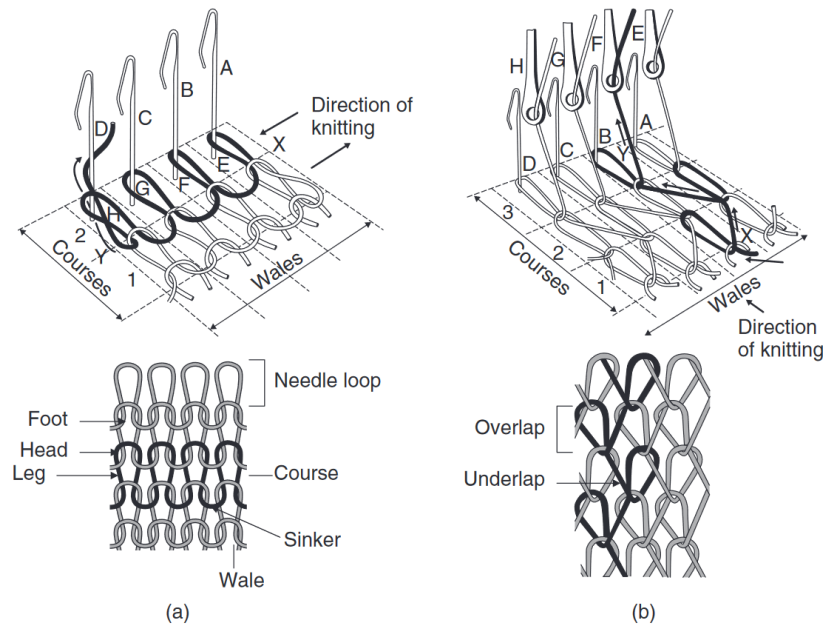
Figure 2.17: (a) Weft and (b) Warp knit fabrics. [15]

Knit fabrics exhibit high elasticity and stretchability compared to woven fabrics due to their loop-forming structure. When they are applied in lightweight structures, the degree of flexibility determines the structure's span and shape possibilities [20]. The fabric's construction does not hinder its mechanical performance, however, it does compromise its durability. Also the gaps present in the fabric necessitate the application of a coating prior to any large-scale outdoor applications. Consequently, knit fabrics and their coated versions have been used in textile architecture to a limited extent; mainly in temporary outdoor structures.

Figure 2.18: Tent structure from coated knit fabric. [20]

2.1.3. Design Principles

While mainstream architecture is focused on defining and realizing orthogonal spaces, textile architecture is concerned with interaction between the structure and the form to achieve efficient lightweight structures. The concept is to rely on tensional forces within the membrane applied through prestressing and curvature to provide a stable structure. Structures in which their shape allows for the transfer of forces through either compression or tension forces only represent the most efficient constructions in terms of load transfer; in that sense, membrane structures could be likened to shell structures where their curved shape follows the lines of compression, largely avoiding bending forces and resulting in minimal surfaces. A requirement for generating surfaces for shell structures, however, is to follow a geometric shape that is possible to define through analytical formulas. This is not the case for tensile structures which depend on the tension applied through the boundary conditions to define the surface geometry. Consequently, tensile surfaces are capable of free-form shapes that surpass the traditional

surfaces, such as in cones and paraboloids, confined by mathematical limitations. The art of designing membranes therefore lies in controlling the boundary conditions and support geometries in order to find the ideal form for the defined purpose.
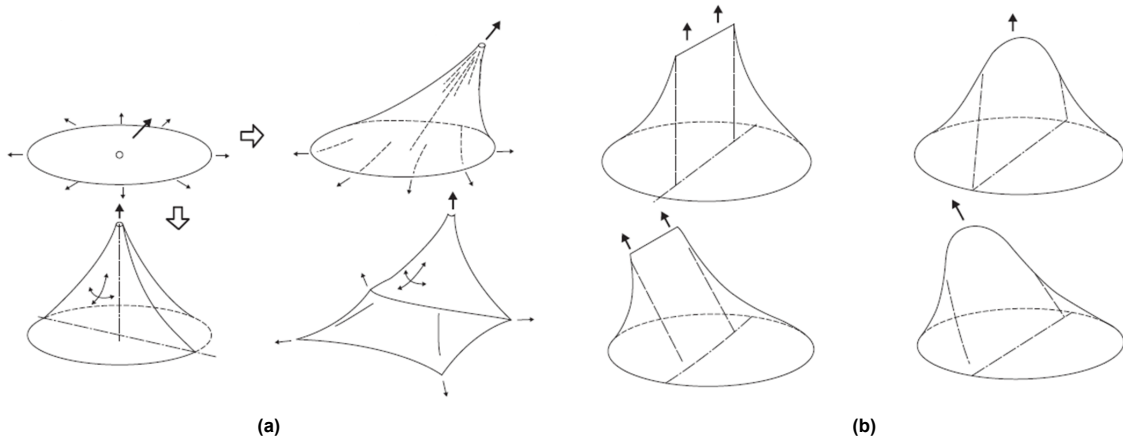

(a)   **(b)**

Figure 2.19: (a) Tensional cones, (b) Tensional conoids. [33]

(a)   **(b)**
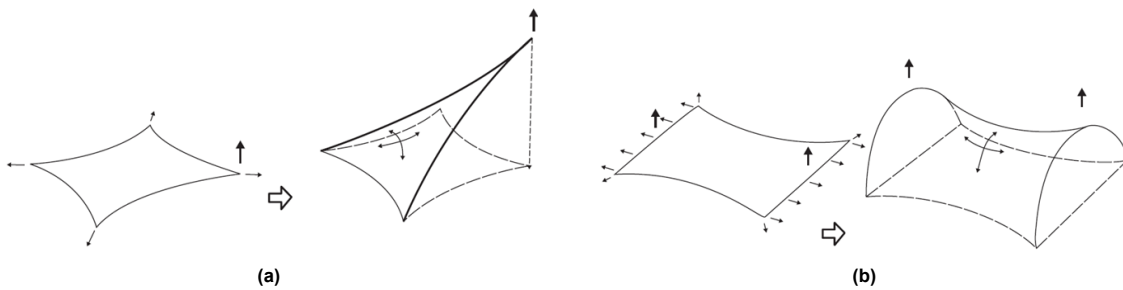
Figure 2.20: Tensional paraboloids with (a) border points, (b) soft borders. [33]

Specifically, the design rests on the choice of three primary structural factors: surface shape, prestress level, and surface deformability. Because fabrics demonstrate a very low surface stiffness, prestress is mandatory to stiffen and shape the tensile structure. The curved geometry then becomes crucial since only through the curved geometry can the textiles limit the deflection caused by loading. This interplay between prestress level and curvature to resist loading is demonstrated by the geometric relationship: T=p×R, where T is the membrane tension, p is the loading pressure applied normal to the surface, and R is the radius of curvature. As the radius increases, the surface becomes flatter, hence increasing the prestress forces required to endure the loads.
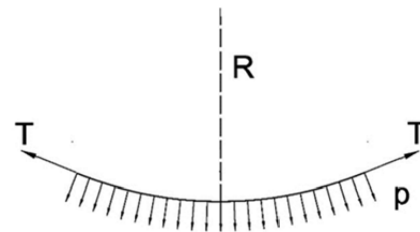
Figure 2.21: Geometric relationship between applied load (P) and cable tension force (T). [53]

In terms of surface shape, or form, tensioned membrane structures are mainly either synclastic or anticlastic. The former pertains to doubly-curved shapes where both principal curvatures are in the same direction (i.e. positive gaussian curvature), whereas the latter relates to doubly-curved shapes where the principal directions are in opposite directions (i.e. negative gaussian curvature). Both shapes differ fundamentally in how they maintain stability. For anticlastic forms, this can be demonstrated through cable mechanics which dictate that three tensile forces are needed to stabilize a point on a cable in a plane. A fourth force, acting in

Figure 2.22: Cable mechanics. [33]

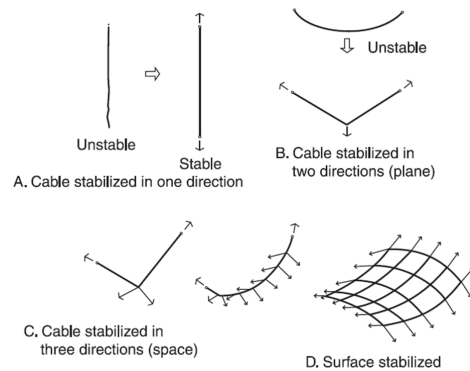the perpendicular plane to the force at that point, is required to stabilize the same point in space. To stabilize all points on a cable, more pairs of opposing forces are necessary. The result becomes similar to introducing an extra set of cables along the perpendicular direction to the main cable, eventually generating a stabilized anticlastic surface.
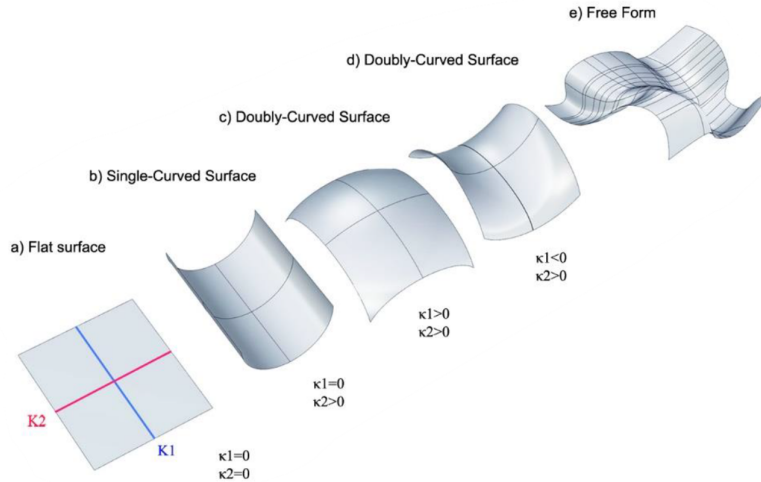

Figure 2.23: Surface typology and the corresponding principal curvatures. [28]

Therefore, the tensioned surface itself becomes the main structural element with two identifiable load paths for inward and outward pressures. It is through the internal equilibrium of prestress within the membrane that anticlastic shapes retain their form and guarantee stability against external loads. Synclastic shapes, on the other hand, require pressure for tension and stability often provided via pneumatic or hydraulic pressure acting perpendicular to the membrane surface.
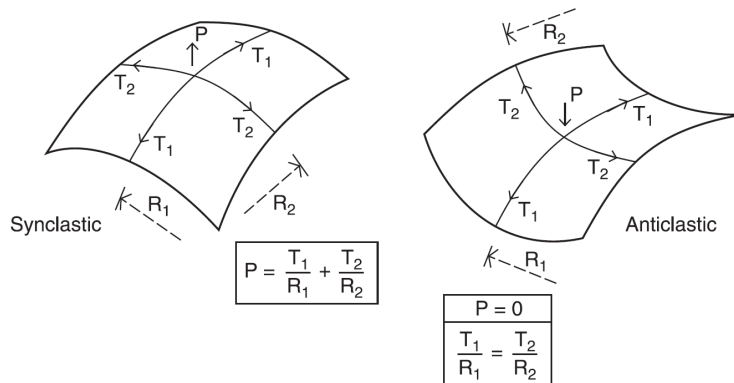
Figure 2.24: Synclastic & Anticlastic curvatures. [33]

The vast majority of fabric structures are of the anticlastic format, where the warp and weft directions coincide with the load paths, or principal curvature directions. The surface is kept in equilibrium by edge reinforcements that are arranged in space by suspending and supporting elements. By manipulating the arrangement of internal and external supports, designers can achieve unique anticlastic doubly-curved forms. The most generic types of anticlastic structures are the cone, hypar, saddle, and ridge-and-valley. Anticlastic structures covering very large areas are preferably constructed by grouping multiple single structures simply because expanding single structures makes the prestressing process cumbersome as the prestress load greatly increases, and most likely, high strength fabrics will be required to cope with the increased stresses.

(a) Sum of cones

(b) Sum of paraboloids/hypars

(c) Sum of cones and paraboloids
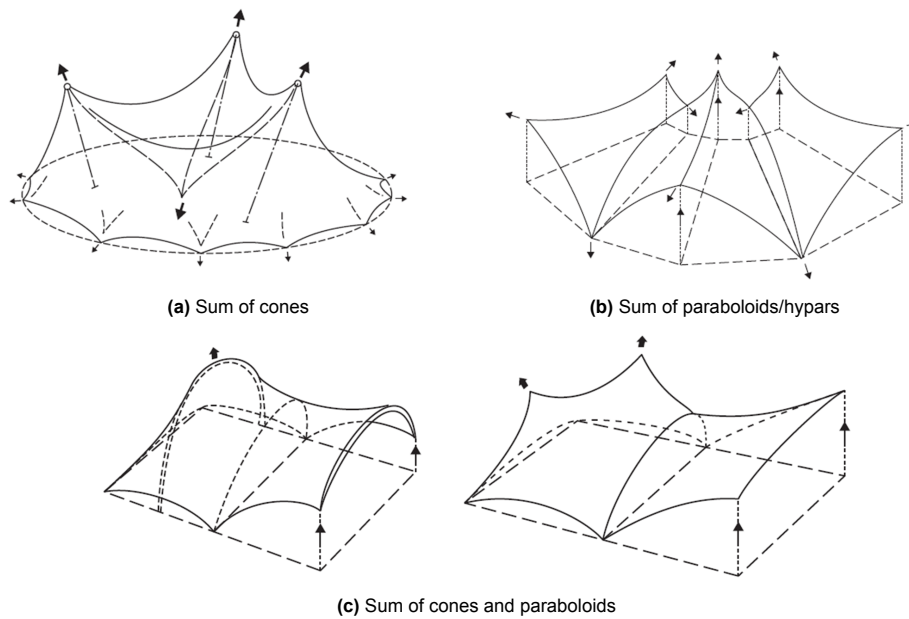
Figure 2.25: Combination of multiple structures. [33]

Synclastic membrane structures are shaped and stabilized by a difference in fluid or gas pressure across the membrane's skin. Typical applications of the synclastic form include air-supported structures, air-inflated cushions, and to a lesser extent, hydrostatically shaped structures. Air supported structures utilize fans to supply air generating pressure into an airtight membrane cover without the need for rigid supporting elements. Another approach to create these structures is through negative air pressure by mechanically evacuating air, and thus, creates a lower air pressure inside. It becomes necessary then to add an additional structure for the membrane to act against to maintain its shape such as a metal framework or inflated membrane ribs. Inflated cushions are also supported by the difference between internal and external pressure; air is pumped into a closed membrane envelope which generates tensile stresses in the membrane surface and retains its shape. Such cushions are typically made from ETFE foils in the form of a single cushion or an array of cushions used for roofs or facades. Hydrostatically shaped structures are those shaped by hydrostatic pressure. What is characteristic to these structures is the change of pressure with height which enables a set of unique shapes. Hence, they are used as lightweight and mobile containers for liquids and viscous substances.
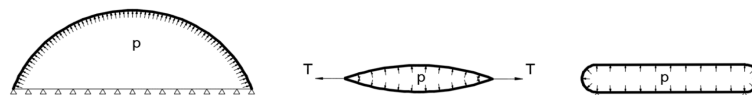
Figure 2.26: Air-supported structure (left), inflated cushion (middle), and inflated beam (right). [53]

All in all, the engineering of membrane structures consists of four interlinked design steps:

- Form finding
- Structural analysis
- Cutting pattern generation
- Construction engineering

The form finding process takes place initially to find the appropriate boundary configuration along with the prestress level. Structural analysis is then performed after applying load assumptions as well as material stiffness assumptions. Since the form is intimately linked to the structure, a change in the structural analysis phase requires amendments to the form finding, and so it becomes a back and forth interaction until stability is guaranteed and architectural requirements are met. The following step is the generation of cutting patterns which is involved with dividing the fabric into individual segments and determining the plane unstressed patterns. This division is necessary due to the limitation to the fabric

width possible by the textile fabrication process. Construction engineering steps could now commence to demonstrate the erection plans and prestressing procedures.

Support & Boundary Systems

One of the main features of the supporting structures is the explicit expression of the membrane structure's lightness using a variety of material possibilities including steel, timber, or a combination of both. Support structures can be classified based on different aspects, yet the most common is based on the stiffness or the location within a structure, i.e. internal, edge, or external support. The classification used here is stiffness based.

I. Flexible membrane support elements

    A. Linear reinforcements

        Soft curvilinear reinforcements in the form of steel cables or textile belts are used at the edges of the membrane to connect support points which are usually arranged on different levels relative to the ground, referred to as high points and low points. The loads from the membrane surface are transferred to the edge cables which in turn carry the load to the supporting structures via axial extension forces. Flexible edges can be constructed by creating a fold, also known as a hem, at the edges using the same textile fabric where a steel reinforcing cable is inserted or laced from the outside, depending on the diameter size of the cable. In case of wide spans, high-tensile steel cables with large diameters are used to collect the membrane edge loads. Fabricating folds from the same fabric is the simplest way to attain an elastically compatible behavior between the tensioned surface and the edge reinforcement especially when large deformations are expected [17]. Sewing woven belts onto the fabric edge is yet another approach to achieve flexible edge supports. Tensioned linear membrane supports are not only used at the edges but also internally. Cables connecting internal high points are referred to as ridge cables whereas those connecting low points are labeled valley cables.

Flexible interior

Flexible exterior

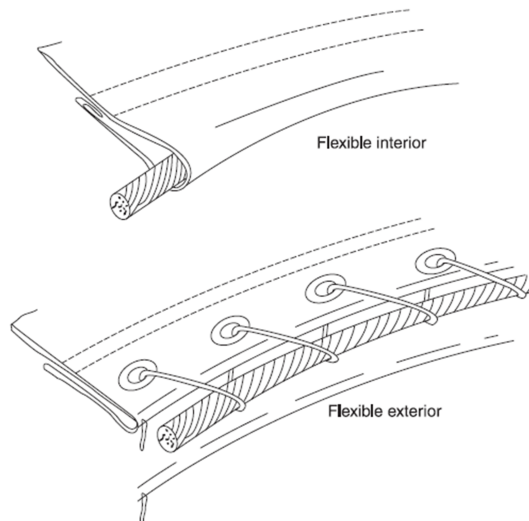**Figure 2.27:** Cable edge. [33]

    B. Point anchorages

        At internal low or high points, a couple of options are possible to join the membrane with the support element transferring the loads to the foundation. A spherical reinforcing cap is an option used for small inflections. For large inflections, the loop is used; it is a special form point anchorage composed of a curved rope reinforcement.

(a) Internal soft point with spherical reinforcement.   **(b)** Internal sharp point with loops.
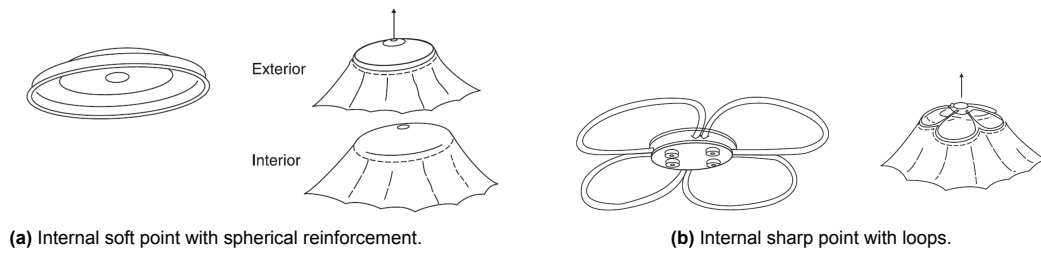
Figure 2.28: Point anchorage variations. [33]

II. Rigid membrane support elements

A. Stiff linear supports

Stiff support structures are continuous boundaries of straight or curved elements arranged
into curves or polygons. They may take the form of a solid bar or a hollow tube inserted in a
fold similar to the flexible reinforcements mentioned above; however, the bar/tube transfers
perpendicular stresses only to the cloth . This solution is exclusively used at the peripheral
membrane edges. A circular ring is another perimetric option typically used in cone struc-
tures to convert the tensile forces from the fabric into axial compressive forces. Arches and
frames are the most common options that are modular and can be applied both internally
and at the edge. Depending on whether they are used internally or externally, hinged or
fixed support conditions can be chosen to stabilize the structure.
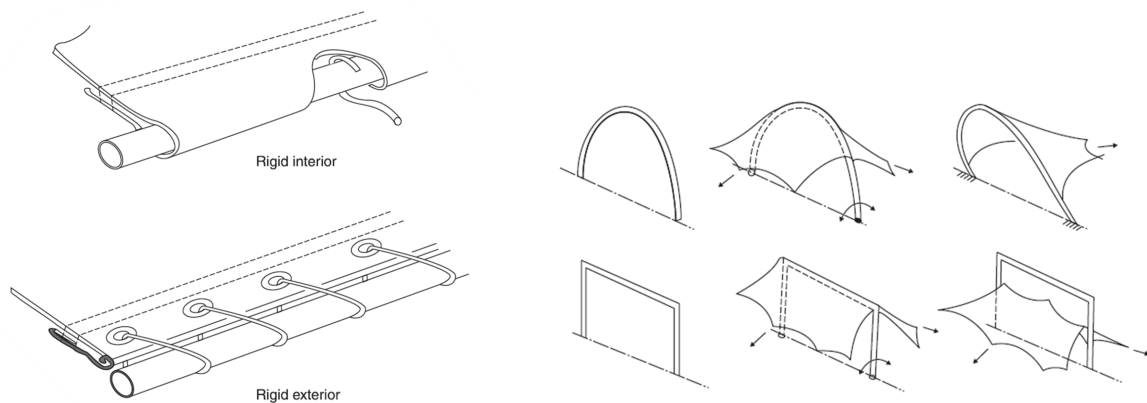
Figure 2.29: Stiff linear edge supports. [33]

Figure 2.30: Internal & external arches and portal frames with
different support conditions. [33]

B. Point anchorages

Rigid point anchorages of hollow steel rings are used for internal points where large point
loads are expected. For smaller membranes, a steel cone may be used instead.

(a)

(b)

Figure 2.31: Internal sharp point with **(a)** rigid junction, **(b)** steel cone. [33]
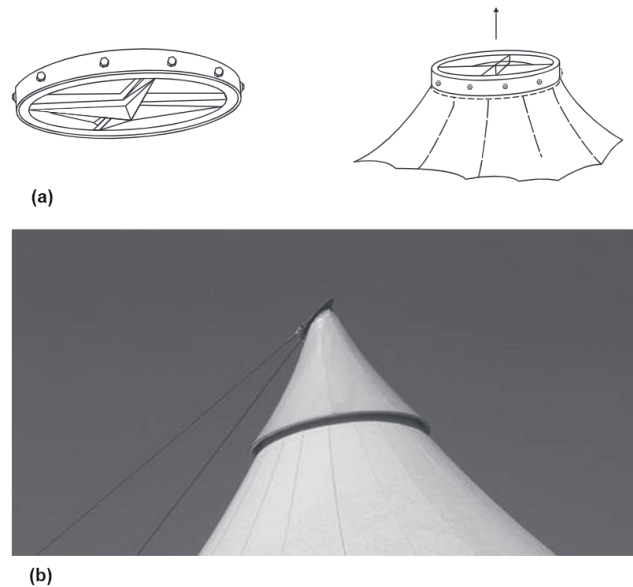
C. Humped supports

These are spherical supports capable of sustaining large membranes through compression. To achieve prestress equilibrium, the diameter of the humped area needs to be large enough in relation to the membrane area in between the humps [17]. They are less traditional support options seen mainly in tent structures.

Figure 2.32: Humped supports. [17]

D. Masts

Masts are compression elements that provide support to the membrane structure and can be placed almost anywhere inside the structure or outside [17]. Three main types of masts could be identified based on location, namely boundary, internal, and external masts. Boundary masts are those at the edge or corner points bisecting the edge cable and anchor cable. Internal masts are those placed inside the enveloping area of the structure pinned to the footing at the bottom and to an internal high point at the top. Stability of the internal masts are maintained by the membrane fabric itself. A special type of internal masts is known as flying masts since they are unconnected to the foundation generally floating midair. They are stabilized via tensioned cables at the bottom and another set of cables or the fabric itself at the top. Lastly, when the design prohibits the presence of structural elements in the covered area, external masts with inclined suspension cables are used to support the structure from the outside.
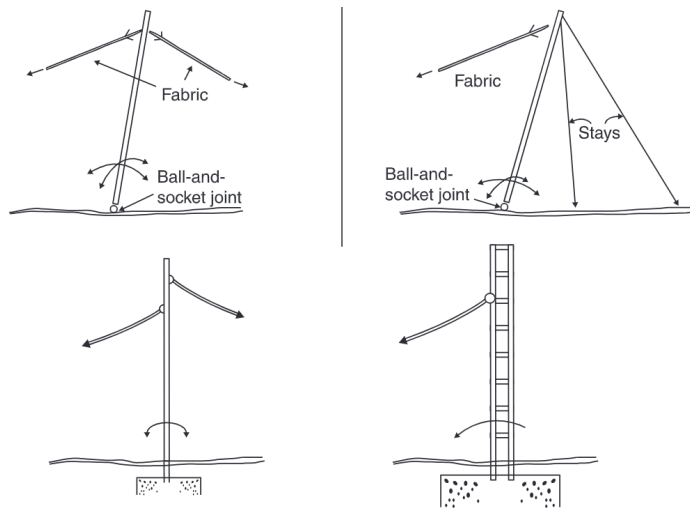
Figure 2.33: Internal & external masts, hinged or restrained. [33]

Figure 2.34: Flying mast. [48]

The final dissipation of the accumulated loads is carried out by the foundation which is required to provide sufficient stability to the membrane system. In case of small anchor loads, earth anchors or sand/water containers could be used. Larger loads require heavy concrete foundations, or alternatively, permanent soil injection could be used for a lower environmental impact [17]. When possible, membrane structures could even be attached to nearby building structures instead.

Form-finding

The process of finding the geometric shape of the tensile membrane where equilibrium is attained is termed form-finding, and it depends primarily on the layout of the boundaries as well as the prestress levels. Form-finding commences by defining the arrangement of internal and external supports and boundary conditions confining the enclosure area for which the equilibrium state is found in an iterative manner. Each layout of boundaries results in a unique surface shape and so the number of possible shapes is as variable as the different boundary/support layouts possible. The prestress level is not a major determinant of the surface shape but rather a means to modify the surface further. A form found shape is therefore one where the combination of support arrangements and the prestress ratios has achieved membrane equilibrium.

Both physical and numerical methods are used for the form-finding process and the development of the design concept. Earlier models were physical ones constructed from soap-films, elastic cloths, or spring systems to simulate the membrane behavior. Soap films are relatively easy to construct using rigid wires and thread supports. Due to their fleeting lifespan, pictures are taken from which relevant geometric data is extracted. However, soap films can only guarantee a constantly stressed surface which poses a limitation on the design efficiency since not always can an optimum design be achieved through constant stresses but rather a variation in stresses might be needed. Alternatively, elastic fabrics are used as they offer better curvature and stress control in addition to the possibility of performing detailed cutting pattern measurements. Current models are mainly numerical ones which also begin with the layout of the boundary conditions, then the 3D model is generated in an iterative numerical process.

The fundamental principle behind most computational systems is equilibrium modeling; once the fixed support points and the edge geometry are inserted, the structure is discretized into a finite element mesh of approximate nodal coordinates. Internal forces occurring at the nodes could then be quantified by the FE technique, and by applying external loads, the residual nodal forces causing instability can be determined. The model then performs adjustments to the mesh positioning until nodal equilibrium is reached, generating an anticlastic surface with similar tensions and curvatures at all points. Several FE methods can be used to carry out form-finding as well as full nonlinear analysis, yet the two main ones remain the force-density and dynamic relaxation methods. All methods discretize the surface into

a network of line elements or orthotropic mesh elements and allow for the inclusion of other element types in the structural model such as masts, beams, and slip elements [17].

Cutting Patterns & Seams

Woven fabrics are typically produced in widths of 2 to 5 meters on a fabric roll, and so to create a curved geometry out of planar fabrics, the designed surface shape needs to be divided into single cut shapes which are eventually joined together using seams. Since doubly curved geometries are formed from two dimensional panels having an orthogonal weave, shearing of the weave must occur. The extent of shearing depends on the coating flexibility, prestress level, and panel's maximum width and length [17]. Fabrics are known to have a limited shear resistance; consequently, the warp and weft directions are aligned along the principal membrane stresses directions to negate any shearing effects. It is necessary for the centerlines of panels to follow geodesic paths over the curved surface as they represent the paths which a flat panel could follow without shearing. In addition, creating panels along geodesic paths allows for material economy and improved accuracy. Another requirement for panel fabrication is to determine the stretch compensation; this is the amount of reduction in the cut pattern's size such that during installation the panel elongates to achieve an initial prestress.

Figure 2.35: Cutting patterns following geodesic paths. [17]

Cutting pattern generation, thus, involves three main aspects: the division of a surface into individually cut fabric shapes, the flattening of the 3D geometry onto a plane, and the determination of the compensation values. The cut patterns are accounted for early on in the design in both the form-finding and analysis stages.

Adjoining adjacent panels requires one of the established seaming techniques depending on the membrane composition and type. Sewing, welding, and adhesives can all be used to that end. Sewing creates a mechanical interlock using overlaps and stitches between the panels, yet still provides flexibility to the fabric which makes it suitable for use in convertible roof structures. Stitching, however, lowers the mechanical strength and water resistance of the fabric. A popular alternative is the welding technique achieved by welding the coating material together in the case of coated fabrics. High frequency welding is used for joining PVC coated polyester panels while heat welding is used in PTFE coated glass and ETFE foils. Vulcanisation is used specifically for silicon coated fabrics otherwise adhesives are applied.

2.1.4. Standardized Testing

The first steps towards standardization of fabric testing were originally carried out in the clothing textile industry to provide quantifiable means for quality control and experimentation. Likewise, a multitude of tests have been developed by standardization entities to verify certain fabric behaviors influencing the functional performance of the fabric in an architectural context. Tests pertaining to strength, stiffness, and the impacting environmental factors are all used to verify the fabrics performance.

Strength Tests

Pure tensile strength of fabrics is merely one crucial strength value amongst others. Seam strength, tear strength, and adhesion strength, in case of coated fabrics, are sought strength values too. For glass fiber fabrics, the tensile strength after crease fold is of utmost importance because of their sensitivity to folding. Strength tests can be classified into short-term and long-term behavior tests, aimed at assessing the resilience of the fabric against strength-decreasing factors including prolonged loading and environmental impacts. Most long-term strength tests are based on adjustments to the following main short-term test protocols:

I. Uniaxial tensile strength tests

EN ISO 1421 and EN ISO 13934-1 are currently the most prominent european and international norms for measuring the fabric's tensile strength for coated and uncoated fabrics, respectively. Both standards require the use of constant rate of extension (CRE) testing machines, as opposed to constant rate of load (CRL) or constant rate of traverse (CRT) machines, and present two methods of possible uniaxial tensile tests to measure a fabric's maximum tensile force: a grab test and a strip test. The fundamental difference lies in how the clamping of the specimens is performed; in a strip test, the whole width of the specimen is clamped while in a grab test, only the middle part of the specimen width is clamped.

EN ISO 1421 proposes the use of the grab test as an interchangeable substitute to the strip test in case of clamping failure to measure the breaking load, whereas EN ISO 13934 presents the two methods as separate tests.

Table 2.4: Comparison of strip and grab test procedure according to EN ISO 1421. [3]

Parameters	Strip Test	Grab Test
Jaw distance	200 mm ±1 mm or 150 mm ±1 mm or 100 mm ±1 mm	100 mm ±1 mm or 75 mm ±1 mm
Width of specimen	50 mm ±1 mm	100 mm
Gripping width	50 mm ±1 mm	25 mm ±0.5 mm
Mounting state	Pretension setting or slack mounting	—
Rate of Extension	Constant rate of 100 mm/min ±10 mm/min	
Slippage	Disregard test results where specimen slips asymmetrically or by more than 2 mm. Or record them when they are useful.	
Jaw breaks	Disregard the test results where test piece breaks within 5 mm of the face of a jaw or outside the reference marks on the specimen. Or record them when they are useful.	Disregard the test results where test piece breaks within 5 mm of the face of a jaw. Or record them when they are useful.
Results	Maximum force, force at break (if it differs from maximum force), elongation at maximum force and elongation at break (if it differs from elongation at maximum force)	Maximum force

For structural design purposes, the strip test is the more representative tensile strength test as it better resembles tensile fabric behavior in which all yarns in the width of the fabric contribute to the strength. It is also possible to measure the strain/elongation at break via the strip test due to the lesser uncertainties in the stress distribution and fairly constant elongation along the specimen's width. In a grab test, however, strain measurements are not possible due to the frequent slippage and large out-of-plane deformations [3]. Not to mention that non-uniform elongations indicate non-uniform stresses and hence, transforming the breaking load into a linear stress is incorrect [3]. Asadi et al. demonstrated that these conclusions are valid regardless of whether coating is present.

Strip tests are performed by first cutting specimens to a length equivalent to the gauge length plus the additional fabric length to be held in the clamps and to a width of 50 mm. In case of uncoated fabrics, the width is cut wider and longitudinal yarns are removed equally from both sides of the specimen until the 50 mm width distance is reached to prevent the unraveling of threads. The specimen is then inserted into the clamps and either left hanging under its own mass (i.e. slack mounting) or prestension is applied. The test now commences with a constant rate of extension

applied until failure and the resulting failure load as well as the extension at break can be obtained. It is necessary to perform this test in both warp and weft directions of the fabric. To include the temperature effects, the same test can be performed at -20 °C, 23 °C, and 70 °C.

II. Seam/connection strength tests

Both the short-term and long-term strength behaviors of the seams and connections can be carried out using the same uniaxial strip tests as in EN ISO 1421. The test specimen then includes the seam and the load is applied perpendicular to it.

III. Tear strength tests

Tear strength is not a requirement for structural design nevertheless it might be needed in special applications where a tearing failure behavior is expected. The principle of tear tests is to load the individual yarns of fabric one after the other. In this manner, the load at which the tear will undergo unstable propagation, hence failure, can be found. Two main tear test standards are used: the Tongue Tear method proposed by ASTM D2261 and the Trapezoidal method by EN 1875-3.
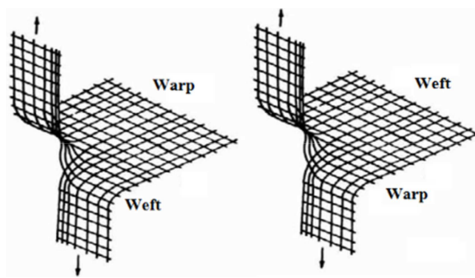
Figure 2.36: Tongue test method in both weave directions. [32]

IV. Adhesion strength tests

Adhesion tests, according to EN ISO 2411, are performed specifically for coated fabrics to determine the mechanical behavior of the adhesion between the coating and the fabric. A specimen of two material strips welded to each other is pulled until separation occurs.
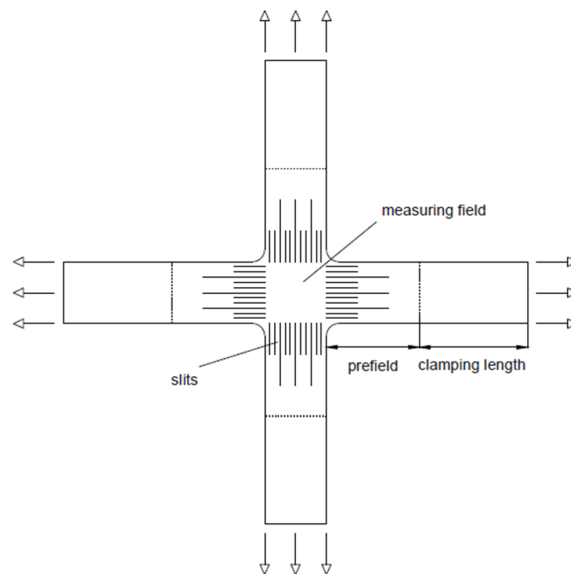
Deformation Behavior Tests

Figure 2.37: Bi-axial test specimen. [53]

Bi-axial stiffness test   Bi-axial tests have become the primary tests used to determine the stress-strain behavior of fabrics and the cut pattern compensation values. Although different variations of biaxial tests are present, the principles followed are the same. The test is designed to measure the elasticity moduli in the principal weave directions to be used in an orthotropic linear-elastic model for the structural design. To conduct the test, a cruciform specimen is biaxially loaded in-plane in a cyclic manner according to different load ratios in warp and weft. It is not intended for the fabric to reach failure but rather mimic the loading in real conditions; thus, a relevant load range is required. The maximum load applied in any of the load ratios, denoted as the working stress, is a portion of the ultimate strength value measured in a uniaxial strip test as a safety margin. A fifth to a tenth of it is then used as prestress. Consequently, the testing load range becomes that in between the prestress and the working stress values. The main load ratios to be tested are 1:1, 1:2, and 2:1, yet higher ratios (1:P & P:1) are also possible if required. Standards normally propose a loading profile similar to the one in **Figure 2.38**, consisting of a series of load ratios from which the stiffness parameters are extracted. EN 17117-1 is currently the European norm associated with bi-axial stiffness testing of textile architecture fabrics.
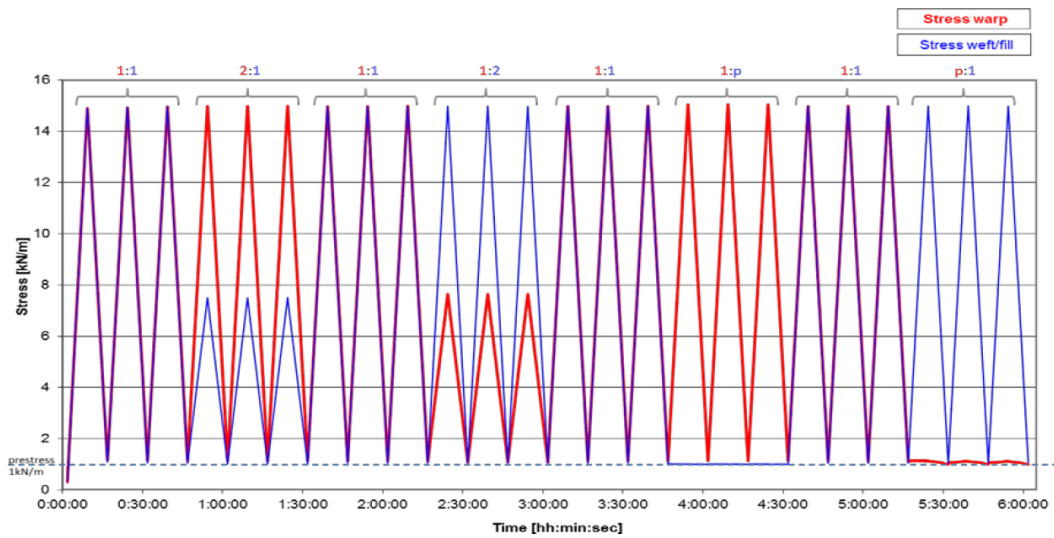

Figure 2.38: Characteristic load regime for the determination of the elastic moduli, CEN TC 248 WG 4 Draft standard [9]
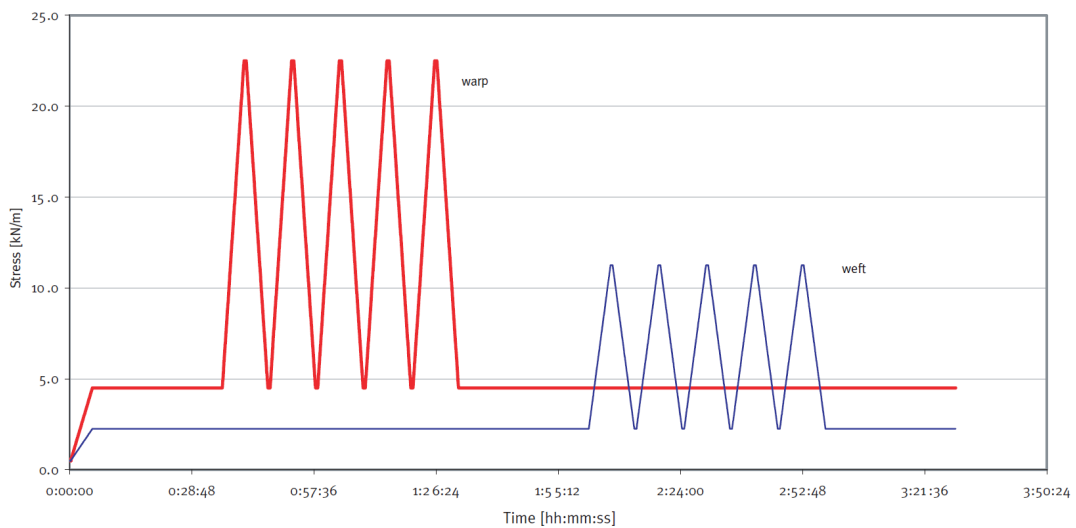

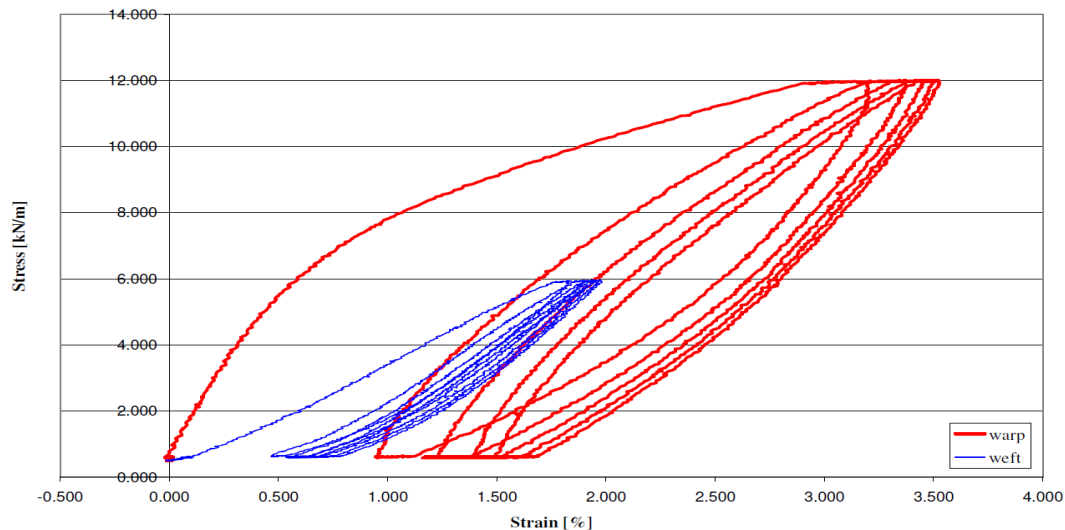**Figure 2.39:** Load history graph for 2:1 warp-to-weft ratio [53]

Figure 2.40: Stress-strain diagram for a 2:1 stress ratio [10]

Shear test   It is important to evaluate the shear behavior of fabrics since it directly influences the stress distribution of orthogonal materials at the seams and edges, especially if the mean axis of anisotropy are not perpendicular to the edge. Multiple tests are devised to measure the shear modulus values using uniaxial methods and variations of biaxial methods; bias extension and picture frame shear tests are the most prominent.

Relaxation & Creep behavior   Creep is defined as the increase in plastic strain under constant stress while relaxation is the decrease in stress under constant strain. They are long-term behaviors that are more relevant in the case of foils in comparison with coated and uncoated fabrics. There are no available standards to assess these properties for coated fabrics as yet nevertheless two tests are used to that end: creep-rupture test and time-to-failure test [2].

Fire Resistance Tests

Assessing the fire behavior of a textile fabric is crucial for its induction into structural membranes. Not only is the strength loss a detrimental outcome but also the occupants safety is compromised in case of excessive smoke or ignited drops release. This is considered by EN 13501 which provides a classification of the building construction products in terms of fire reaction labeled Euroclasses, ranked as A1, A2, B, C, D, E, & F. A product classified A1 is non-combustible whereas F corresponds to products which do not have another classification or have not undergone testing. Additionally, the standard also provides classification concerning smoke production (s1, s2, s3) and the production of molten droplets (d0, d1, d2). In order to verify the classification of a material, a variety of different fire tests can be carried out. Non-combustibility test (EN ISO 1182), Heat of combustion test (EN ISO 1716), Single burning item test (EN 13823), and Single-flame source test (EN ISO 11925-2) are some of the available fire-reaction tests.

2.2. Solar Cell Technology

Solar cell technology is by far the most researched sustainable energy-harvesting technique. It has seen a myriad of advancements throughout the years in terms of materials and layout composition, technically referred to by generations. First generation solar cells refer to the earliest form of solar cells made of crystalline silicon (c-Si) wafers that are being used to this day with an efficiency as high as 22 to 25% [43]. Their bulkiness, however, heavily impacts their application, limiting it to merely large desolated areas and buildings' roofs. Thin-film or second-generation solar cells were developed as a result to allow for more flexible applications with comparative efficiencies using less energy-intensive production methods. Copper indium gallium selenide (CIGS), cadmium telluride (CdTe), and amorphous silicon (a-Si) are the typical thin-film types used. Third generation solar cells, commonly termed

emerging photovoltaics, share the flexibility and low environmental impact properties with their predecessor, and they include organic photovoltaics (OPV), dye-sensitized solar cells (DSSC), multijunction solar cells (MJSC), and perovskite solar cells (PSC). Additionally, they are faster to manufacture as well as install and can be printed in various patterns and colors. MJSCs currently hold the highest efficiencies recorded at the research level of higher than 45%.

(a)   **(b)**   **(c)**   **(d)**
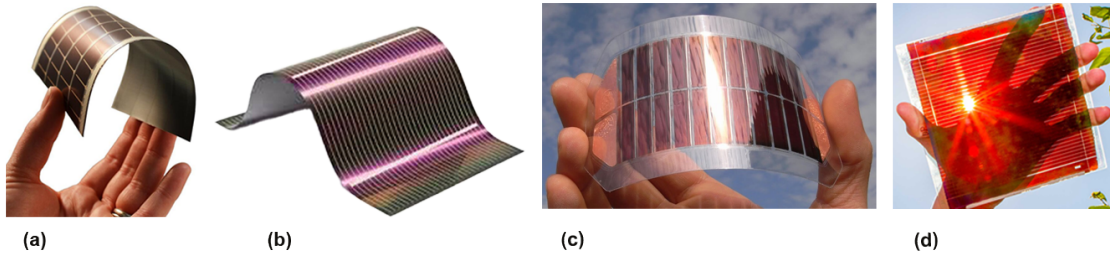
Figure 2.41: Thin film solar cells: **(a)** Amorphous silicon [58], **(b)** CIGS [13]; Third generation solar cells: **(c)** Organic photovoltaics [39], **(d)** Perovskite solar cells [60]
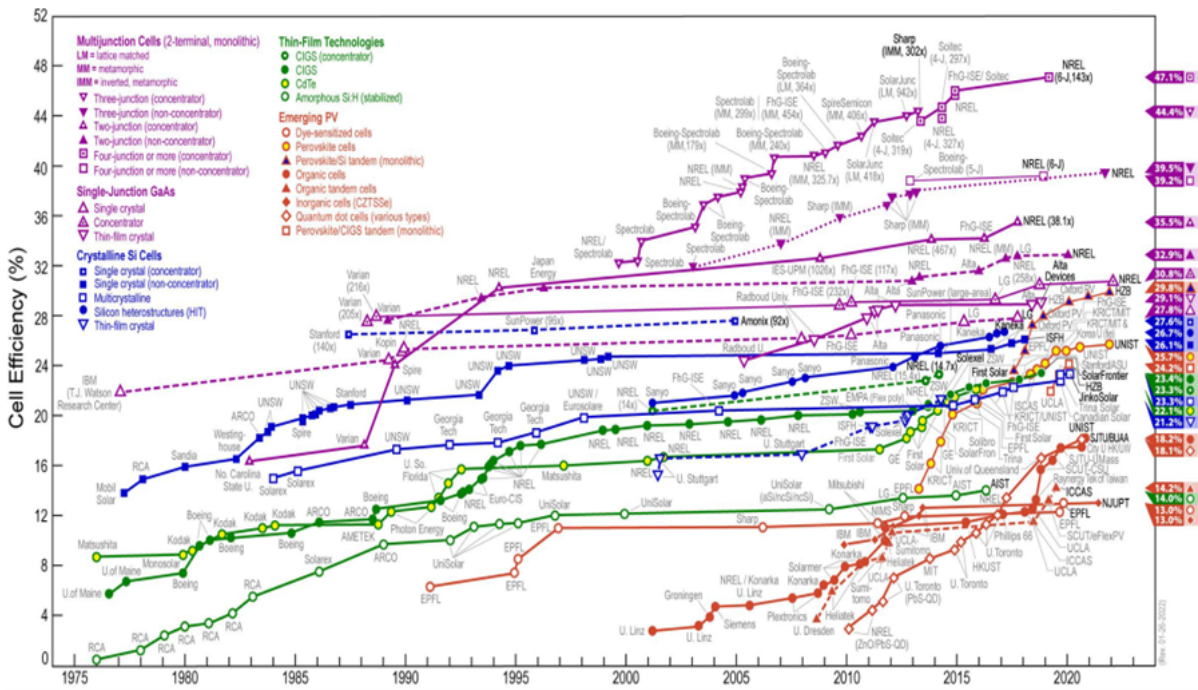
Figure 2.42: Best PV cell efficiencies achieved through research from 1976 to 2022. Multijunction cells are represented in purple, Crystalline Silicon cells in blue, Thin-film cells in green, and Emerging PVs in red. [8]

2.2.1. Photovoltaics

Photovoltaics is formally defined as the branch of technology concerned with the production of electric current at the junction of two substances. The smallest photovoltaic unit is the cell which is connected in series and/or parallel to produce larger circuits yielding higher current, voltages, and power. Different terminologies are thus used to distinguish the hierarchical levels of solar cell circuitry namely, modules, panels, and arrays (**Figure 2.43**). The photovoltaic modules consist of PV cell circuits sealed in an environmentally protective laminate known as the encapsulant, and are the fundamental building blocks of PV systems. Photovoltaic panels are composed of one or more PV modules assembled as a pre-wired, field-installable unit. When several PV panels are connected, a photovoltaic array is formed which is the complete power-generating unit.
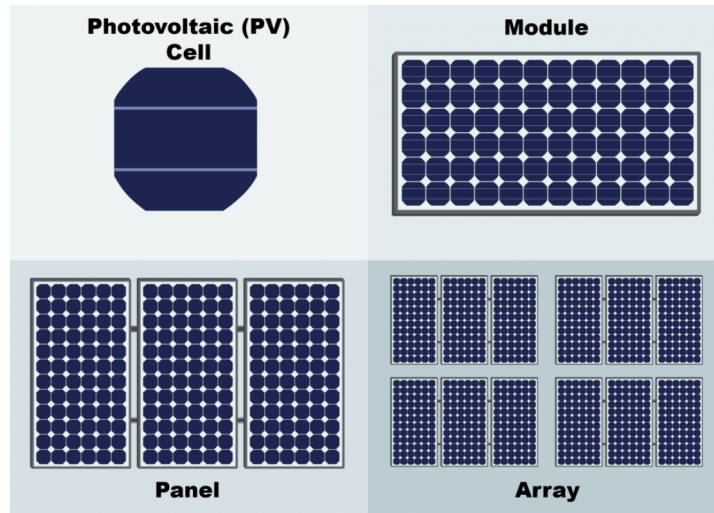
Figure 2.43: Photovoltaic cell, module, panel, and array. [12]

PV modules and arrays are typically rated in terms of their maximum DC power output (in watts) under Standard Testing Conditions (STC); these conditions are defined by an incident solar irradiance level of 1000 W/m2, operating temperature of 25°C, and an air mass of 1.5 spectral distribution. Since these conditions are not the actual field conditions, the actual performance is usually 85 to 90 percent of the STC rating.

2.2.2. PV module parameters

A set of parameters are commonly used to characterize the photovoltaic behavior at both the solar cell and module levels [43][45]:

I. Open circuit voltage (V_{OC}): represents the maximum voltage of a solar cell under a specific illumination level.

II. Short circuit current (I_{SC}): represents the maximum current delivered by a cell under a specific illumination level.

III. Fill factor (FF): is the ratio between maximum power and the product of (I_{SC}) and (V_{OC}) used to indicate the output quality of a cell;

$$FF = \frac{P_{MPP}}{V_{oc} \cdot I_{SC}} = \frac{V_{MPP} \cdot I_{MPP}}{V_{oc} \cdot I_{SC}} \tag{2.1}$$

IV. Efficiency (η): is the ratio of the electrical energy output to the total input sunlight energy and also serves as an indication of a cell's performance;

$$\eta = \frac{V_{MPP} \cdot I_{MPP}}{P_{in}} \tag{2.2}$$

For modules, it is necessary to distinguish between *aperture area efficiency* and *module efficiency*. The former is also known as the active area efficiency which pertains to the area of the PV-active parts only, whereas the latter relates to the total area including the aperture area and the dead areas, such as at the edges or areas with interconnections.

Ideally, the efficiency and fill factor at both module and cell levels should be the same; however, this is not the case in real life. The interconnects connecting the cells to each other induce resistive losses. Additionally, individual cells exhibit a mismatch caused by inhomogeneities occurring during the production process. The result is a loss in performance translated into a loss of efficiency at the module level compared to ideally matching interconnected cells.

Illuminated solar cell behavior is characterized by a so-called I-V curve, where the relationship between current and voltage is depicted. The graph is confined by two points corresponding to the

(V_{OC}) and (I_{SC}) values, and so the maximum power, calculated by the relationship $P = I \times V$, is indicated by the point along the curve with the maximum current (I_{mpp}) and voltage (V_{mpp}). This is known as the maximum power point (MPP). The I-V curve is dependent on the module temperature and the irradiance, or power received by the solar cell area. An increase in solar cell temperature shifts the I-V graph, decreasing the open circuit voltage while slightly increasing the short circuit current. This in turn results in an efficiency decrease. Higher irradiance, on the other hand, increases the power output of the cell and hence, the efficiency. Due to the dependency of the MPP on the ambient conditions, solar cell modules in field applications undergo continuous tracking of changes in the I-V curve to identify the MPP and use it as the operating point for maximum efficiency; a process which is termed maximum power point tracking, or MPPT.
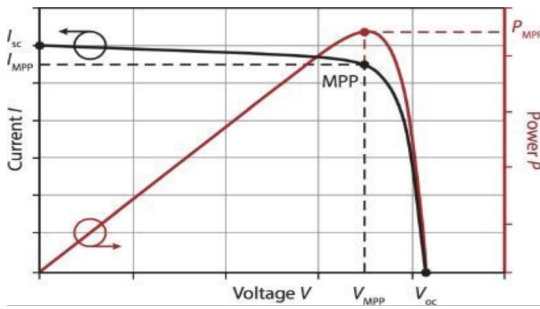
Figure 2.44: A generic I-V curve and the associated P-V curve. [51]
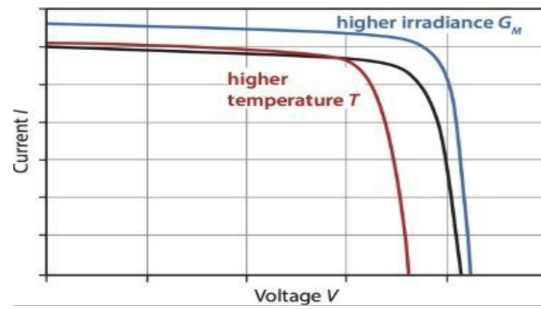
Figure 2.45: Effect of temperature and irradiance increase on I-V curve. [51]

2.2.3. Serial & Parallel Connections

Individual solar cells can be connected in either a series connection, also known as string, or a parallel connection to form a solar module. In a series connection, the voltages of the single cells add up yet the total string's current remains that of the single cell. The current of the whole string is therefore dictated by the cell that delivers the smallest current. A parallel connection does the exact opposite in which the total module's voltage is equal to the single cell's voltage, while the module's current becomes the added value of all the single cell's currents. Depending on the connection type, the I-V curve behaves differently.
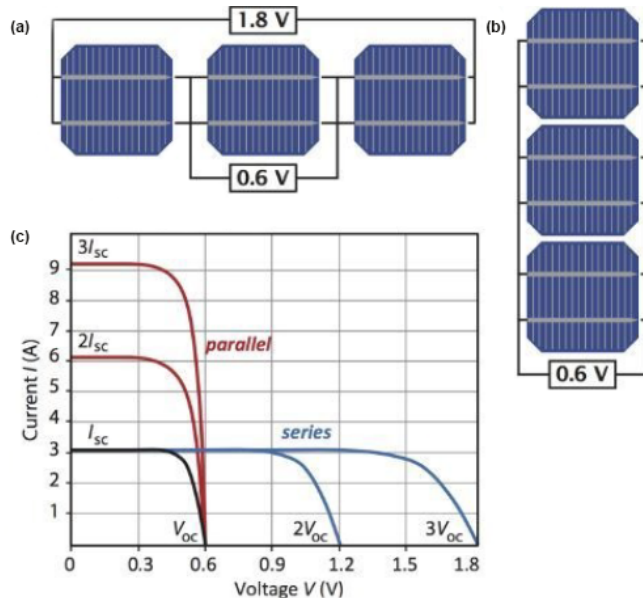
Figure 2.46: (a) Serial connection, **(b)** Parallel connection, **(c)** I-V curves for different connections. [51]

Multiple strings of series-connected solar cells are often connected in parallel to increase the energy yield. In theory, several parallel-connected cells can also be connected in series; however, it is not

performed in reality because as the current increases by the parallel behavior effect, the resistivity losses in the cables increase as well. As a result, modern PV modules often contain 60, 72, or 96 solar cells connected in series to achieve high voltages with minimal resistance [51].

2.2.4. Bypass Diodes

When PV modules are used in real-life conditions, partial shading of cells might occur from neighboring objects. Any partial shading of solar cells in a module is detrimental to the output. The performance of a module with a series connection for instance, becomes compromised once a single solar cell is shaded since in a string, the current is limited by the cell with the lowest current. That is why PV modules are integrated with bypass diodes which conduct current via an alternative route around a shaded cell, and by doing so, the module can still produce current equal to that in the unshaded cell scenario [51]. Groups of cells in a module normally share one diode instead of having a diode per cell.
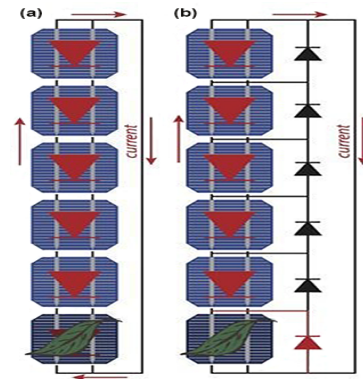
Figure 2.47: (a) A string of six solar cells of which one is partially shaded; **(b)** effect of bypass diodes on circuitry. [51]

2.3. Integration Techniques

The term "integration" is used in textile architecture when solar cells are involved to refer to the process where the solar cells merge with the membrane/foil material. Three main integration modes are possible [27]; the first is mechanical integration in which flexible photovoltaics (FPVs) are welded to the textile at the edges. Lamination is another strategy performed by applying adhesive with sufficient bonding strength in between the PV module's substrate[1] and the textile. The last and most promising technique is through the direct printing of PV cells onto the textile. In this case, the textile itself becomes the substrate for the solar cells hence, printing is the least invasive as well as the most versatile measure compared to mechanical integration and lamination.
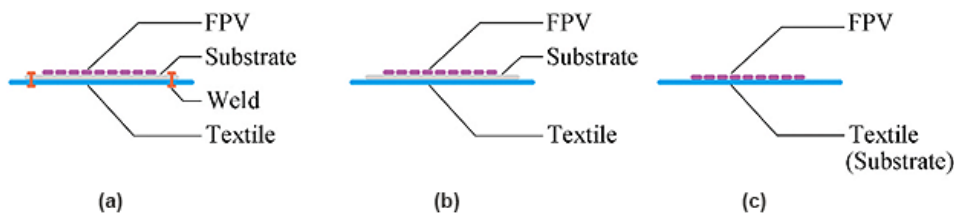
Figure 2.48: Flexible photovoltaics (FPV) to textile integration methods: **(a)** mechanical integration, **(b)** lamination, **(c)** direct printing. [27]

Several realized projects have employed these techniques using thin-film and OPV technologies. Buildings, greenhouses, and carports were all equipped with membrane-integrated photovoltaics to harness solar energy while providing shade or even structural support (**Table 2.5**).

---

[1]Underlying material which provides the surface onto which the active material is deposited or inscribed.

Table 2.5: An overview of projects with textiles integrated with flexible photovoltaics [27].

Year	Project name	Building type	Location	Membrane	FPV	Envelope type	Integration mode	Membrane transparency	PV transparency
1998	Under the Sun	Pavilion	New York, USA	PVC	a-Si PV	Canopy one-layer fabric	Mechanical integration	Translucent	Opaque
1999		Industry building	Jena, Germany	ETFE	c-Si PV	Roof one-layer fabric	Mechanical integration	Opaque	Opaque
2007	Hightex Office	Office building	Rimsting, Germany	ETFE	a-Si PV	Roof two-layer cushion	Mechanical integration	Transparent	Opaque
2010	Breathing Organism	Pavilion	Shangai, China	ETFE	a-Si PV	Envelope two-layer cushion		Translucent	Opaque
2010		Greenhouse	Shimane, Japan	Polyolefin	a-Si PV	Roof one-layer foil	Mechanical integration	Transparent	Opaque
2011	AWM carport	Carport	Munich, German	ETFE	a-Si PV	Roof three-layer cushion	Mechanical integration	Transparent	Opaque
2012	Staten Island Children's Museum	Sunshade	New York, USA	PTFE	c-Si PV	Canopy one-layer fabric		Opaque	Opaque
2013	Soft House	Residential building	Hamburg, Germany	PTFE	OPV	Roof one-layer fabric	Mechanical integration	Translucent	Opaque
2014	Pure Tension Pavilion	Carport	Milan, Italy	Vinyl encapsulated polyester	CIGS	Skin mesh	Mechanical integration	Translucent	Opaque
2015	Fields of Ideas	Pavilion	Milan, Italy	ETFE	OPV	Canopy one-layer foil	Printing	Transparent	Translucent
2015	Masterpiece	Carport	MountainView, USA			Canopy, fabric	Lamination	Opaque	Opaque
2016		Bridge	Tallahassee, USA	Polyethylene		Canopy one-layer fabric		Opaque	Opaque
2017		Greenhouse	Thessaloniki, Greece	Low density polyethylene	OPV	Roof one-layer foil	Mechanical integration	Transparent	Translucent
2018		Greenhouse		Polyethylene	OPV	Roof one-layer foil	Mechanical integration	Transparent	Translucent
2018	Merck KGaA Building	Building retrofit	Darmstadt, German	ETFE	OPV	Façade one-layer foil	Lamination	Translucent	Opaque
2019		Bus station	Tilburg, Netherlands	ETFE		Roof one-layer foil		Translucent	Opaque

Figure 2.49: (a) Techstyle Haus - Mechanical integration [52], **(b)** Merck KGaA building - Lamination [57][27], **(c)** Germaon pavilion at Milan EXPO 2015 - Direct printing [38].

Integration is interpreted differently for solar textiles: true integration is sought and is defined as the uncompromising combination of the two components without the textile hindering the solar cell performance nor the solar cell limiting the textile mechanical properties or flexibility, a product of which is called a solar textile. Similar to the membranes in architectural textiles, printing of solar cells onto the fabric is one possibility. Imbibing the solar cell's active material into the textile matrix is another, yet the most unique integration mode is through the weaving process itself by using solar cell fiber, yarn, or tape [24]. Laminating or stitching PV cells on top of fabrics is an obvious possibility but is disregarded due to its impact on the aesthetic, physical, and mechanical properties of the fabric.

Printing and/or imbibing PV material on textiles is a promising approach given the relative ease of creating designs and the possible manufacturing efficiency nevertheless, it places limitations on the type of textile and solar cells used due to the high temperature needed in the process. More importantly, it still needs to overcome operational efficiency and stability challenges. Weaving of PV fibers/yarns into fabrics presents a practical solution in terms of manufacturing and is especially useful in maintaining the fabric's flexibility and mechanics. It does however lack operational stability as the PV material is not yet capable of handling stresses from abrasion or stretching. Additionally, creating a correct and error-free contacting to the positive and negative terminals becomes challenging. Even though the tape approach could seem inferior to the fiber/yarn approach from the mechanical stability and flexibility standpoint, it provides better control over the position of the terminals. Solar cell tapes could also be encapsulated by a barrier foil for enhanced operational stability. Consequently, amongst the three methods, weaving of solar cell tapes is the most feasible and readily available mode of integration for creating solar textiles [24] [29].

3

Weave Analysis

3.1. Weave Structures

Woven structures consist of two sets of yarns namely, warp and weft that are interlaced orthogonally in a recurring pattern. Warp yarns move along the length and weft yarns along the width of the fabric. Upon the microscopic examination of the fabric, the weave pattern can be identified. If the side view of a warp yarn is examined, it is observed to ride on top of a weft yarn at certain locations and fall below the weft at others in a continuous fashion across the fabric. The weave structure is thus represented by a checkered schematic of rows and columns to indicate this behavior, as seen in **Figure 3.1**.
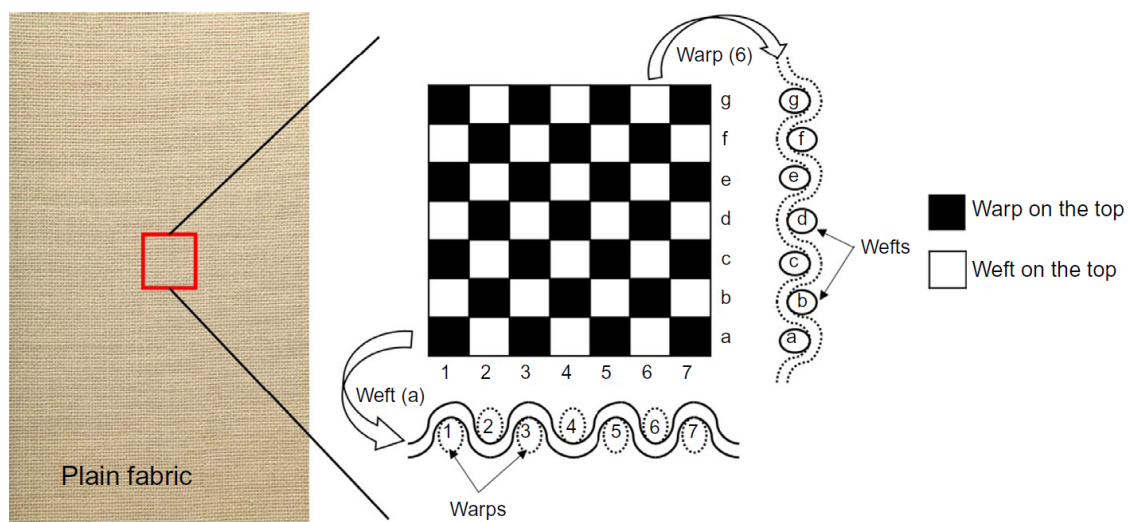
Figure 3.1: Plain weave representative scheme. [26]

Each individual row and column represents a single weft and warp, respectively. It is often the case where the pattern is represented by its weave repeat and that is the maximum possible frequency of interlacements to create a fabric structure, or in other words, the smallest repeating unit in a fabric. Woven fabrics can have almost infinite possibilities of interlacement patterns including the most generic formats: plain, twill, and satin weaves.
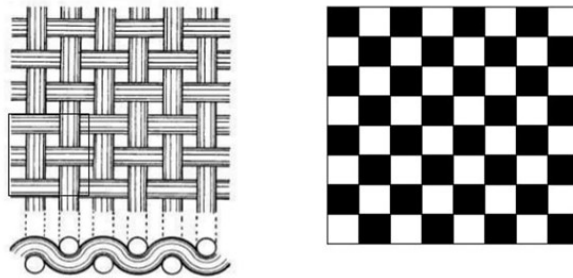
3.1.1. Plain weave

Figure 3.2: Plain weave structure.

Plain weaves possess the simplest yarn inerlacement, yet they exhibit a strong and stable fabric due their high interlacing frequency. In this weave, every weft yarn goes under and over the warp yarns across the width of the fabric. Several variations of the plain weave are possible such as the warp rib, weft rib, matt, and ripstop weaves.

Warp/Weft rib weave

Warp ribs are a modified form of plain weaves where 1/1 interlacements appear only in the weft/filling direction. This modified interlacement results in the formation of cords, ridges, or texture across the warp direction of the fabric due to the grouping of the filling yarns. The first warp yarn follows the weave formula, while the second warp yarn is in the opposite direction of the first one. In its regular format, warp rib structure is obtained by a weave formula where the numerator and denominator are equal, like in 2/2 or 3/3 warp ribs. Irregular warp rib, on the other hand, is one where the numerator is different from the denominator. Weft ribs are the inverse of the warp ribs such that warp and weft directions are interchanged.

Warp rib
Unit repeat

Regular 2/2 warp rib

Irregular 2/3 warp rib

Weft rib
Unit repeat

Regular 2/2 weft rib

Irregular 2/3 weft rib
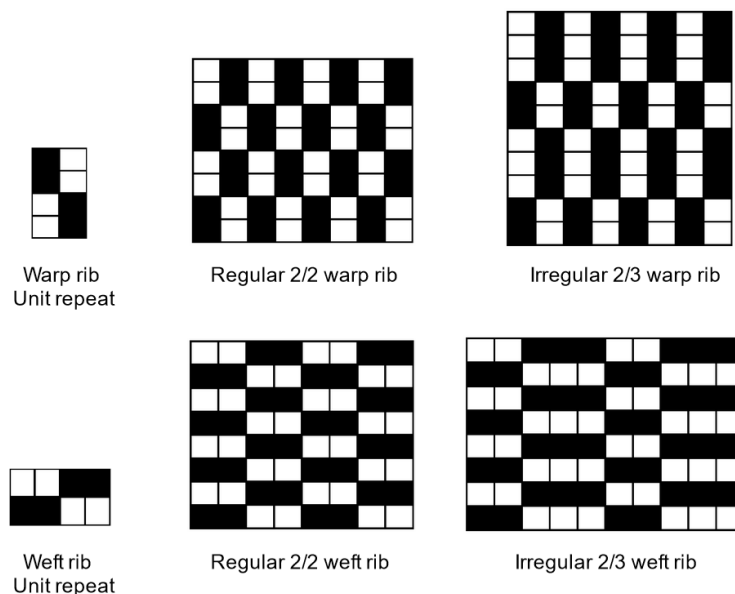
Figure 3.3: Plain rib weaves

Matt weave

This type of weave is constructed by extending the plain weave in warp and weft directions at the same time so that two or more yarns work alike in both directions. The same size of squares appear on both sides of the fabric showing the same number of warp and weft yarns on front and back of the fabric. This is not the case for irregular types of the matt weaves. Fabrics constructed from this weave

are flexible with a looser construction than traditional plain weave yet they are less durable. A matt weave is also known as basket, hopsack, or panama weave.
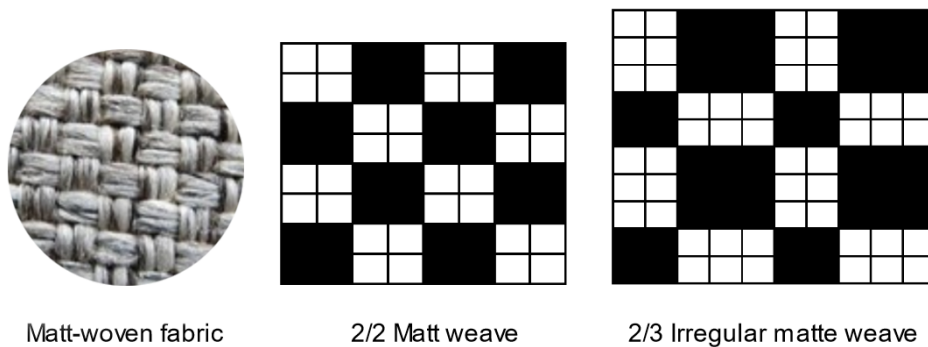

Matt-woven fabric   2/2 Matt weave   2/3 Irregular matte weave

Figure 3.4: Matt weave structures

Ripstop weave

This is a plain weave in which a coarser and stronger extra thread (ripstop yarn) is incorporated as reinforcement at regular intervals. The ripstop yarn along the weft and warp gives the look of a checkered pattern on the fabric and increases the strength as well as the resistance of the fabric against ripping/tearing. The same ripstop effect can also be achieved by weaving 2 or 3 yarns at the same time to stop the spreading of the rupture in the fabric. It is used more commonly in light, highly durable fabric such as hot air balloons and parachutes, or in heavy, highly durable fabrics such as tactical clothing and tent structures.

Typical fabric weave   Ripstop fabric weave
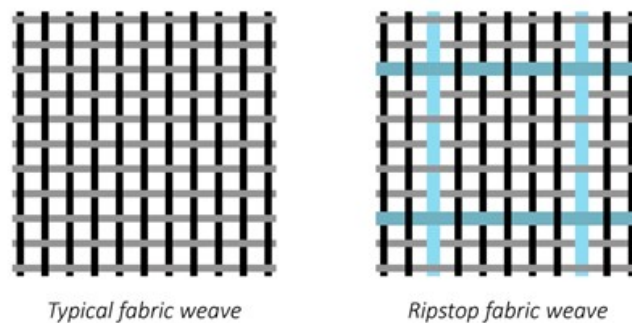
Figure 3.5: Ripstop weave structure [44]

3.1.2. Twill weave

Twill is one of the basic weave structures in which the weft yarns are woven over and under two or more warp yarns, producing a characteristic diagonal pattern. The direction of the diagonal lines on the surface of the cloth generally describes the type of the twill. When the diagonal lines are running upward to the right, they are "Z twill" and when they run in the opposite direction, they are "S twill". Twill weaves can be produced in a wide variety of forms, and so they could be classified broadly into the following categories [35]:

   i. Ordinary or continuous twills
  ii. Zigzag/wave/pointed twill
 iii. Rearranged/transposed twill
  iv. Combination twill
   v. Broken twill
  vi. Figured or other related twills

Their angle and definition can be varied by changing the yarn spacing and/or the linear density of the warp and weft yarns. For any construction, twills will have longer floats, fewer intersections, and a

more open construction than a plain weave fabric with the same cloth elements. The smallest repeat of a twill weave consists of 3 ends & 3 picks (i.e., 3 warp yarns & 3 weft yarns). There is no theoretical upper limit to the size of twill weaves, but the need to produce stable fabrics with floats of reasonable length imposes practical limits. Twill weaves have become symbols for carbon fiber fabrics used in engineering composite materials.

Balanced 2/2 Twill   1/3 Weft faced (Z twill)   3/1 Warp faced (S twill)
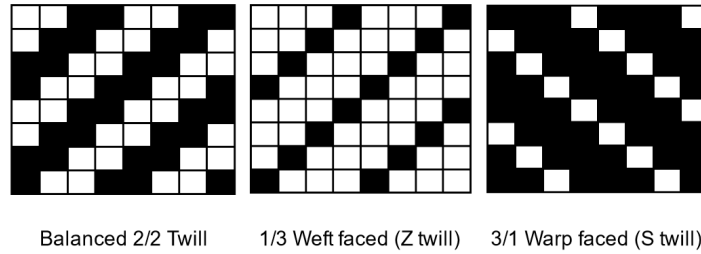
Figure 3.6: Ordinary Twill Weaves.

Pointed Twill

Zigzag or pointed twill weave constructions are formed by reversing the twill line at specific intervals to combine Z-twills and S-twills in a single design. The reversing of the twill may be done horizontally or vertically.

(a) 2/2 Horizontal Pointed Twill

(b) 2/2 Vertical Pointed Twill
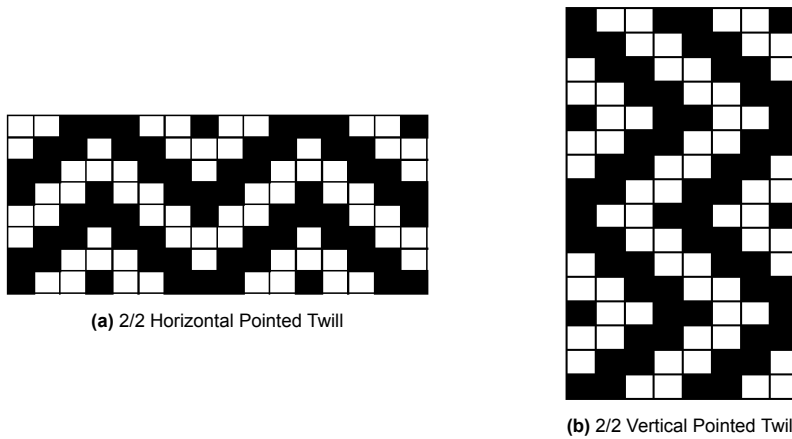
Figure 3.7: Pointed Twill Weaves.

Transposed Twill

In this version of a twill weave, only rearrangement of the original twill weave is done to get more aesthetic designs. The transposition interrupts the basic twill line at specific intervals according to the break unit (**Figure 3.8**). The process of transposition is much similar to the breaking of the twill. The weave repeats on the same number of ends as the original weave if break unit is a factor of the original weave. Transposed twills are also referred to as rearranged twills.

4/4 Transposed
twill (break unit of 4)   4/4 Transposed twill

Figure 3.8: Transposed Twill Weaves.

Combination Twill

For this twill structure, a number of weaves are grouped in a single end, creating a combined visual effect of these weaves. The repeat of the combination twill will be equal to the aggregate of constituting weaves. For example, the repeat of a 2/1+2/2 will be on 7 ends and 7 picks.

Figure 3.9: Weave repeat of 2/1+2/2 Combination Twill.

Broken Twill

This twill type is achieved by breaking the regular twill at specific intervals. A variety of distinctive designs can be drawn by using this weave. T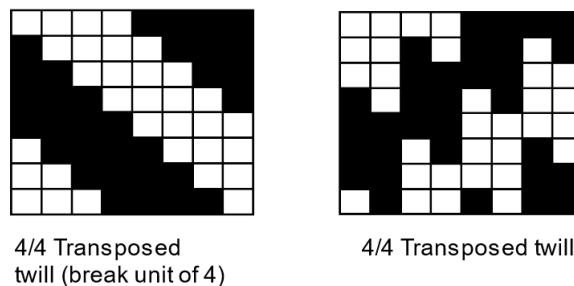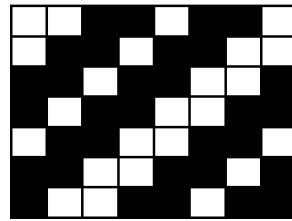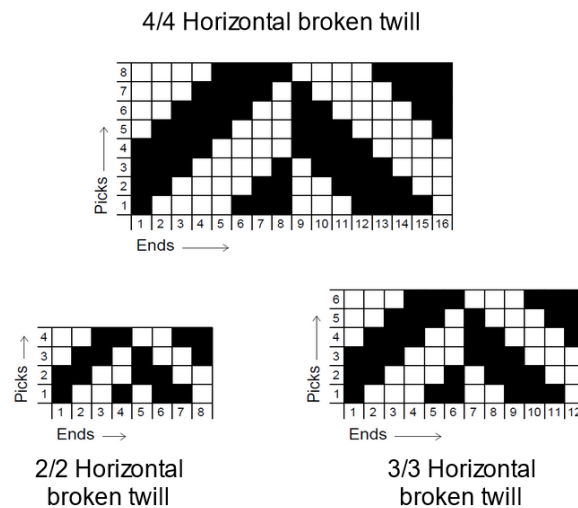he regular twill can be broken in a number of ways, but the most simple and common way is to stop the regular twill and reverse the next ends according to the break unit.

4/4 Horizontal broken twill

2/2 Horizontal
broken twill

3/3 Horizontal
broken twill

Figure 3.10: Broken Twill Weaves.

Related Twill weaves

Diamond and herringbone twill weaves are two distinctive twill figures that can be created as well, however, they are mainly variations of other twill structures. The diamond weave is achieved by combining horizontal and vertical zigzag/pointed twills, whereas the herringbone weave is based on a broken twill form.

3.1.3. Satin weave

Satin/sateen is the final basic weave that does not have any regular pattern like twill. The surface of the fabric is either warp or weft-faced. Satin is warp-faced which means that all the surface of the fabric will show the warp yarns except for the one yarn interlacement with other series of yarn. If it is weft-faced, then it will be known as sateen and will mostly show the weft yarns. The single interlacement of warp and weft yarns in a single repeating unit is a trait unique to this weave structure rendering it the basic weave with the least interlacement. As a result, fabrics with this weave demonstrate a loose structure.

The satin or sateen weaves that do not follow any specific move number are termed as irregular satin and sateen weaves. Four and six-yarns satin/sateen do not follow any specific move number and

so are labelled irregular. These are the only irregular satin or sateen weaves that are constructed using a combination of move numbers.

Satin (left) and sateen (right) weaves, 5 ends   Irregular sateen with 4 ends (left) and 6 ends (right)
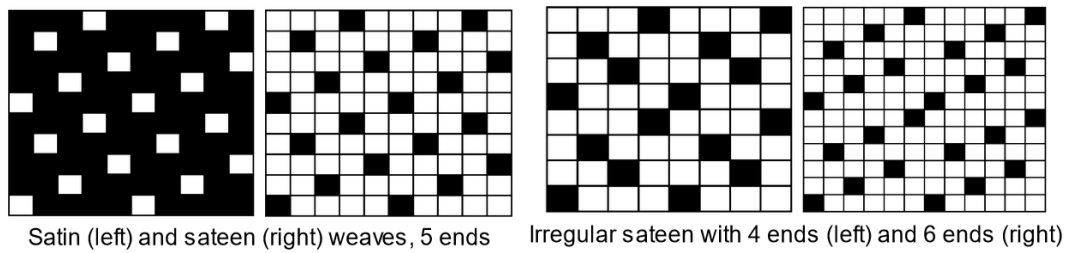
Figure 3.11: Satin & Sateen Weaves.

3.1.4. Special weaves

Some weaves are used occasionally either on their own or as part of a basic weave to achieve specific fabric effects and properties; honey comb and huck-a-back are weaves typically used to create moisture absorbing textiles. Leno and mock leno weaves, on the other hand, are used to convey a perforated appearance. When a weave does not have a specific pattern, it is labeled crepe weave and is usually employed for a rough appearance.

(a) Huck a back weave

(b) Mock leno weave

(c) Honeycomb weave

(d) Honeycomb fabric showing three-dimensional effect
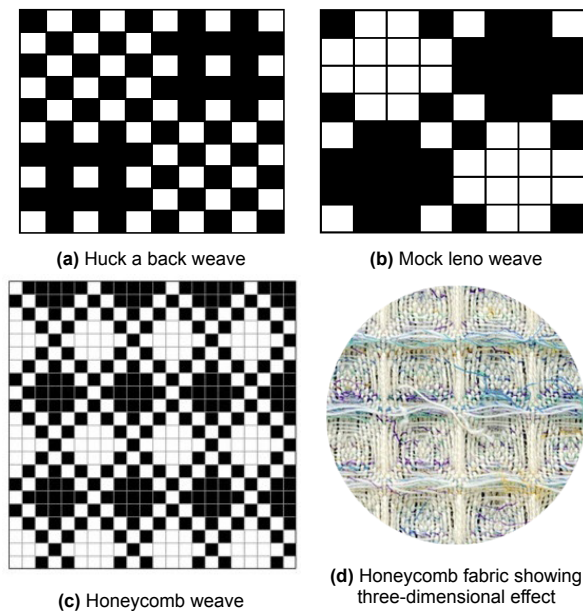
Figure 3.12: Special weaves schematics.

Leno weave

Leno weaves require leno weaving which is the process in which the warp yarns are twisted around one another locking the weft yarns in place and preventing yarn slippage. This weave type is used where a relatively low number of yarns are involved, resulting in a sheer yet durable fabric that is permeable to air and light. Leno weaves are normally used in a fabric in conjunction with other weave structures because if used alone, their openness could not produce an effective composite component; therefore, they are used in open-meshed fabrics with low yarn count to improve the fabric's stability.
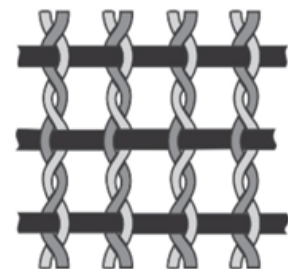
Figure 3.13: Leno/gauze weave [46]

3.2. Structural Parameters

In textile engineering, a number of technical jargon is used to describe the structure of a fabric. The following structural parameters are the most important elements used to design and shape fabric [26]:

i. **Yarn count:** represents the fineness or coarseness of a yarn, usually expressed in Tex (weight of 1000 m of yarn in gram).

ii. **Yarn density/fabric count:** indicates the number of warp or weft yarns per unit length (i.e., warps/cm or wefts/inch). It can also be calculated by either multiplying or adding the yarn densities in both directions as indicated in **Figure 3.14**.

iii. **Areal density:** is the weight of one square meter fabric in grams, expressed in g/m^2.

iv. **Weave repeat:** a complete unit of the weave, or alternatively, the minimum number of warp-and-weft yarns for a given weave.

v. **Weave factor:** is a number that accounts for the total number of interlacements of warp and weft in a given repeat. It is expressed as

$$M = E/I$$

where E is the number of yarns per repeat, and I is the number of intersections per repeat of the cross-yarn.

vi. **Float:** indicates the length of floating yarns on the surface of fabric between two consecutive intersection points. It is counted by the number of consecutive black boxes or white boxes in a weave repeat.

vii. **Crimp:** by virtue of interlacing, both warp-and-weft yarns assume a wavy path; hence, the length of the fabric is smaller than the straight length of the yarn. The crimp thus represents the degree of yarn waviness in the fabric which is expressed by:

$$\text{Crimp}(c) = \frac{\text{Length of yarn - length of fabric}}{\text{length of fabric}} \tag{3.1}$$

viii. **Fabric cover/cover factor:** is defined as the fraction of total fabric area covered by the component yarns. The weft or warp cover is also calculated to indicate their effect individually on the overall fabric cover.

ix. **Fabric specific volume:** is the ratio between fabric thickness (cm) and fabric mass (g/cm2).

x. **Fabric packing factor:** is the ratio between the specific volume of fiber (g/cm3) and the specific volume of the fabric (g/cm3). It indicates the presence of void or air inside the fabric.
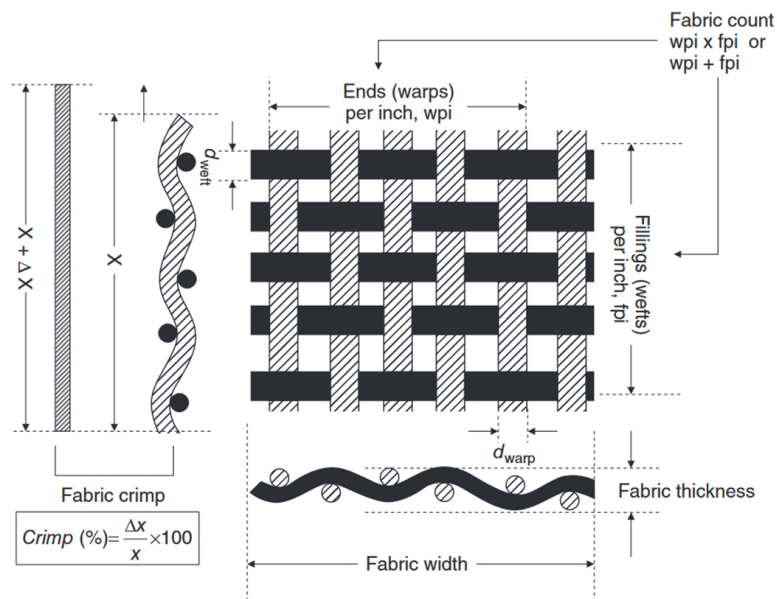
Figure 3.14: Woven fabric basic specifications. [15]

The aforementioned structural elements are convenient in describing and quantifying important fabric properties. The fabric cover, for instance, indicates the availability of free gaps within the fabric which determines multiple properties of the woven fabric such as air and water vapor permeability, UV light protection, and transparency. Adjusting the cover factor parameter through the yarn density and fabric count can then result in different fabric performances suited for a desired application. Similarly, the fabric packing factor indicates the fabric's porosity which is the volume within the fabric occupied by air and as a result, both the thermal conductivity and the liquid transmission properties of the fabric can be manipulated. Furthermore, the fabric crimp indicates its tendency to extend. Since a plain weave possesses the maximum intersection points amongst its counterparts, it exhibits higher extensibility. A fabric's shearing properties on the other hand is influenced by the number of floats in the structure.

Many of the discussed factors are also used by geometrical and empirical models for predicting the mechanical properties of woven textiles [32].

## 3.3. Mechanical Properties of Woven Fabric

Tensile, shear, tearing, bending, and buckling are some of the most important mechanical properties that determine the fabric performances in several applications. As discussed in section 2.1.1, fiber/yarn material primarily influences the mechanical properties of the fabric. For fibers, their morphology, including orientations, crystallinity, and amorphousness, is the key determinant of their strength, stiffness, and extensibility. Yarn properties, however, are dependant on the twist, fiber length, and fiber orientation which in turn, affects the fabric properties.

In this section, the most critical mechanical behaviours of fabrics from the textile architecture perspective will be addressed and the contributing factors discussed.

3.3.1. Tensile behavior

Woven fabrics are anisotropic and asymmetrical structures with different properties in the two main orthogonal directions. Their tensile behavior is evaluated via tests that measure the stress, strain, and elastic modulus. The stress value quantifies the resistance of the material to external deformation, expressed as the ratio of the applied force to the cross-sectional area of the specimen perpendicular to the force while the strain indicates the amount of deformation induced by the material. The modulus is the ratio of the stress to the strain when the deformation is below the elastic limit. A typical tensile behaviour trend is a nonlinear one with a varying modulus that changes with the extension of the fabric. **Figure 3.15** shows the generalized load-elongation curve of a woven fabric. Three distinct regions can be identified;

1. Initial region (OA) where the extension only involves the inter fiber friction effect.
2. The decrimping region (AB) where the crimp in the yarn is diminished.
3. Region (BC) in which the yarn extends.
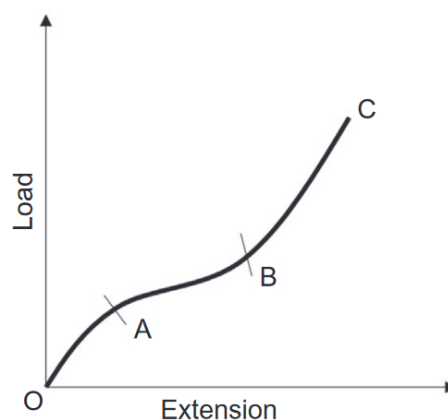
Figure 3.15: Load elongation behavior of woven fabric. [26]

A number of structural changes are also bound to happen under tensioning which may result in lower tensile strength. The fabric, for instance, could become jammed, causing local areas to wrinkle. Fibers may also slip through the engulfing yarn. In addition, crimp interchange might take place which is the contraction of the fabric occurring in the direction perpendicular to the applied tension causing the crimp to increase in the contraction direction and decrease in the stretching direction. The fabric jamming affects the crimp interchange during extension, so there is a possibility of reduction in the strength and extensibility if the jamming is found before crimp exchange.

Several structural parameters, such as yarn strength, yarn twist, weave, crimp, and cover, determine the tensile properties of the fabric [6]. The extent of yarn twist is inversely proportional to the fabric's extensibility such that a higher twist results is a loss of extensibility. Twisting additionally improves the fabric cover and so reduces the fabric's permeability. An increase in the yarn density improves the strength and durability of the fabric; however, it increases the elongation at break. On the other hand, the crimp decreases the strength of the fabric as well as the initial modulus (i.e., before actual yarn extension).

3.3.2. Shear behavior

Shear stress is defined as the component of the stress parallel to the cross-section of the material, whereas the shear strain refers to the amount of deformation perpendicular to the applied load. The shear stress to the shear strain ratio is defined as shear modulus. In woven textiles, shearing results in an angular deformation between warp and weft yarns and with further deformation, the angle reduces until the locking angle is reached (see **Figure 3.16**). The locking angle is identified as the smallest angle between the warp and weft yarns beyond which the fabric becomes unstable. Similar to tensile behavior, the shear behavior is also dependant on the loading direction of the testing specimen.

Shear stiffness can be linked to multiple fabric parameters. A high cover factor and yarn density are linked to an increased shear rigidity and shear hysteresis [6]. The free yarn length between two cross-over points (i.e., floats) also affects the shear behavior; the longer the float length, the lower the shear stiffness; this implies that the more intersections there are, the higher the shear rigidity. Plain weaves are thus stiffer against shear deformation than both twill and satin weaves.
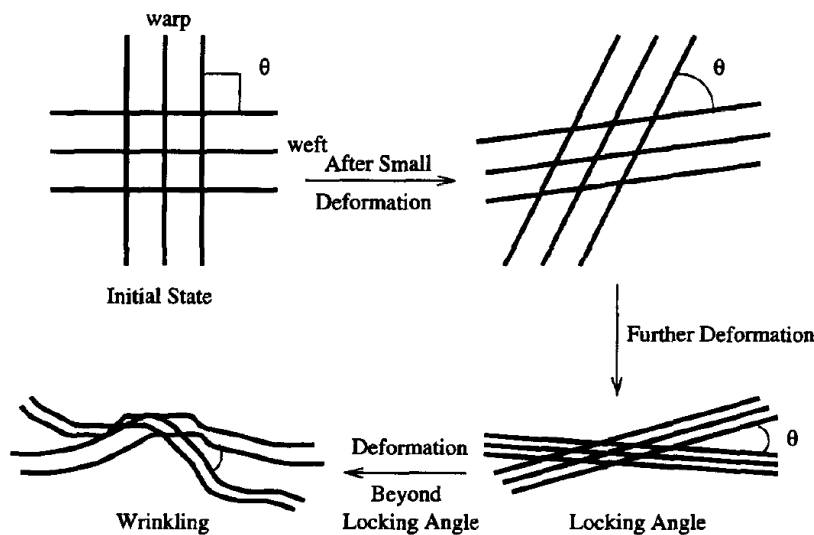
Figure 3.16: Shear deformation behavior. [42]

3.3.3. Tear behavior

Under certain circumstances, fabrics may rupture by tearing which is defined as the occurrence of local stress concentration on a single yarn leading to its breakage followed by a progressive failure of the adjacent yarns. The ability of a fabric to resist tear propagation is known as the tear strength, and that is highly linked to the yarn's ability to slide within a weave. Consequently, the higher the number

of yarn intersections, the lower the tear strength [4][16]. This is translated physically to the float's length parameter since the longer the yarn floats, the lesser the yarn intersections and the higher the tear strength. Moreover, the bundling of multiple yarns together increases the tear resistance, so for instance, a 2/2 matt weave has a higher tear strength than 1/1 plain weave. Yarn properties also play a major role; the higher the tensile strength of the yarns and the more slippery the yarns are, the more tear resistance a fabric possesses. This approach is seen in ripstop weaves applied to mitigate tear failure.

<div align="right">

4

</div>

Design Approach

4.1. Fabric Components & Design

To design a structural fabric capable of harnessing solar energy dictates the need for unconventional measures to guarantee safe outdoor performance. For conventional fabrics, the coating applied is the main protective ingredient responsible for water and UV-light resistance as well as fire retardancy. Given the dual-function nature of a solar fabric with PV modules integrated in the weave, the presence of a traditional coating becomes meaningless as it requires the covering of the entire fabric with the solar modules included. This would detrimentally affect the efficiency of the solar films and thus compromise the fabric's solar energy-harnessing function. Conventional coating made of polymeric compounds also takes a toll on the sustainability dimension of this endeavor [63]. Therefore, without a coating, the individual components of the fabric must provide the necessary water, fire, UV resistance, and the necessary shear stiffness at the seams as discussed in Chapter 2.

The proposed solar-fabric design is a 50 cm × 50 cm uncoated fabric module that is built up of three different yarn types with the addition of solar films; main yarns form the weave structure which in turn provides the fabric's strength. Transparent monofilament yarns are added to create floats on top of the solar cells intended to mechanically hold the solar film in place without negatively influencing the photovoltaic performance nor the fabric's strength. Additionally, conductive yarns are inserted to link the solar modules' contacts together, creating a parallel circuit. The solar films used are 45 cm × 2.5 cm organic photovoltaic modules capable of generating 170 mW of maximum power under standard testing conditions (**Figure 4.1**). This type of PV modules provides the flexibility needed to allow for curvatures iconic to tensile structures. For the different yarns, weather protection properties mentioned earlier are achieved through two strategies: either by using coated yarns to construct the weave or by using uncoated yarns made of a material with inherent weather-proof properties. For the OPV modules, however, a PET (Polyethylene Terephthalate) encapsulation layer is the component responsible for these properties.

Figure 4.1: Organic solar module produced by ASCA.

The presence of different components with different mechanical properties within a weave poses several structural challenges since the fabric becomes as strong as its weakest link. Further yarn analysis becomes necessary to obtain close mechanical properties across the yarns to avoid creating a weak link and ultimately achieve the required strength. **Table 4.1** presents a comparison between different commercial yarn types; breaking load, linear density (or yarn count), and elongation at failure are the mechanical criteria governing the choice of all three yarns. For conductive yarns, however, electrical resistivity is an additional property that needs to be considered to assess the extent of conductivity. A

typically favorable structural behavior is one where the tensile strength is high yet with a low elongation at failure (**Figure 4.3**) to ensure appropriate strength and stiffness behaviors for the final fabric. Just as the large discrepancies in yarn strengths may result in weaker fabric, the overall layout of the fabric directly influences the fabric's strength; hence, the following influencing parameters can be identified within the layout:

1. Weave Pattern
2. Solar module dimensions
3. Spacing between OPV module
4. Solar module insertion direction
5. Number of floats
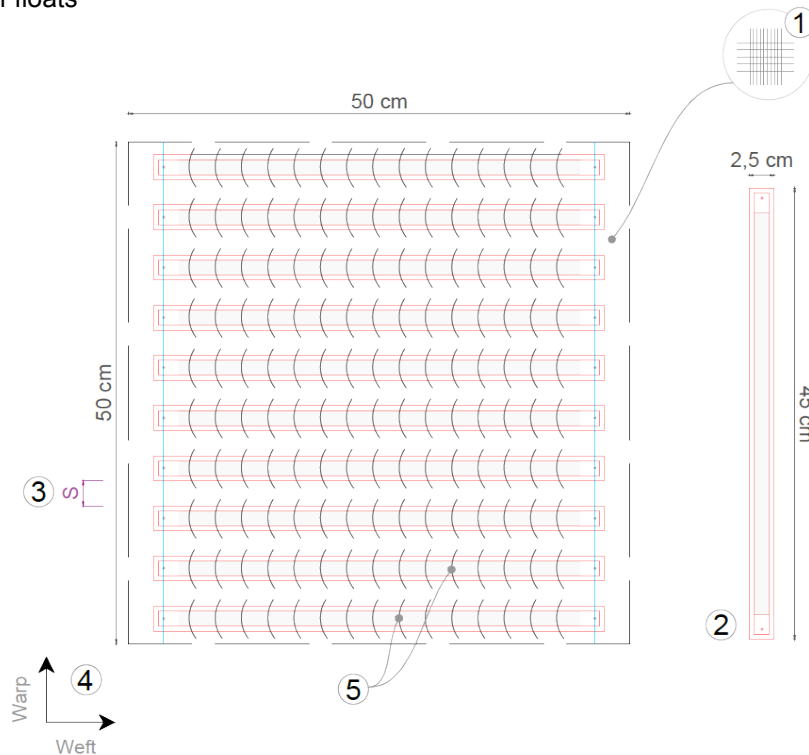
Figure 4.2: Fabric module layout with design parameters.

Not only do these parameters impact the strength and stiffness of the fabric, but also influence the energy efficiency of the photovoltaic cells, complicating the design decisioning process. So, for instance, a larger number of floats would mean an increase in fabric stability at the solar cell weave sections, but this would also implicate a reduction in efficiency due to the larger area covering of the solar cells or even a low fabric strength in case low stiffness monofilaments are used. Consequently, design decisions will have to reach a common ground so as not to compromise any of the desired fabric functions. This is the case for the weave pattern and the solar film insertion direction parameters for which an assessment and a feasibility study will be performed, respectively. The remaining design parameters, however, were controlled more by the weaving process, availability of material, final fabric objectives, or a combination of these factors; the OPV module size was dictated for the solar cell dimensions parameter mainly due to availability, but this size also guarantees it fits within the loom. The spacing between OPV modules will then have to be 2.5 cm in order to attain the 50% fabric to solar-module area ratio objective. As for the number of floats, it was decided to apply them alternatively (i.e., half of the yarns along the floats direction) as a starting point which will be verified by testing.

Table 4.1: Compilation of yarn properties from different manufacturers.

	Yarn Name	Core Material	Coating Material	Linear density (dtex)	Breaking load (cN)	Tenacity (cN/dtex)	Elongation at failure %
CoatYarn	TPU Evolution 01- 1300 dtex Type 64	PES	TPU high abrasion	1300	1770.6	1.36	12.55
	TPU Evolution 01-930 dtex	PES	TPU	930	1259.6	1.35	11.11
SwicoFil	SwicoFil PET	PET HT	—	20-6600	8400	up to 8.4	13 to 24
	SwicoStop	PET HT FR	—			6.3	N/A
Recytex	PUR 2434	PES HT	TPU	900	700	0.778	15
Kuraray	Vectran HT	Polyarylate HT	—		N/A	22.9	3.8
	Vectran UM	Polyarylate	—		N/A	20.3	2.7
Senbis	PLA 9210	PLA	—	550	2145	3.9	25
	PLA 9210	PLA	—	1100	4070	3.7	38
	PLA 9210	PLA	—	2200	7480	3.4	40
	PLA 9210 LS "Low shrinkage"	PLA	—	1100	3850	3.5	43
Fibers International	FI Low elongation	PES HT	—	1100-4400	18260	8.3	12 [+/-2]
	FI Super Low Shrinkage	PES HT	—	550-2200	7700	7	23 [+/-2]
MSP-Emmen	White MOPET-r Yarn 4835T	rPET (recycled PET)	—	1100	8430	7.54	13.8
	White MOPET-r Yarn 4835T	rPET (recycled PET)	—	1670	12410	7.35	14.9
	White MOPET-r Yarn 4835T	rPET (recycled PET)	—	2200	16470	7.36	15.1
	White MOPET-r Yarn 4835T	rPET (recycled PET)	—	3300	24410	7.34	15.5
Lenzing Profilen	MHG044T30 (1-ply, twisted)	PTFE	—	440	1760	4	2.5
	MHG044T30 (1-ply, twisted)	PTFE	—	470	2350	5	3.6
Trevira	Trevira 41071054 4UVT	PES	—	432	906	2.10	39.4
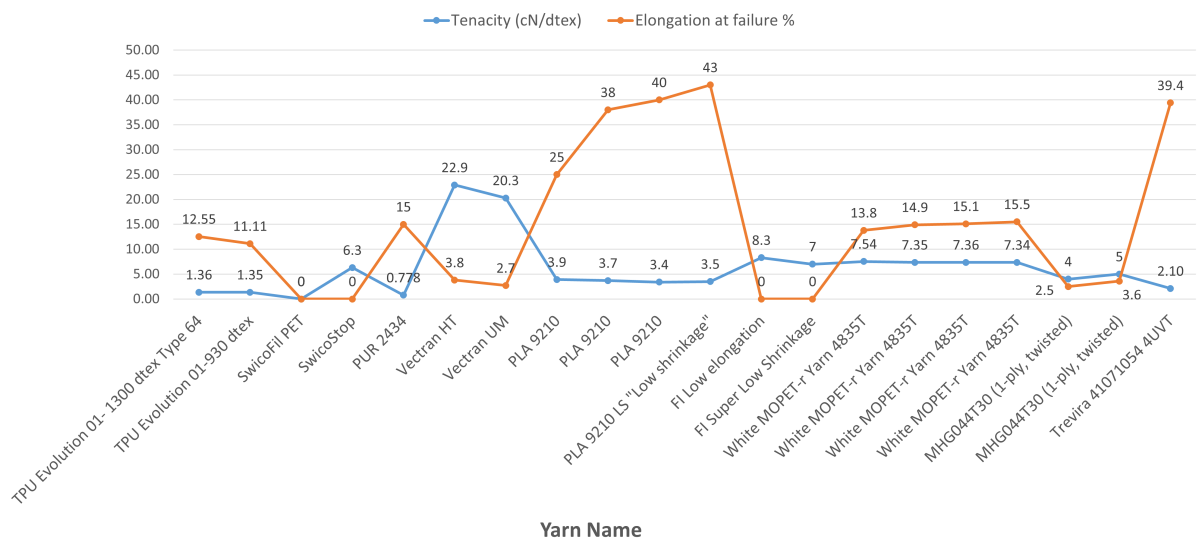
Figure 4.3: Yarn tenacity & elongation at break comparison.

4.2. Weave Pattern

The weave pattern/structure has a direct effect on the mechanical properties of woven fabrics, especially for uncoated fabrics. As discussed in Chapter 3, each of the main weaves (i.e., plain, twill, and satin) possesses a different behaviour in terms of tensile strength, shear rigidity, and tear resistance. It is, therefore, necessary to select a weave structure that allows for the insertion of the OPV film without complicating the weaving process nor compromising the fabric's strength and dimensional stability.

Amongst the main traditional weave structures, plain weaves have the highest tensile strength and shear resistance due to their high yarn density and cover factors. They also possess the highest extensibility based on their high crimp values. Twill weaves, on the other hand, have a more open construction as a result of longer floats and fewer yarn intersections which allow them to perform better in resisting

tear compared to plain structures. Satin weaves demonstrate an even more open construction and has the highest tear strength, yet they have the least shear rigidity.

Satin weaves are not considered a suitable option for the integration of solar films due to their lower strength and loose construction which does not allow the modules to remain in position and thus, under loading, would damage the electrical connections at the contacts. Additionally, their low shear resistance prevents their application in tensile structures as the fabric is more prone to carry loads axially rather than orthogonally along the warp and weft leading to wrinkling and ultimately failure. On the other hand, plain and twill weaves are more stable constructions that should allow for integrating rectangular solar modules and provide the necessary strength and stiffness. Balanced/regular versions of both weaves are the most suitable since they do not introduce large variations within the weave that are likely to create weak links. As a result, 1/1 plain weave (**Figure 3.1**), 2/2 basket (or panama) weave (**Figure 3.4**), 2/2 twill weave (**Figure 3.6**), and 2/2 broken twill weave (**Figure 3.10**) represent possible suitable candidates for the weave structure.

4.3. Solar Module Insertion (Warp vs. Weft)

During the weaving process, the encapsulated OPV modules can be inserted into the fabric either in the warp or weft direction. The weft insertion option is the more readily feasible option, whereas warp insertion requires further adaptations to the loom prior to weaving. Each method has its implications on the final fabric's strength and the extent of load transfer to the OPV module; therefore, each approach necessitates a fundamentally different design strategy than the other to ensure the dual-functionality of the fabric.

In order to decide on the insertion direction, four main factors were identified that are largely influenced by the insertion direction, namely:

1. Tensile strength along the warp.
2. Dimension of solar modules.
3. Weaving complexity.
4. Shaping possibility.

Each factor was weighed based on its importance to generating an operational fabric between 1 and 5, with 5 being the most essential. The implications of each insertion technique with regards to those factors were then identified, and based on their individual performance, each method was given a score between 1 and 5; the higher the score, the better the performance, or the more feasible the option is. Finally, each factor's weight is multiplied by the insertion methods' performance score for that factor and the results added for each method. The results are summarised in **Figure 4.4** followed by further elaboration:

Factor	Weight (1-5)	Weft Insertion	Score /5	Sub-total	Warp Insertion	Score /5	Sub-total
TENSILE STRENGTH WARP	5	▪ Loss of weft yarns.	5	25	▪ Loss of warp yarns. ▪ Leno binding required to minimize solar panel movement.	2	10
DIMENSION OF SOLAR CELLS	5	▪ SF length limited to the width of the loom. ▪ Fit for disassembly.	4	20	▪ Continuous roll with electrical interruptions. ▪ Complex disassembly. ▪ Post-weaving insertion is labor intensive.	2	10
COMPLEXITY OF WEAVING	5	▪ For non-manual insertion, a special gripper is needed. ▪ The reed needs to be set to avoid SF crushing.	2	10	▪ Adjustment is needed to the reed & heddles.	2	10
POSSIBILITY OF SHAPING	3	▪ Allows for different cutting patterns by leaving out SF.	4	12	▪ Continuous SF impedes cutting patterns.	2	6
				Σ = 67			Σ = 36

Figure 4.4: Truth table for solar film insertion direction.

Since the warp direction of a fabric is normally the strongest, the effect of the the insertion strategy had to be linked to the warp's tensile strength. Regardless of the weave direction used, including the OPV modules requires the removal of yarns in the direction of insertion which is detrimental in the case of warp insertion. Leno binding will also be required to minimize the movements in the solar modules. As for the solar cell dimension factor, weft insertion requires the modules to remain within the weaving looms' width, but this option also allows for future replacement of malfunctioning modules. Warp insertion, on the other hand, will require the OPV module to be continuous with regular zone interruptions where strain relief mechanisms and electrical connections must be included. This option proves complex for disassembly and labor intensive if post-weaving insertion is considered.

Both insertion techniques will require adjustments to the loom to facilitate integrating the solar modules; weft insertion allows for the manual placement of modules, but the reed's speed needs to be adjusted to prevent the crushing of modules, whereas the reed and heddles themselves have to be adjusted in the warp insertion's case. Moreover, the weft insertion technique is more suited for scaling and re-shaping as opposed to the warp method which obstructs the production of cutting patterns. Considering all of the discussed points, the weft insertion method was found to be the most suitable option for the fabric layout.

5

Experimental Testing

5.1. Testing Overview

A series of tests have been devised to measure the strength of the fabric with the proposed layout in addition to the performance of the solar modules under stresses and under coverage by float yarns. In this chapter, the testing methodology, purpose, and foreseen complexities pertaining to each test type is outlined first. The tests procedures, results, and analysis are then discussed for each test series, starting with the tensile mono-axial fabric tests, followed by the electro-mechanical OPV module tests, and, finally, the floats' shading effect tests.

5.1.1. Uniaxial Tensile Strength Testing

Mono-axial strip testing carried out according to EN ISO 13934-1 [36] was the chosen procedure to determine the maximum force and elongation at failure of the fabric. It was also decided to perform at least six tests per fabric sample/layout, three specimens per weave direction. Each sample would include main yarns with/without monofilament yarns in addition to cardboard paper or PET plastic strips to simulate the solar films behavior; the used OPV replicas allows for cutting/clamping the specimens without destroying actual solar film especially that only strength values are measured via this test. In addition, measurements of the specimens' strain will be aided with Digital Image Correlation (DIC) which is a non-contact method used to create accurate strain field measurements applicable to dense fabrics [22]. The objective of the test is to verify whether the strength of the fabric has achieved a type I fabric criteria where the strength is 3000N/5cm and the elongation at break is approximately $\leq 17\%$. The four main strategies that will be followed to achieve the desired strength is changing the yarn strength, material, or thickness, increasing yarn density, using twisted/plied yarns, or changing the weave structure. The process is summarized by the flowchart in **Figure 5.1**.
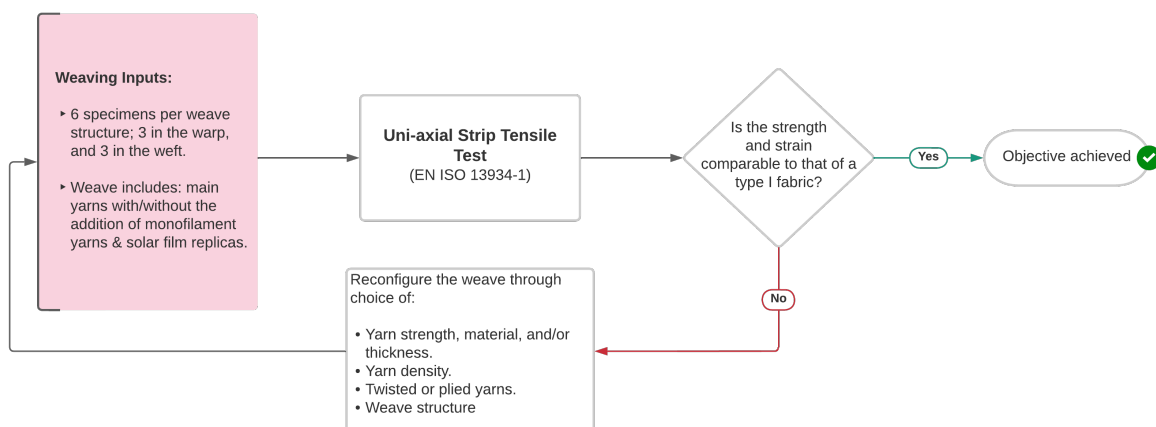

Figure 5.1: Uni-axial tests process

The EN ISO 13934-1 test protocol should be straightforward to apply on uncoated woven fabrics without SF replica insertions, but for those with SF replica insertions, the specimen dimensions and clamping process will have to be adjusted to better represent the final solar fabric's behavior. The standard stipulates a specimen dimension of 5 cm in width and a maximum gauge length of 20 cm whereas the solar cell dimensions are 45 × 2.5 cm. This means the solar film would be included and extend beyond the clamps for a specimen in the weft direction, causing the variance in stiffness between the SF replica and fabric to influence the failure behavior. Additionally, the remaining fabric width adjacent to the solar film becomes 1.25 cm on each side which could probably emphasize the stiffness variance effect. If the tests truly simulate the final composite fabric behavior now becomes questionable. Initial calibration tests will have to be performed to address these concerns prior to the actual uni-axial strength tests.

5.1.2. OPV module Testing

Regardless of the insertion method the SF tape will have to undergo tension throughout its service life whether it be by a direct tensile force or tension induced by bending. The OPV module is a composite in itself built up of electrodes/conductive material and a PET encapsulant. The electrodes tend to be more sensitive to straining compared to the encapsulant, and so the modules can be expected to lose electrical efficiency at a lesser tensile force and strain than those reached at mechanical failure as demonstrated by Fang et al. [40]; however, this failure behavior cannot be generalized over all OPV modules since each OPV structure is built up of different components, yet a similar testing approach can be taken with the ASCA OPV module to identify the two critical failure points via a uniaxial tensile test with electrical performance logging. Benchmarking the OPV module's ultimate tensile capacity beyond its electrical failure provides insight into the amount of tensile strength reserve available which allows for quantifying a safety reserve prior to failure. It also allows for quantifying the stiffness of the tape, thus enabling direct comparison with the fabric stiffness which will guide the fabric design as to what extent the solar modules can be fixated within the fabric.

An efficacious electro-mechanical test is one where the current, voltage, tensile force and extension/displacement can all be measured. Hence, a correlation can be established linking the solar cells performance and the force, stress, or strain. This is only possible if the tension is applied at intervals followed by a pause in which the voltage and current are measured to generate the I-V curve using a source meter. Since the main purpose of the test is to identify the load at electric failure rather than the whole degradation of the module due to straining, a less complex alternative could be used; this is done by identifying the maximum power point (refer to section **2.2.2**) for the OPV module under constant lighting conditions then performing the tensile test until mechanical failure. The load corresponding to the lowest measured power (I × V) is the electric failure load which can be found by correlating the time of both the electrical and mechanical measurements. The accuracy of this test is, therefore, dependent on the simultaneous timing accuracy and the difference between the rate at which data is measured for both tests.

Multiple challenges can be identified prior to carrying out the proposed test. Firstly, clamping of the OPV module will be difficult in order to avoid both slippage and the damaging of the contact points by clamp compression. Secondly, the temperature of the module should be kept constant during the tests since both the OPV module's electrical and mechanical performances are influenced by temperature. Lastly, the lighting source will need to provide sufficient irradiance to stimulate the module without increasing the samples temperature.

5.1.3. Float Effect Testing

In the designed fabric layout, transparent monofilament yarns were used as float yarns along the warp to provide stability to the OPV modules without majorly influencing the module's efficiency. The float tests aim to verify the shading effect of monofilaments and the impact of increasing the float yarn frequency on the OPV module's performance.

The test can be performed by creating a fabric with multiple float segments having different yarn material or variable frequencies that can accommodate the module length (see **Figure 5.42**). A solar film could then be inserted into each of the pockets created by the floating yarns and their electrical

efficiency measured using a source meter under lighting from a high-irradiance light source. Similar to the electro-mechanical test, the light source should adequately stimulate the modules without heating them up. It is necessary, however, for this test to have the temperature controlled since the measured efficiency value is highly influenced by the temperature.

## 5.2. Testing Procedures, Results, & Analysis

5.2.1. Calibration Tests

Calibration tests were performed using Instron 1561 uniaxial tensile testing machine initially on a fabric with known strength properties to verify the testing process, evaluate the concerns discussed in section **5.1.1**, and in general, test the applicability of the EN ISO 1421 & EN ISO 13934-1 specifications. The first specimens were from Soltis 86, a commercial fabric typically used in external blinds for facades, greenhouses, and verandas. The fabric is constructed from open mesh PVC-coated PES yarns in a plain weave with a tensile strength of 2300 and 1600 N/5 cm in the warp and weft, respectively. Test samples of 5 cm width by 20 cm length were mounted into the clamps and pre-tensioned to approximately 20-40 N before commencing the tests. A constant extension rate of 10 mm/min was applied during testing while the load and elongation values were recorded. The extension rate applied is less than that proposed by both standards (i.e., 100 mm/min) because at this speed, the failure behavior can be easily followed by the naked eye for the next coated-yarn woven test specimens. And so, the same rate would need to be applied for the Soltis fabric specimens to allow for a comparison with other fabric material as well as verify the effect of reducing the rate on the fabric strength.

Table 5.1: Soltis 86 fabric specimens test results.

	General Properties				Weave specifications		Test samples criteria					
Specimen Name	Material	Weight (g/m^2)	Thickness (mm)	Tensile Strength (warp/weft) (N/5cm)	Warp density (yarns/cm)	Weft density (yarns/cm)	Dimensions (cm^2)	Initial Length (cm)	Extension (mm)	Elongation (%)	Failure Load (kN/5 cm)	Extension Rate (mm/min)
CF 01	PES/PVC	380	0.43	2300/1600	7.2	5	5x24.3	18.45	—	—	No failure	10
CF 02	PES/PVC	380	0.43	2300/1600	7.2	5	5x19.5	9.25	21.82	23.6	2.198	10
CF 03	PES/PVC	380	0.43	2300/1600	7.2	5	5x20	9.65	24.11	25.0	1.696	10
CF 04	PES/PVC	380	0.43	2300/1600	7.2	5	5x20	9.65	22.08	22.9	1.597	10
CF 05 F1	PES/PVC	380	0.43	2300/1600	7.2	5	5x20	9.65	24.05	24.9	1.645	10
CF 06 F2	PES/PVC	380	0.43	2300/1600	7.2	5	5x20	9.65	25.05	26.0	1.715	10
CF 07 F3	PES/PVC	380	0.43	2300/1600	7.2	5	5x20	9.65	20.74	21.5	1.476	10
CF 08 w1	PES/PVC	380	0.43	2300/1600	7.2	5	5x20	9.65	21.91	22.7	2.428	10
CF 09 w2	PES/PVC	380	0.43	2300/1600	7.2	5	5x20	9.65	21.73	22.5	2.303	10
CF 10 w3	PES/PVC	380	0.43	2300/1600	7.2	5	5x20	9.55	23.40	24.5	2.503	10

— Incomplete test where the max. stroke was reached before failure.
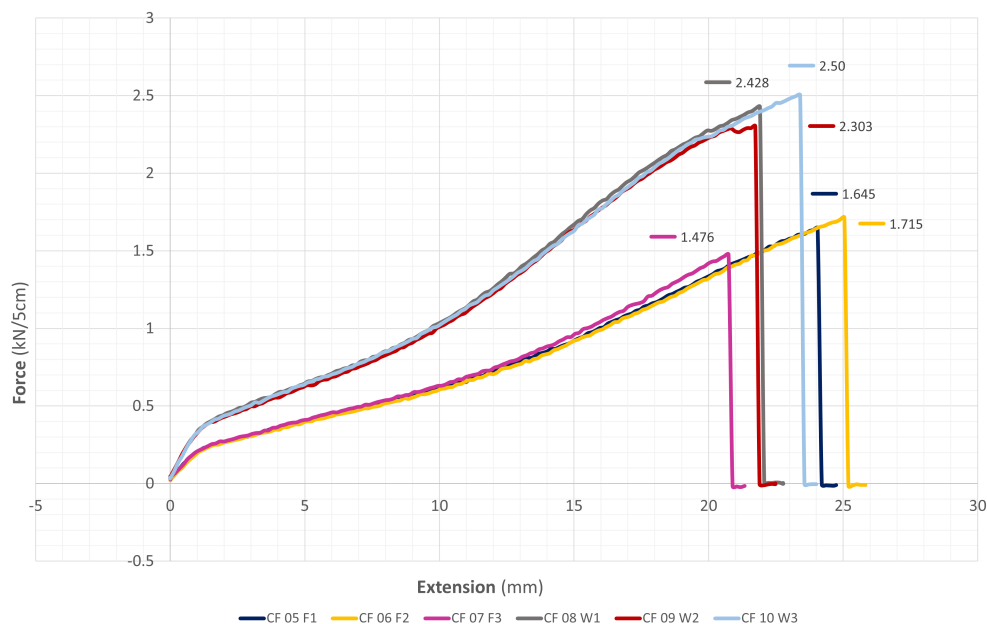
Figure 5.2: Load-extension behavior.

CF 05 to CF 10 represent the six tested strip specimens with the first three taken in the weft direction and the following three taken in the warp direction. An average failure load of 2.41 kN corresponding to 23.2% elongation was measured in the warp compared to 1.61 kN for 24.1% elongation in the weft. In all specimens except CF 07 F3, failure occurred near the clamps approximately within the 5 mm margin stipulated in EN ISO 1421 which is considered a jaw break, and hence requires the disregard of the collected measurements; however, the failure load measured for these specimens were consistent with the fabrics strength provided in its specifications data. In fact, only

Figure 5.3: Specimens' CF05-CF10 after failure.

specimen CF 07 F3 exhibited failure within the tested zone yet showed a lower failure load than expected compared to the other weft specimens. It could therefore be deduced that the failure near the clamps is an acceptable failure behavior, and that initial faults in the fabric or faults in the specimen edges are probably the cause of the premature failure in the 3rd weft specimen.
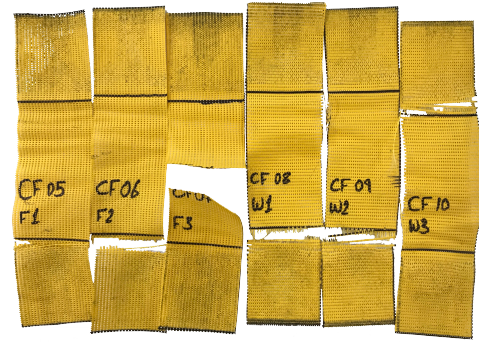
A second calibration test was performed using the same machine on a hand woven fabric from CoatYarn 930 dtex coated TPU yarns structured in a plain weave. Cardboard solar cell replicas were inserted in the weft direction with a 2.5 cm spacing in between adjacent replicas. Warp yarns created the floats going above and under the replicas intermittently along the warp width, holding the cardboard in place. Specimens were initially cut to 6×20 cm in the warp and 6×17 cm in the weft, then frayed by removing equal threads from each side in both directions for a total of five warp specimens and four weft ones. Again the specimens were mounted into the clamps with low pretension prior to testing. For weft specimens in specific, two variations were performed to address the question of whether the solar cell replicas should be included in the clamping. Therefore, one specimen, CYF 02, was mounted into the clamps with the cardboard replicas included while the remaining three had the replicas cut near the clamps such that only the fabric is included in the clamps. The results are shown in **Table 5.2** below.

Table 5.2: CoatYarn specimens results

General Properties			Weave specifications			Test samples criteria					
Specimen Name	Material	Thickness (mm)	Pattern	Warp density (yarns/cm)	Weft density (yarns/cm)	Dimensions (cm²)	Initial Length (cm)	Extension (mm)	Elongation (%)	Failure Load (kN/5 cm)	Extension Rate (mm/min)
CYW 01	PES/TPU	0.61	Plain	10	10	5x19.5	14.55	16.53	11.4	0.497	10
CYW 02	PES/TPU	0.61	Plain	10	10	5x19.5	14.85	15.89	10.7	0.568	10
CYW 03	PES/TPU	0.61	Plain	10	10	5x19.5	14.85	17.84	12.0	0.552	10
CYW 04	PES/TPU	0.61	Plain	10	10	5x19.5	14.85	16.40	11.0	0.548	10
CYW 05	PES/TPU	0.61	Plain	10	10	5x19.5	14.85	15.91	10.7	0.524	10
CYF 02	PES/TPU	0.61	Plain	10	10	5x16	10.75	—	—	—	10
CYF 03	PES/TPU	0.61	Plain	10	10	5x16	11.15	9.47	8.5	0.179	10
CYF 04	PES/TPU	0.61	Plain	10	10	5x16	11.25	9.20	8.2	0.149	10
CYF 05	PES/TPU	0.61	Plain	10	10	5x16	11.25	8.58	7.6	0.171	10

– Incomplete test where the max. stroke was reached before failure.
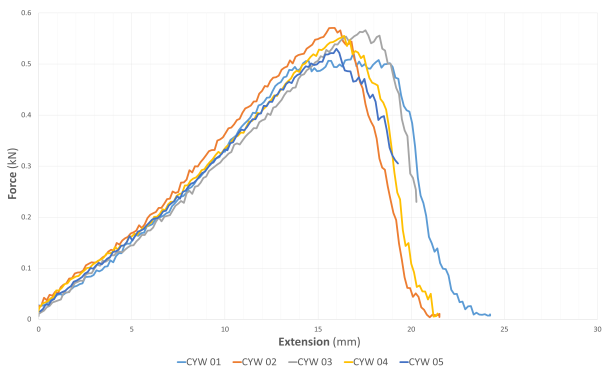

Figure 5.4: CoatYarn warp specimens Load-Extension behavior.
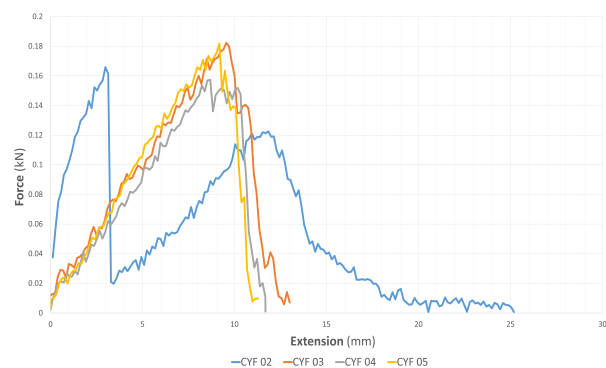

Figure 5.5: CoatYarn weft specimens Load-Extension behavior.

An average failure load of 0.538 kN was obtained in the warp direction against 0.166 kN in the weft, excluding specimen CYF 02. This is attained with 11.2% average warp elongation and 8.1% average fill elongation. No uniform-cut failure pattern was visible but rather individual yarns failing separately at different moments in time until multiple yarns rupture simultaneously signaling ultimate failure. Additionally, the force against extension graphs showed a kinked plot which can be related to the stress redistribution across the longitudinal yarns after every yarn tear as well as the consequent yarn movement especially with a slow extension rate such as the 10 mm/min. Specimen CYF 02 experienced a different failure behavior than the rest of the specimens where a peak load of 0.166 kN was reached and the cardboard replica ruptured followed by a sudden drop in measured force.

The force then started increasing again until it reached a second peak of 0.123 kN before failure. Due to the difference in stiffness between the replica and the fabric, emphasized by the lower number of longitudinal yarns on either side of the replica, the stiffer element (i.e. cardboard) started taking more of the force until it reached failure beyond which the fabric started taking over the applied force until the second peak failure. Furthermore, all other specimens failed at the zone close to the clamps; warp specimens failed at the floats adjacent to the cardboard insertions whereas weft ones failed at the longitudinal yarns near the corner of the insertions.

(a) Warp specimens: CYW02-CYW05   (b) Weft specimens: CYF02-CYF05
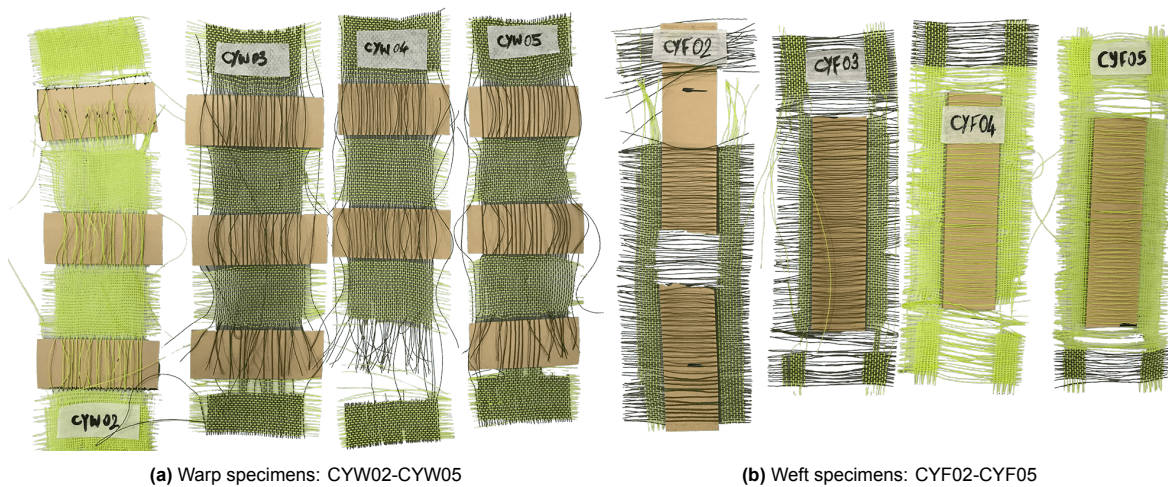
Figure 5.6: CoatYarn specimens failure patterns.

It can be generally concluded that weaker links develop, due to the fabric's configuration, which tend to break first resulting in low force transfer to the SF replicas, except for specimen CYF 02. Failure patterns of the 3rd to the 5th weft specimens, however, can be considered unrepresentative of the composite fabric strength due to the limited number of longitudinal yarns on both sides of the inserts which seem to induce local failure. Further investigation via another test with wider specimens is needed inorder to verify the failure pattern and gain reliable strength results. Specimen CYF 02 clearly showed the damaging impact of fixating the solar film ends into the fabric on the final composite fabric behavior. This is an undesired behavior that should be avoided so as to not transfer excessive loads to the solar cells and risk electrical failure.
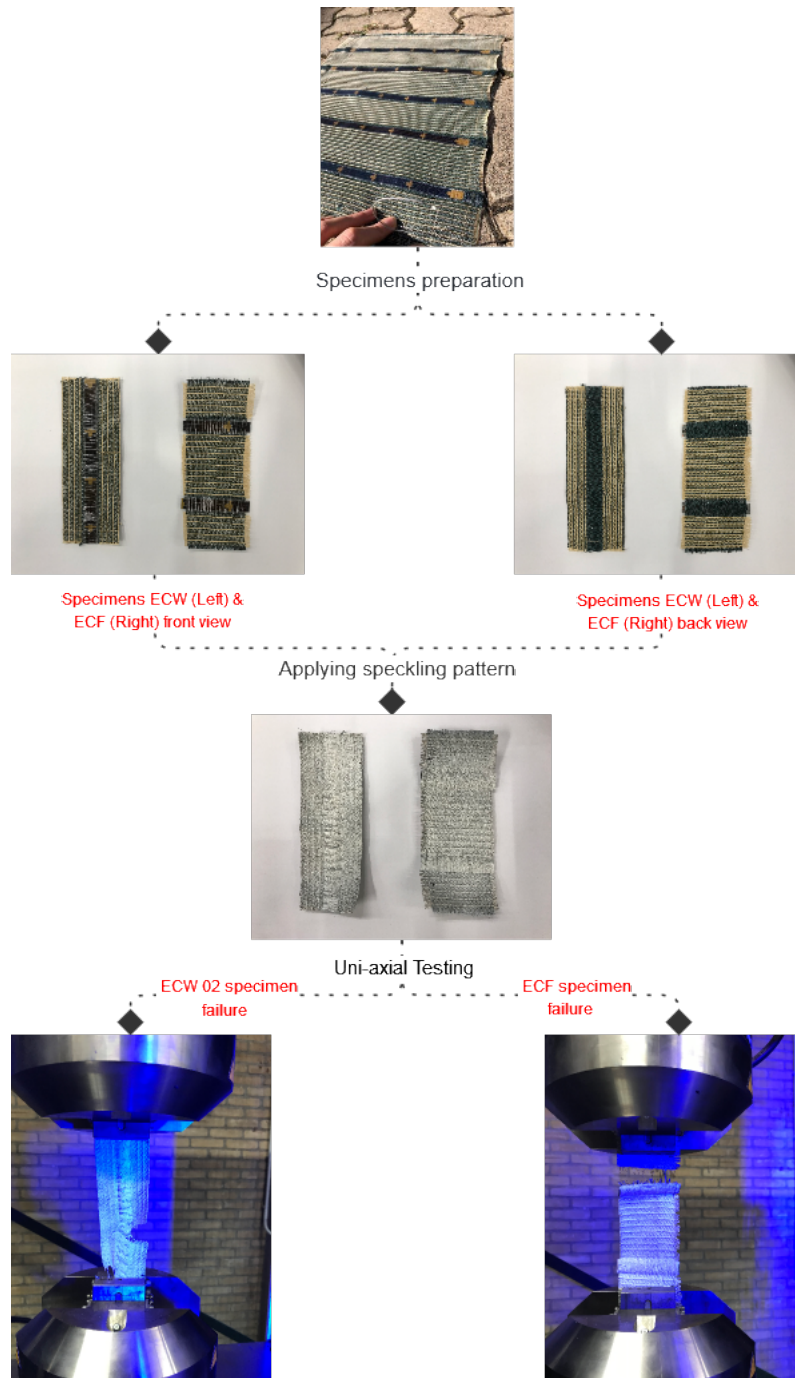
Figure 5.7: EC specimens preparation & testing process.

In contrast to the open-meshed fabric already tested, a denser woven fabric was used for a final calibration test. The fabric was originally meant to be an initial endeavor into the combination of textiles and solar cells, which explains the presence of CIGS solar cell tape instead of OPVs. Other key differences include the presence of different weave combinations within the fabric, most prominently leno weaves in warp, the use of weft yarns to create a SF-backing, and the insertion of the SF tape in the warp direction rather than weft. Two specimens were cut to 5×15 cm for testing, one in each direction. Multiple layers of elastomer were applied to the specimens to create a speckling pattern for digital image correlation measurements (DIC) made possible by the high density of the fabric. The specimens were then placed 2.5 cm into the clamps before load application to failure; CIGS tape was included in the clamps when testing the warp specimen due to the difficulty in cutting it close to the

clamp edges.

The warp specimen exhibited the same failure behavior as that of CYF 02. CIGS tape ruptured first causing a sudden loss of strength followed by a gradual increase in strength until the machine's maximum stroke was reached. Another test run (ECW 02) was carried out using the same specimen to reach failure and the ultimate load recorded at an average value of 707 N/5cm. On the other hand, weft specimen ECF 01 showed a gradual rise in strength until failure at 1270 N/5cm. **Figure 5.9** & **5.10** capture the strain field of ECW 02 which shows increased strains around the leno weave and on top of the solar cells at peak load. Failure initiated at the left side of the bottom clamp where warp yarns were partially torn, putting more stresses on the right side of the specimen. Wrinkling around the solar cell area at the bottom of the fabric was then seen before the ultimate failure caused by a shearing motion of the fabric. ECF 01 strain field demonstrated higher stresses at the borders of the SF tape at peak load with stresses also transferred to the solar cells. Ultimate failure occurred at the upper border of the top SF.

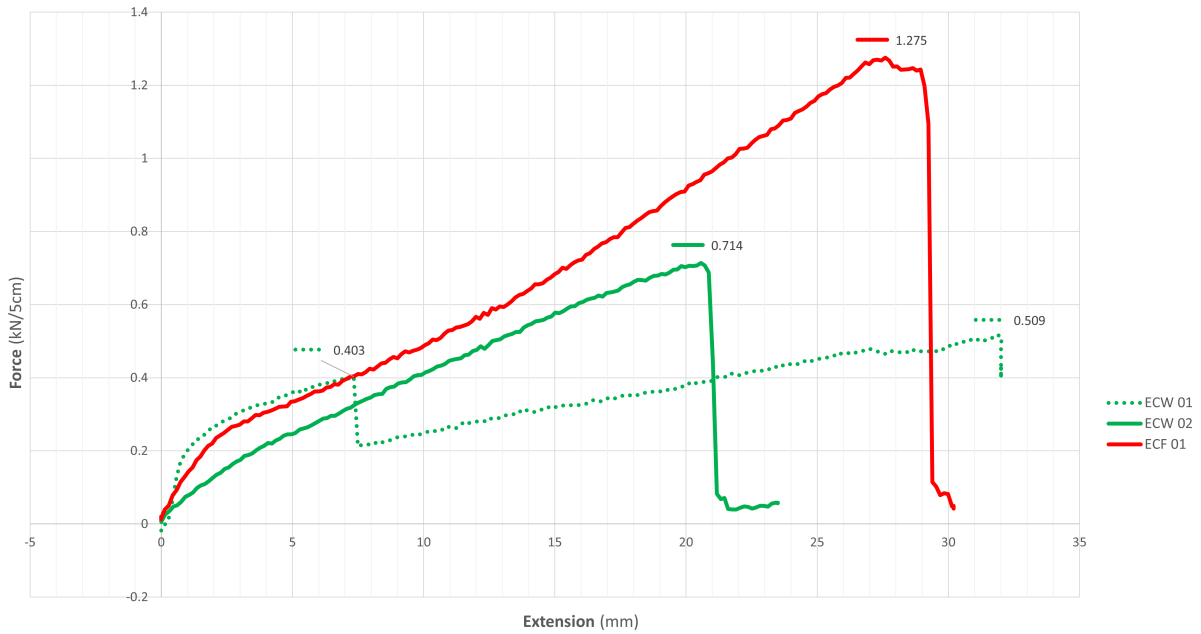**Figure 5.8:** Load-extension graph for EC specimens.

Table 5.3: EC sample test results.

Specimen Name	Weave Pattern	Dimensions (cm^2)	Initial Length (cm)	Extension (mm)	Elongation %	Failure Load (kN/5 cm)	Extension Rate (mm/min)
ECW 01	Mixed	5x15	10.75	—	—	—	10
ECW 02	Mixed	5x15	10.75	20.57	19.1	0.714	10
ECF 01	Mixed	5x15	10.75	27.52	25.6	1.270	10

− Incomplete test where the max. stroke was reached before failure.
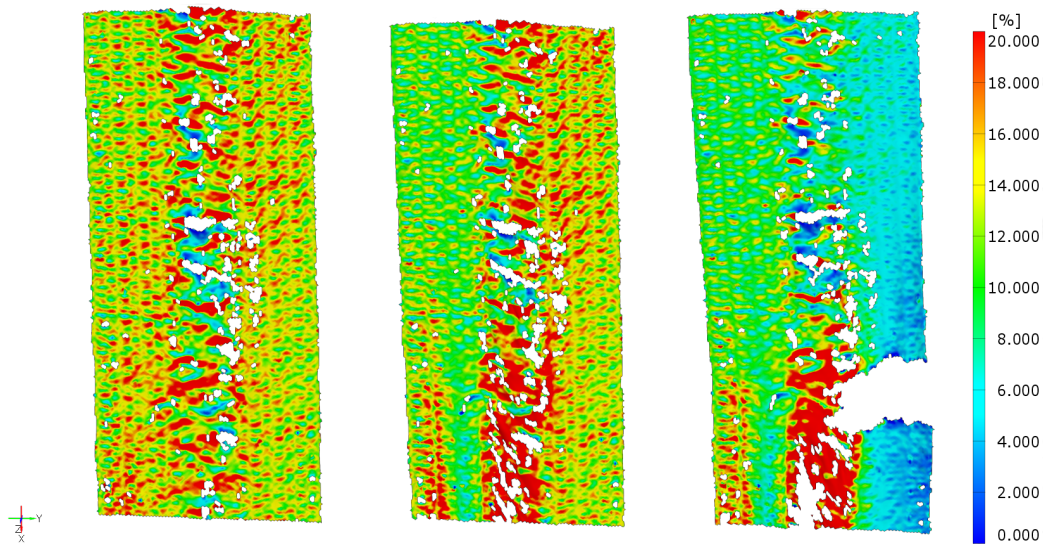
Figure 5.9: Strain field of specimen ECW 02 at three different stages: peak load just prior to failure (Left), failure initiation & wrinkling (middle), and ultimate failure (Right).
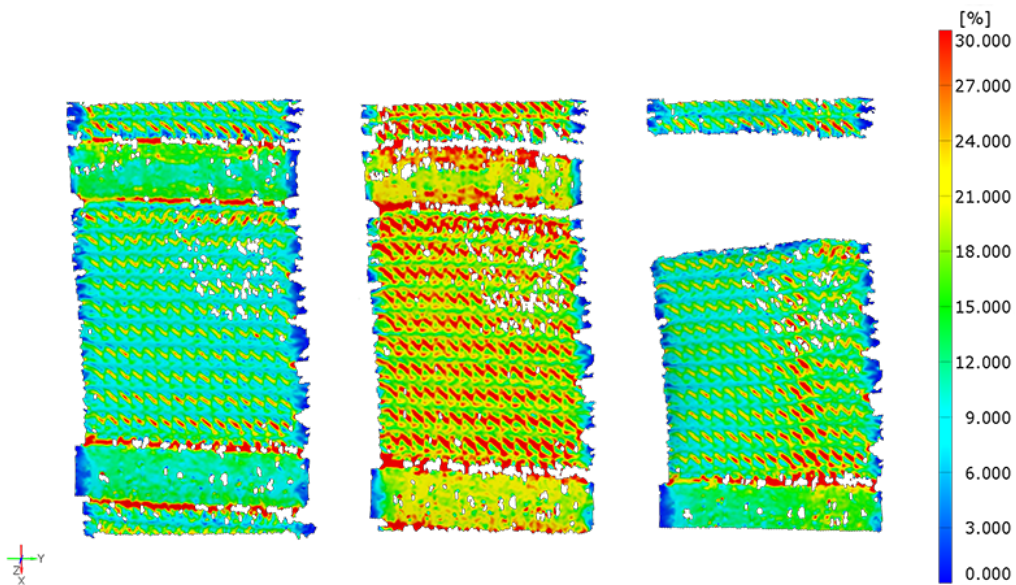
Figure 5.10: Strain field of specimen ECF 01 before reaching maximum load (Left), at peak load (middle), and at ultimate failure (Right).

Conclusion

Several key understandings can be deduced from the different calibration tests performed; firstly, if the solar cell tape is fixated at any point in the fabric in the longitudinal direction of the SF and tension is applied along the same direction, the solar cells will undergo straining that may lead to electrical failure. Due to the fabric configuration, local stress concentrations also occur at the SF borders when load is applied in the perpendicular direction to the SF. These areas become the weakest elements that initiate failure. Furthermore, increasing the yarn density of the fabric allows for more representative mechanical measurements due to the more longitudinal yarns present within the clamp as well as the better application of the elastomer that creates less voids, compared to open-mesh fabrics, for DIC measurements. Lastly, adding a fabric behind the solar film increases the fabric's strength as demonstrated by EC specimens.

5.2.2. Uniaxial Tests

In order to address the possibility of potential premature failure due to the local stresses incited by the low longitudinal yarn count in weft direction and, most importantly, to explore the effect of the weave configuration on the solar cell tape, larger fabric specimens were tested. All the fabric tensile tests mentioned herein were carried out using Instron 1122 tensile testing machine.

TPU Fabric

The same TPU fabric previously tested during the calibration tests was once again tested but for larger specimens with a gauge length of 20 cm and a width of 7.5 cm. The test speed was also increased to 100 mm/min, as recommended by EN ISO 13934-1. To incorporate the wider size of the specimens, customized steel clamps were installed. The fabric was mounted in between two steel plates pressed against each other by screws then by additional clamps. This procedure was found to limit the slippage and clamp-influenced failure in preliminary check tests. Six specimens were tested in total, three in each weave direction.
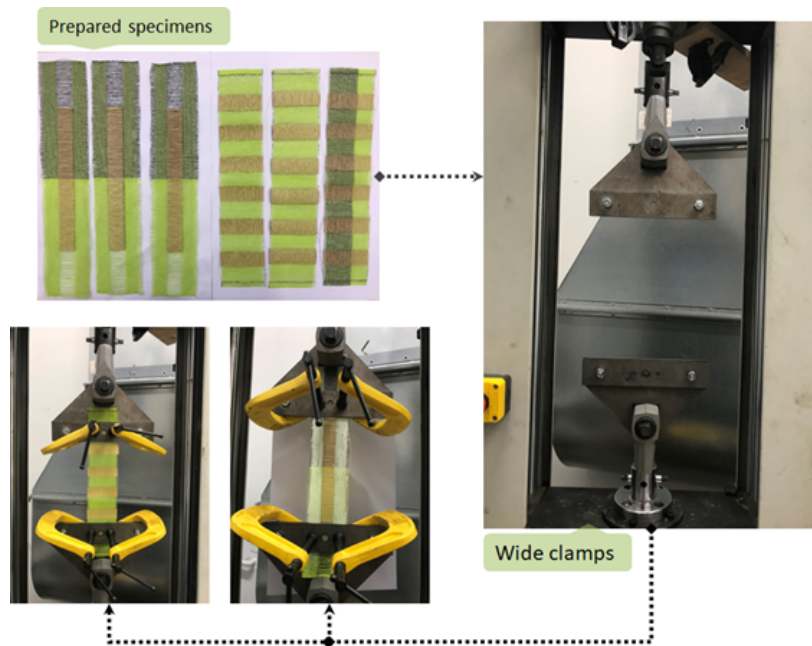
Figure 5.11: TPU specimens test process.

It was observed that warp specimens failed at the edges of the solar cells at an average load of 850.6 N/7.5 cm and 14.2% elongation. Weft specimens, on the other hand, averaged 426.7 N/7.5cm with 10.6% elongation at break; non-uniform failure, similar to that from the calibration tests, was seen at the fabric sides of the cardboard replicas.

Figure 5.12: Specimen CY 7.5cm W1 after failure.

Figure 5.13: Specimen CY 7.5cm F2 after failure.

Figure 5.14: CY 7.5cm specimens' force vs. extension behavior.
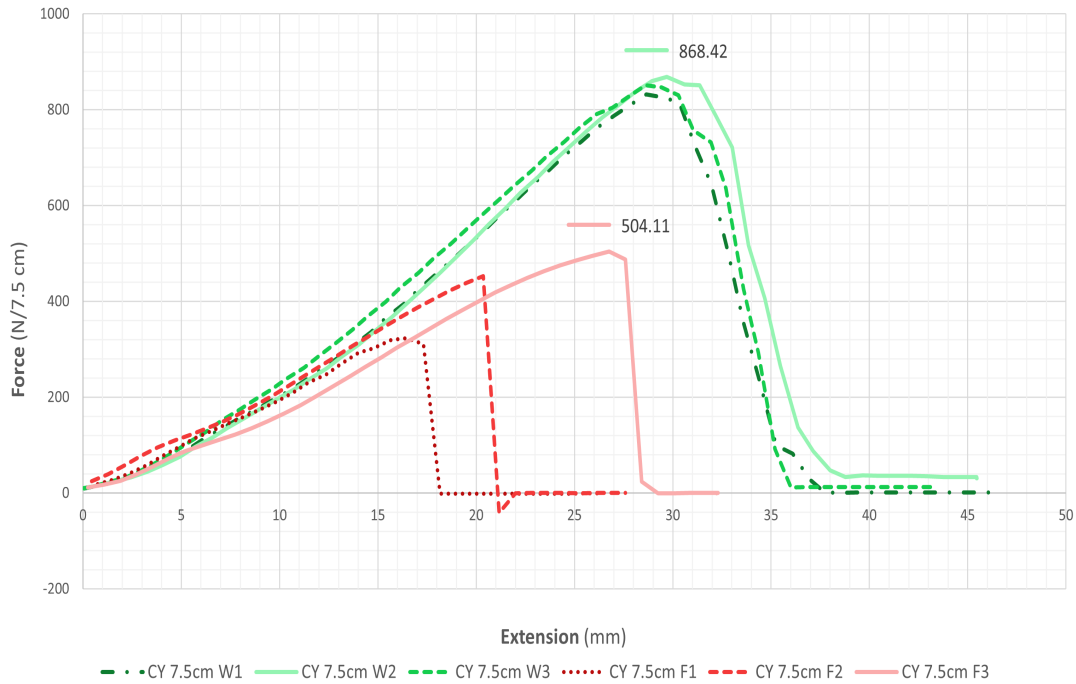
Table 5.4: TPU fabric specimens description & test results.

General Info			Weave specifications			Test samples criteria					
Specimen Name	Material	Thickness (mm)	Weave Pattern	Warp density (yarns/cm)	Weft density ** (yarns/cm)	Dimensions* (cm²)	Initial length (cm)	Extension (mm)	Elongation %	Failure Load (N/7.5cm)	Extension Rate (mm/min)
CY 7.5cm W1	PES/TPU	0.61	Plain weave	10	10	7.5×20	20.3	28.7	14.1	832.24	100
CY 7.5cm W2	PES/TPU	0.61	Plain weave	10	10	7.5×20	20.7	29.7	14.3	868.42	100
CY 7.5cm W3	PES/TPU	0.61	Plain weave	10	10	7.5×20	20.3	28.6	14.1	851.09	100
CY 7.5cm F1	PES/TPU	0.61	Plain weave	10	10	7.5×20	20.2	17.3	8.6	323.07	100
CY 7.5cm F2	PES/TPU	0.61	Plain weave	10	10	7.5×20	20.5	20.4	9.9	452.78	100
CY 7.5cm F3	PES/TPU	0.61	Plain weave	10	10	7.5×20	20.6	27.6	13.4	504.11	100

* Length measured is gauge length.

** Indicates the number of yarns in the adjacent sections to the insertions.

Conclusion

The weave configuration demonstrated insufficient strength in both weave directions. Weft specimens experienced lower failure load due to the lesser number of longitudinal yarns present, and the difficulty of achieving a straight fabric within the clamps which led to yarns being loaded unevenly. This is demonstrated by both the failure pattern and large discrepancy in the failure load between weft specimens. Moreover, the solar cell replicas did not experience straining in any direction.

TPU Fabric Composite
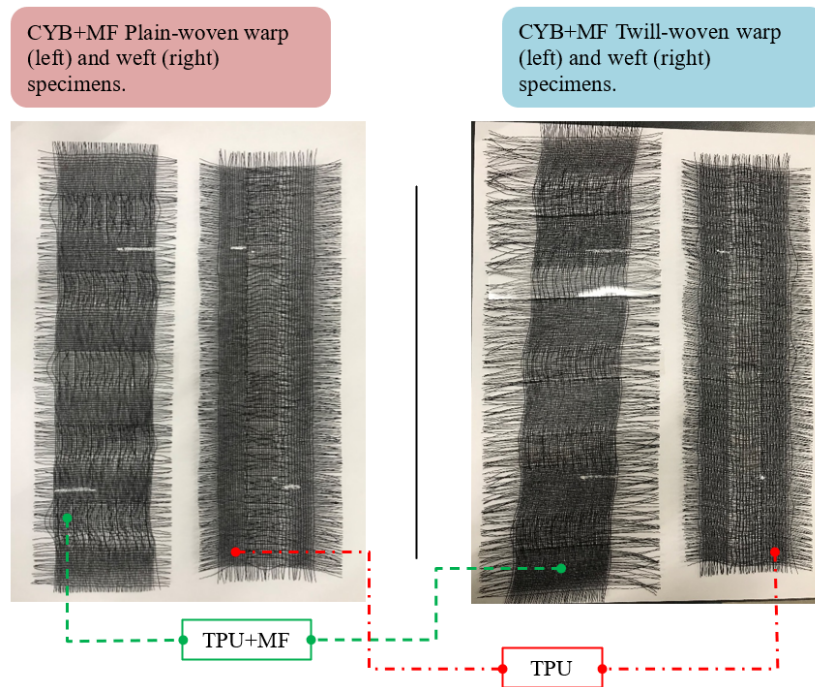


Figure 5.15: Typical TPU fabric-composite specimens.

Another test study was conducted on large fabric specimens with an adjusted weave configuration, aimed at simulating the proposed fabric design. To study the failure behavior and the impact of varying the weave structure, a plain and a 2/2 twill samples were woven on a power loom. The samples were woven from alternating PES/TPU (1300 dtex) yarns and monofilaments (1600 dtex) in the warp direction, but only PES/TPU yarns in the weft. PET films were also inserted along the weft to mimic the solar modules. As opposed to the previous fabric, longitudinal yarns were added to the weave along the weft behind the plastic films to increase the strength of the fabric in that direction. The samples were cut into 6 plain-woven specimens and 6 twill-woven specimens, half of which were taken along the warp and the remaining half along the fill. Each specimen was then clamped and tensioned individually to failure in the same manner used for the TPU fabric tests.

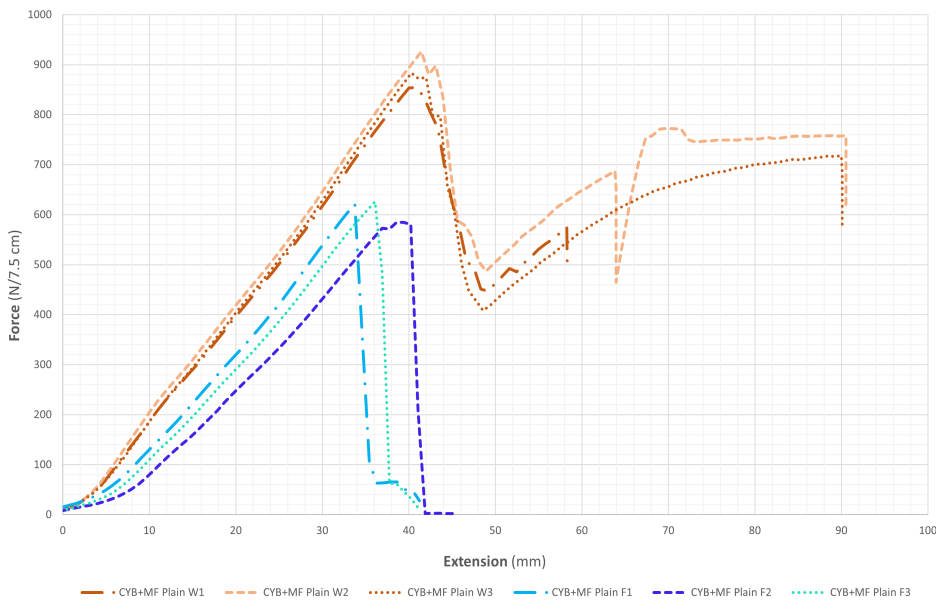**Figure 5.16:** Plain & 2/2 Twill specimens' failure in both weave directions.
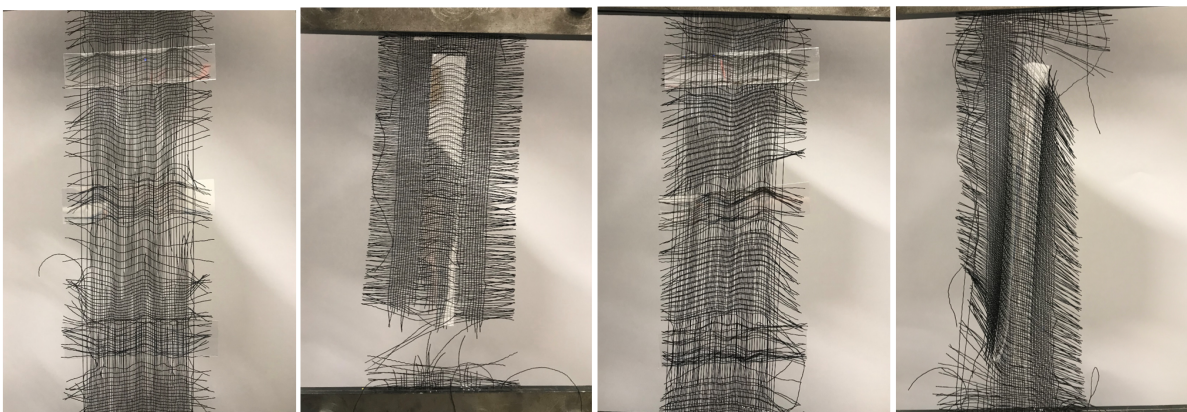

(a) Specimen CYB+MF Plain W2   **(b)** Specimen CYB+MF Plain F3   **(c)** Specimen CYB+MF Twill W2   **(d)** Specimen CYB+MF Twill F3

During the warp specimens' tests, the TPU-coated polyester yarns started breaking one at a time as the tension force applied approached the maximum load. At a certain force above 800 N, the maximum

load was reached followed by a reduction in the measured force, corresponding to a rapid progressive failure of the PES/TPU yarns. The monofilament yarns then started taking over the tensile force as the applied force increased. The weft specimens exhibited typical fabric failure where the measured force gradually increased until the peak load was reached followed by a sharp decline in force.

Figure 5.17: Force-extension behavior of CYB+MF plain specimens.
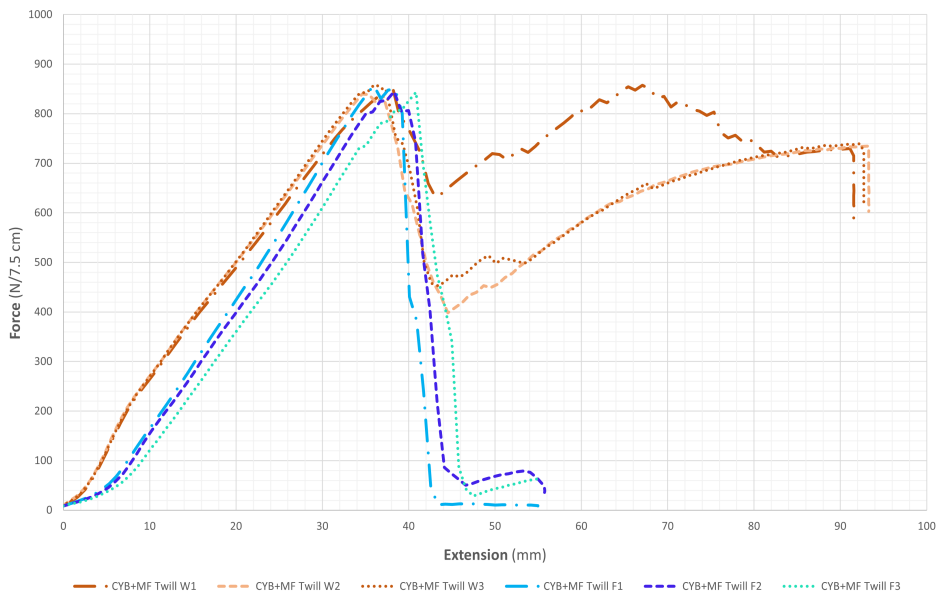
Figure 5.18: Force-extension behavior of CYB+MF twill specimens.

For plain-woven specimens, the warp direction achieved a higher failure load and elongation than the fill; warp specimens had an average failure load of 887.8 N/7.5cm with an elongation at break of 19.8%, whereas the fill specimens failed at 610.7 N/7.5 cm at 18% elongation. On the other hand, twill-woven specimens obtained approximately the same failure load in both weave directions, measured at 851.2 N/7.5cm and 848.3 N/7.5cm in warp and weft, respectively; however, the elongations were lower in the warp direction, amounting to 17.7% against 18.4% in weft. The following table summarizes the fabric properties and the test results:

**Table 5.5:** TPU fabric composite specimens description & test results.

General Info		Weave specifications			Test samples criteria					
Specimen Name	Material	Weave Pattern	Warp density (yarns/cm)	Weft density (yarns/cm)	Dimensions* (cm^2)	Initial length (cm)	Extension (mm)	Elongation %	Failure Load (N/7.5cm)	Extension Rate (mm/min)
CYB+MF Plain W1	PES/TPU + Monofilament	Plain weave	10	8	7.5×20.5	20.8	40.9	19.6	853.95	100
CYB+MF Plain W2	PES/TPU + Monofilament	Plain weave	10	8	7.5×20.5	20.4	41.5	20.3	926.14	100
CYB+MF Plain W3	PES/TPU + Monofilament	Plain weave	10	8	7.5×20.5	20.8	40.3	19.4	883.16	100
CYB+MF Plain F1	PES/TPU + Monofilament	Plain weave	10	8	7.5×20.2	20.6	35.4	17.2	621.67	100
CYB+MF Plain F2	PES/TPU + Monofilament	Plain weave	10	8	7.5×20.2	20.9	40.2	19.3	584.79	100
CYB+MF Plain F3	PES/TPU + Monofilament	Plain weave	10	8	7.5×20.2	20.7	36.1	17.4	625.75	100
CYB+MF Twill W1	PES/TPU + Monofilament	2/2 Twill weave	10	8	7.5×20	20.4	38.1	18.7	854.95	100
CYB+MF Twill W2	PES/TPU + Monofilament	2/2 Twill weave	10	8	7.5×20	20.5	34.6	16.9	839.90	100
CYB+MF Twill W3	PES/TPU + Monofilament	2/2 Twill weave	10	8	7.5×20	20.5	36.0	17.6	858.63	100
CYB+MF Twill F1	PES/TPU + Monofilament	2/2 Twill weave	10	8	7.5×20	20.8	35.9	17.3	857.11	100
CYB+MF Twill F2	PES/TPU + Monofilament	2/2 Twill weave	10	8	7.5×20	20.8	38.3	18.4	844.29	100
CYB+MF Twill F3	PES/TPU + Monofilament	2/2 Twill weave	10	8	7.5×20	20.8	40.8	19.6	843.39	100

* Length measured is gauge length.

Conclusion

- The failure behavior seen in the warp specimens is most probably due to the difference in stiffness between the yarns which makes the stiffer PES/TPU yarns carry most of the load until failure then the load is transferred to the less stiff monofilaments. Lower failure load is measured for the plain-woven weft specimens. This is most likely caused by the lesser number of picks per cm and the fact that the yarns were not clamped linearly along a single line. Furthermore, adding a backing fabric layer to the solar film did not contribute to avoiding the uneven loading of the weft specimens; however, it did prevent the tear propagation initiating at the solar film end.

- Overall, the twill weave performed better in terms of strength; however, the dimension skew seen in the sample after the weaving process implies that if used in tensile structures, more work will be needed during seaming and installation to avoid fabric shearing.

Broken Twill Fabric Composite
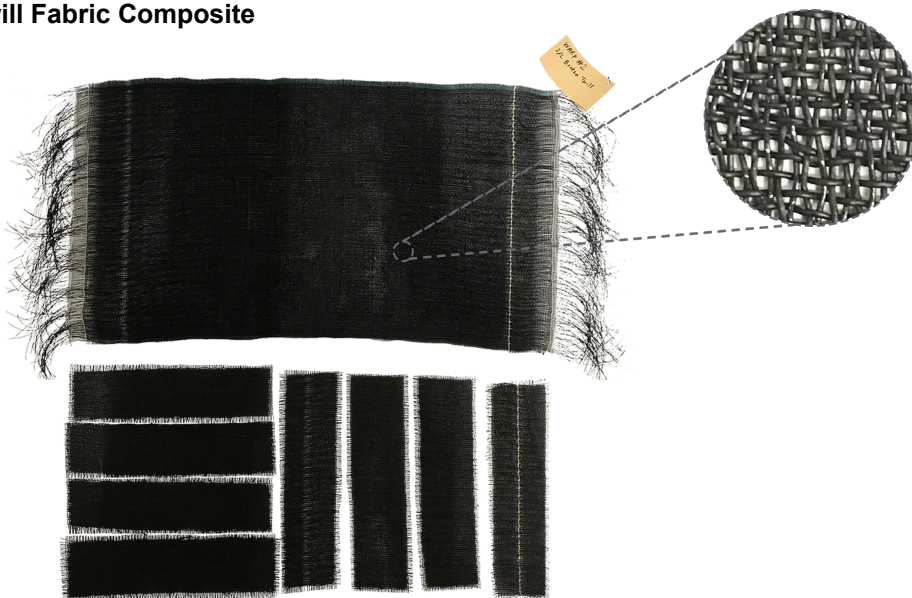
Figure 5.19: Broken twill sample preparation.

A 2/2 broken twill fabric sample composed of PES/TPU 1300 dtex yarns and monofilament yarns was also woven for strength testing. No solar cell replicas were used so as to study the weave configuration's strength if it is sufficient by itself in the first place. Eight specimens of 5×20 cm were tested,

four in each direction. Specimen CYB W1, which was the only specimen with conductive yarns present in the middle, underwent excessive slippage at a low force. An increase in measured force was seen with tightening of the clamps however no useful mechanical information could be extracted from this specimen. The remaining warp specimens showed a different failure pattern to those seen in the calibration tests; the measured force increased gradually until approximately 680 N beyond which single yarns started snapping accompanied by a loss in force. A second gradual rise in force then occurred until an average breaking force of 722.24 N was reached. This behavior can again be explained by the difference in stiffness between the TPU and monofilament yarns:

*Assuming an elastic behavior and the same yarn thickness,*

$$TPU\,yarn\,stiffness = \sigma/\epsilon = 17.7N/mm^2 \div (12.55/100) = 141N/mm^2$$
$$Monofilament\,yarn\,stiffness = \sigma/\epsilon = 27.45N/mm^2 \div (97/100) = 28.3N/mm^2$$

The stiffer TPU yarns carried more of the applied load and thus failed first and continued breaking over a transition zone after which the monofilaments started taking over the load. In **Figure 5.20**, a sudden reduction in force is seen at around 100 mm extension which is the maximum stroke of the upper clamp. At this instant a transition was made to use the lower clamp instead to apply extension, and so this kink is not indicative of a loss in fabric strength. Due to the monofilament's high elongation capacity at failure, the specimens continued to elongate until the maximum breaking force was reached. The elongation measured 104.3% on average. For specimen CYB W3, the rate of extension was increased from 10 to 20 mm/min after the first peak, and similarly for CYB W4, the test was performed at 20 mm/min to check the effect of a relatively minor increase in speed on the force-extension trend.
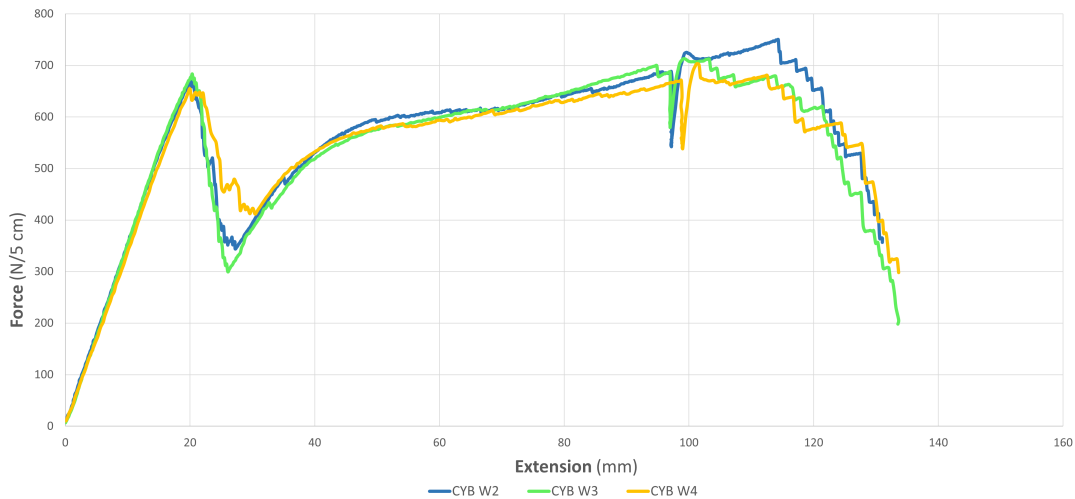
Figure 5.20: CYB warp specimens behavior under tension.
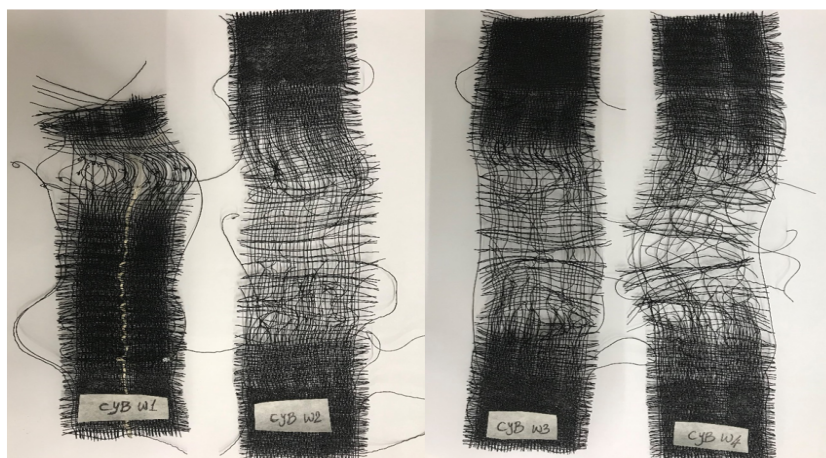
Figure 5.21: CYB warp specimens after failure.

On the other hand, weft specimens portrayed a typical open-mesh fabric failure behavior, as seen during the calibration tests, where the force measured gradually increased until a breaking point was obtained. Maximum load's average arithmetic mean was calculated at 721.73 N corresponding to an average 29.6% elongation.
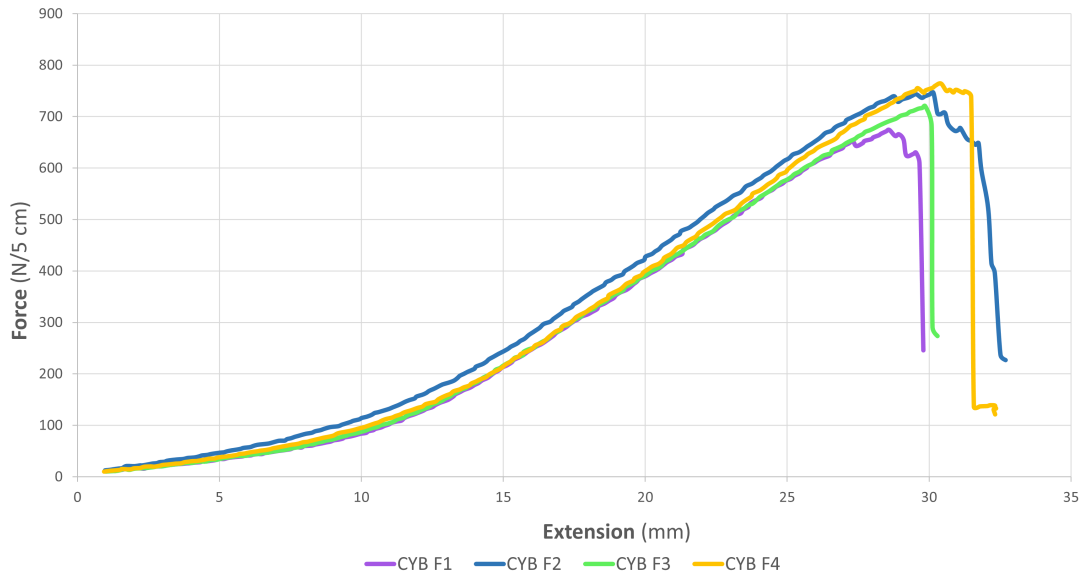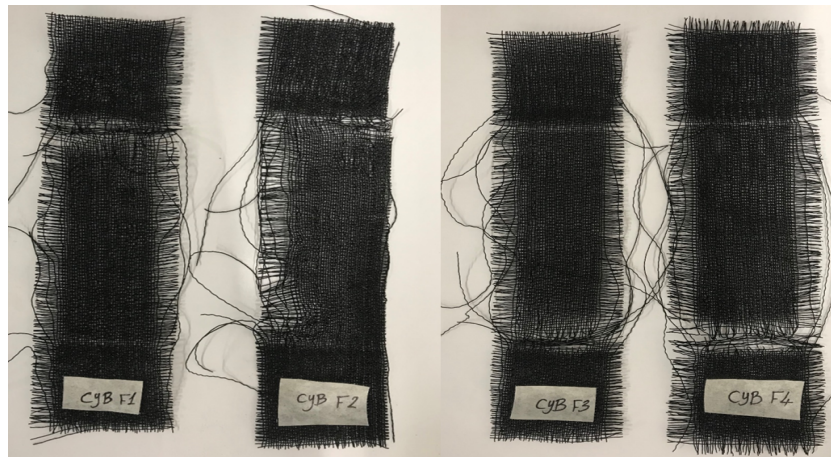

Figure 5.22: CYB weft specimens behavior under tension.

Figure 5.23: CYB weft specimens after failure.

Table 5.6: 2/2 Broken Twill specimens' specifications & test results.

General Info	Weave specifications			Test samples criteria					
Specimen Name	Weave Pattern	Warp density (yarns/cm)	Weft density (yarns/cm)	Dimensions (cm²)	Initial length (cm)	Extension (mm)	Elongation %	Failure Load (N/5cm)	Extension Rate (mm/min)
CYB W1	Plain weave	12	10	5×20	10	**	**	**	10
CYB W2	Plain weave	12	10	5×20	10.15	114.3	112.6	750.39	10
CYB W3	Plain weave	12	10	5×20	10	99.1	99.1	713.00	10 and 20
CYB W4	Plain weave	12	10	5×20	10	101.3	101.3	703.33	20
CYB F1	Plain weave	12	10	5×20	10	28.6	28.6	674.13	10
CYB F2	Plain weave	12	10	5×20	10	29.8	29.8	741.85	10
CYB F3	Plain weave	12	10	5×20	10	29.9	29.9	720.18	10
CYB F4	Plain weave	12	10	5×20	10.05	30.4	30.2	750.74	10

** Faulty test.

Flat rPET Fabric

The CoatYarn-monofilament weave configuration demonstrated a high strength deficiency accompanied with excessively large elongations in the warp direction, which is not befitting of a structural fabric. And so, a weave configuration with stronger yarns was handwoven from flat recycled polyethylene terephthalate (rPET) and tested for tensile strength using Instron 1122. Six specimens of flat rPET yarns were extracted from the woven samples to serve as control tests, all of which were in the warp direction only because the warp is the strongest direction and should give a quick yet decisive indication of the configuration's strength. Three of the specimens were plain-woven while the remaining three included plain woven areas in between cardboard SF replicas and a twill-woven backing fabric behind the replicas which serves to improve the strength as demonstrated by the calibration tests results.

During testing, only the first specimen (rPET W1) was performed at an extension rate of 100 mm/min and the breaking load recorded, yet it was not possible to record neither the extension nor the elongation due to a machine malfunction. The rest of the specimens, however, were extended at 10 mm/min with both force and extension recorded. Specimen rPET W1 achieved the highest strength of the three control specimens, influenced by the higher test speed. The average strength of the remaining two specimens amounted to 1924.28 N with an elongation of 13.7%. When comparing this strength value with the maximum theoretical calculated strength, a large strength reduction of 54% is measured.

Maximum theoretical strength = strength of a single yarn × No. of yarns per cm × width of the specimen in cm $= 84.3N \times 10 \times 5 = 4215N$

Naturally, the calculation neglects the effect of the weft yarns and the nonlinearity of the fabric on the fabric's strength which guarantees the highest theoretical strength that is impossible to attain; nevertheless, it still provides an indication of an underlying cause for strength reduction mainly due to the large discrepancy between calculated and measured strengths. It became evident from visual inspection that a tearing failure mechanism is the most probable cause behind this phenomena. All specimens experienced failure initiation at one of the clamps corners after which a tearing behavior was seen. This is further supported by the bulging behavior of the failed specimens to one side, in addition to the fact that plain weaves are comparatively weak against tear.

Specimens with insertions, nevertheless, showed a unique failure behavior where the specimens experienced shearing of the fabric as the twill backing started to differentially slide behind the solar insertions until the breaking load was reached via local rupture of floats. This is presumably due to the difference in crimp between the twill and plain areas; the plain areas compressed (i.e. decrimped) more at the longitudinal edges, or regions with higher stresses, triggering this shearing mechanism in the twill zone until jamming of the fabric took place. Once jamming is reached,

Figure 5.24: rPET W1-W3 specimens failure patterns

more force is transferred to the floats where jamming occurred leading to local yarn breakage, progressing to the adjacent yarns in a tear failure behavior. Specimens rPET SF W4 & W5 demonstrated this behavior resulting in an average strength value of 1672.63 N. Specimen rPET SF W6, on the other hand, showed the highest strength of 2181.87 N without shearing failure. This is most likely due to the seen rupture of some longitudinal yarns at the left edge of the specimen early on during the test influenced by the cutting during specimen preparation, hence releasing the stresses at this region such that the shearing action cannot take place. Ultimate failure occurred at the right hand corner of the upper clamp. Furthermore, an average elongation for the specimens was calculated at 12.6%, compared to the 13.7% for the control specimens, indicating an increase in stiffness caused by the presence of the stiffer twill weave zones.

Figure 5.25: Fabric shearing

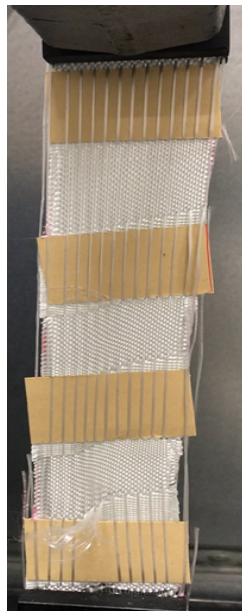**Figure 5.26:** rPET SF W4-W6 failure pattern

(a) Specimens without insertions

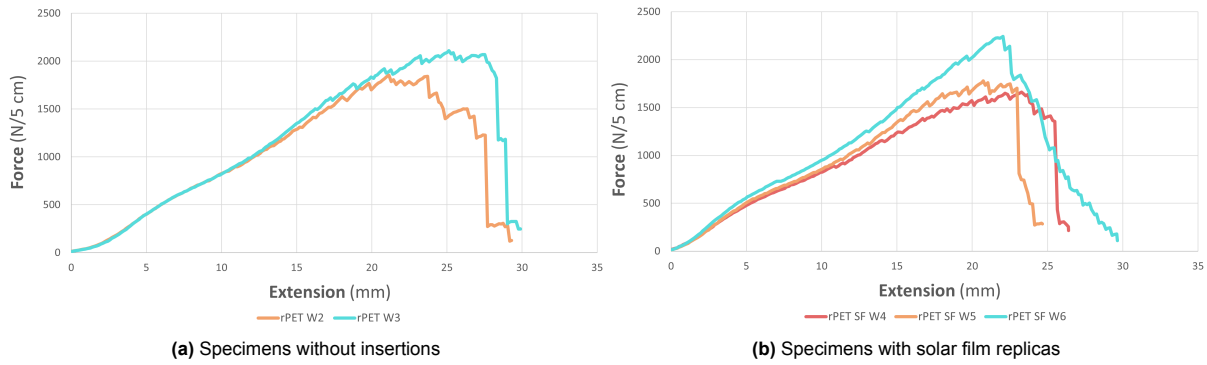**(b)** Specimens with solar film replicas

Figure 5.27: Flat rPET specimens' load-extension behavior.

Table 5.7: Flat rPET specimens' tests & results.

General Info	Weave specifications			Test samples criteria					
Specimen Name	**Weave Pattern**	**Warp density (yarns/cm)**	**Weft density (yarns/cm)**	**Dimensions (cm^2)**	**Initial length (cm)**	**Extension (mm)**	**Elongation %**	**Failure Load (N/5cm)**	**Extension Rate (mm/min)**
rPET W1	Plain weave	10	12.4	5×23.5	17.6	N/A	N/A	2114.22	100
rPET W2	Plain weave	10	12.4	5×23.5	17.6	22.3	12.7	1794.21	10
rPET W3	Plain weave	10	12.4	5×23.5	17.6	26.0	14.8	2054.35	10
rPET SF W4	Plain/twill back-layer	10	12.4	5×23.5	17.6	22.7	12.9	1629.53	10
rPET SF W5	Plain/twill back-layer	10	12.4	5×23.5	17.6	21.6	12.3	1715.73	10
rPET SF W6	Plain/twill back-layer	10	12.4	5×23.5	17.6	22.0	12.5	2181.87	10

Conclusion

Even though the rPET weave configuration exhibited higher strength than the CoatYarn-monofilaments weave, it still demonstrated a lower strength than required for a 3000 N/5cm type I fabric caused by the tearing failures. The solar cell insertions were also affected by the transfer of the compressive forces caused by shearing at the point of contact with the floats after fabric jamming. Thus, the weave structure will have to be fine-tuned further to resolve these setbacks.

Twisted rPET Fabric

A subsequent testing series involved six warp fabric specimens composed of hand-woven twisted rPET yarns of the same count, weave, and testing conditions as the previous tests. In this testing iteration, however, testing speed was increased to 100 mm/min and three of the specimens contained SF replicas from PET instead of cardboard paper. Yarn density in the weft direction also changed where it decreased for the specimens without insertions to 11 picks/cm and increased to 16.6 picks/cm for the specimens with replicas inserted. This difference in density is mainly due to the chosen weave configuration and the yarn type which has a limit to the distance it can be packed closer to the adjacent yarns during weaving. Additionally, the DIC system was used as well to better analyze the strain field given the incoherent nature of the fabric.


**Figure 5.28:** Twisted rPET specimens failure pattern.

Figure 5.29: Twisted rPET SF specimens failure pattern.

All specimens exhibited a substantial increase in failure load averaging 2692.4 N & 2545.21 N for the plain-woven specimens (excluding Twisted rPET W2) and the specimens with SF insertions (excluding Twisted rPET SF W1), respectively. Two of the specimens without the replicas portrayed a similar failure trend where the fabric failed at one of the clamps in the middle of the clamped width, whereas one specimen achieved the highest tensile load of 2959.46 N, following a shear failure pattern. The former specimens experienced high stresses at the corners of the lower clamp and as the lateral contraction increased with loading, the longitudinal yarns at the edges started to decrimp and slightly slip, causing a lesser increase in stresses at the edges compared to the higher stress build up in the middle zone. For the latter specimen, however, the result is rather considered unrepresentative of the strength. The strain field diagram for Twisted rPET W2 indicates a higher stress on one side of the clamp that initiated a shear failure pattern and thus, the higher failure load as plain weaves possess good shear resistance [6].
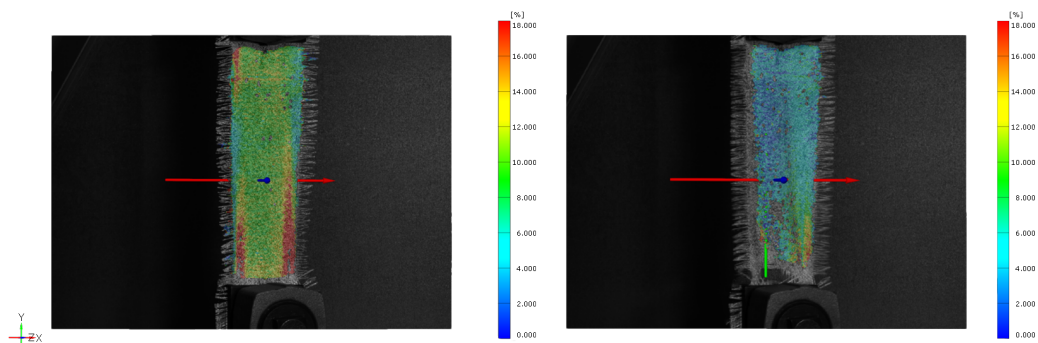
Figure 5.30: Strain field of Twisted rPET fabric specimens.
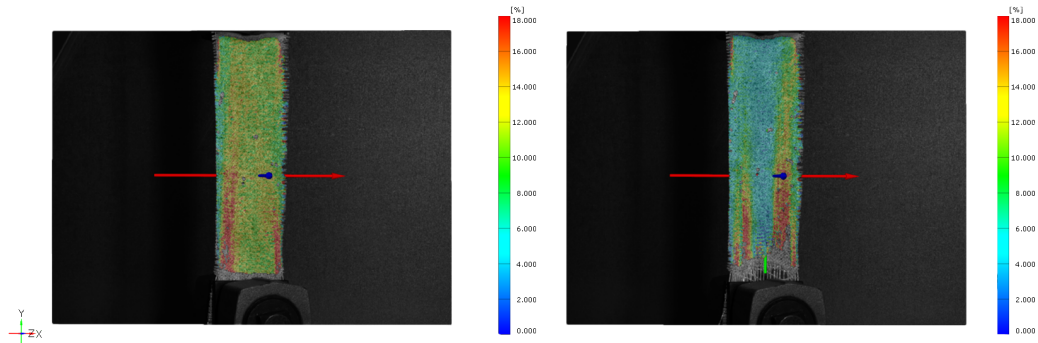
(a) Twisted rPET W1 strain field along the longitudinal direction at failure (left) & directly after failure (right).
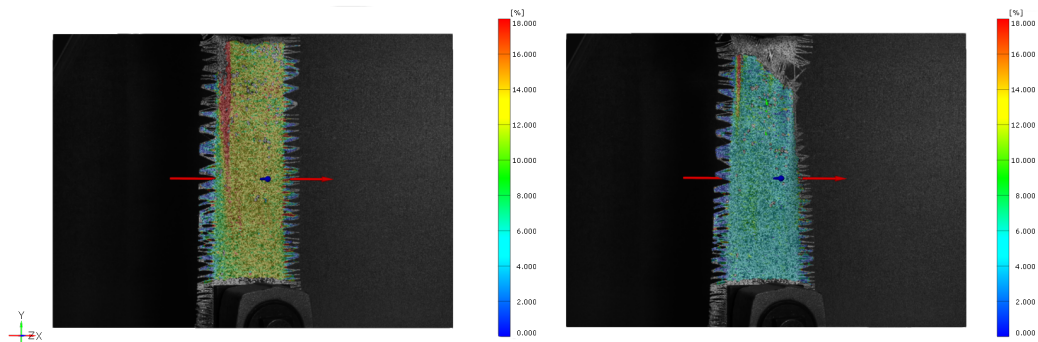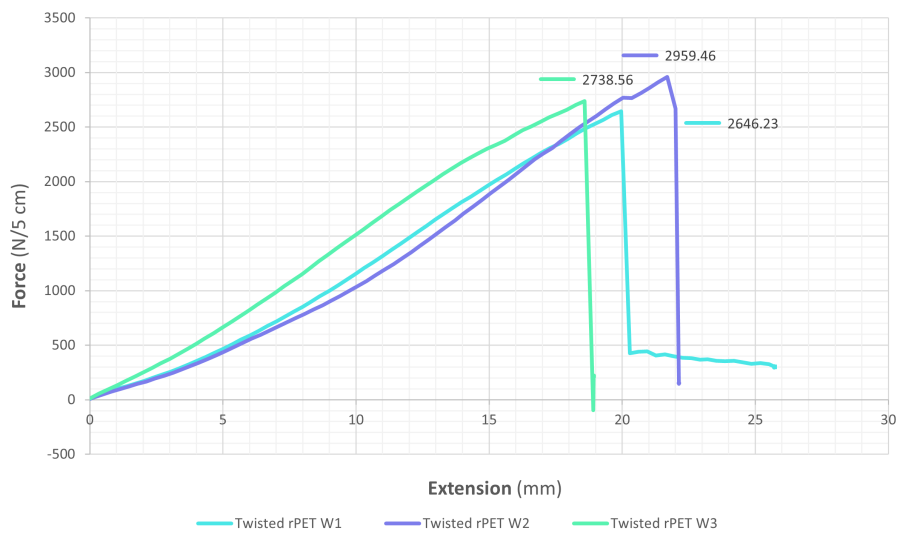

(b) Twisted rPET W2 strain field along the longitudinal direction at failure (left) & directly after failure (right).

(c) Twisted rPET W3 strain field along the longitudinal direction at failure (left) & directly after failure (right).

**Figure 5.31:** Load-extension graphs for Twisted rPET specimens W1-W3.

The specimens with PET replicas inserted also demonstrated a consistent failure load in two of the specimens, namely twisted rPET SF W2 & W3. Twisted rPET SF W1 experienced uniform slippage across the width where the weft yarns completely slipped over the longitudinal yarns with no visible breaking in longitudinal yarns. Therefore, it is disregarded as far as mechanical strength is concerned. Twisted rPET SF W2 fractured in a similar fashion to plain woven specimens W1 & W3 at the longitudinal yarns in the middle of the clamp but with the addition of a wrinkling effect in the twill zones that presumably aided the premature failure. Twisted rPET SF W3, on the other hand, exemplified a typical tearing behavior. Just as the load applied approached failure load, the specimen underwent shearing action momentarily and more stresses can be seen at the corner of the lower clamp where tear started propagation. Furthermore, all specimens showed a higher strain in the plain woven zones than in the twill zones until at least 1.5 kN which implies lesser stresses transferred to the solar insertions. All specimens also experienced out of plane curvature, in other words wrinkling, at some point during loading initiating at the twill SF backing.

Figure 5.32: Strain field of Twisted rPET fabric specimens with SF insertions.
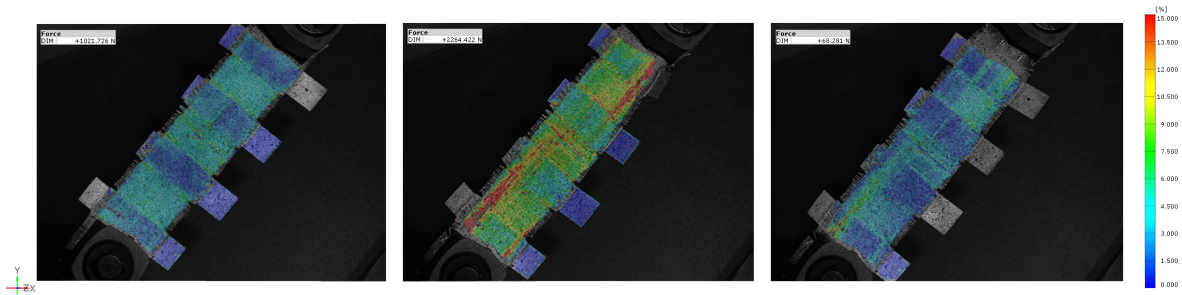
(a) Twisted rPET SF W1 strain field at approximately 1 kN load (left), at maximum load (middle), and after slippage (right).
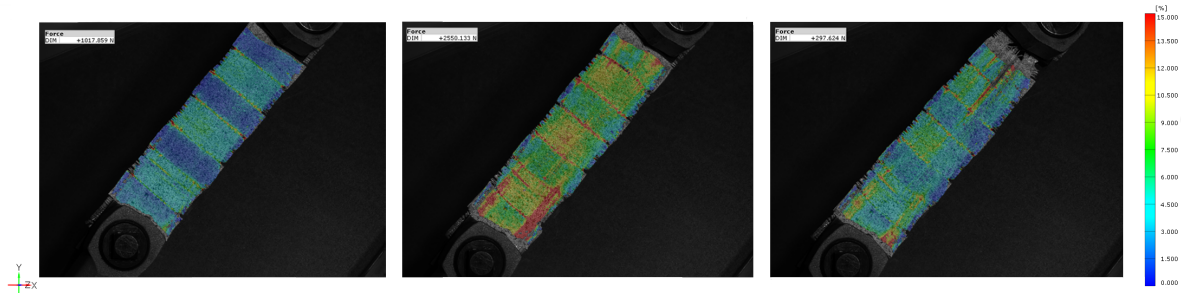
(b) Twisted rPET SF W2 strain field at approximately 1 kN load (left), at maximum load (middle), and after failure (right).
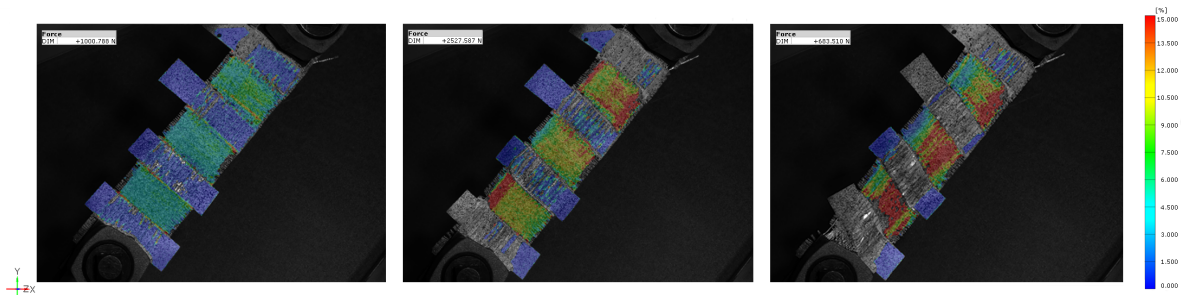
(c) Twisted rPET SF W3 strain field at approximately 1 kN load (left), at maximum load (middle), and during tearing failure (right).

Figure 5.33: Load-extension graphs for Twisted rPET SF specimens W1-W3.

Table 5.8: Twisted rPET test results

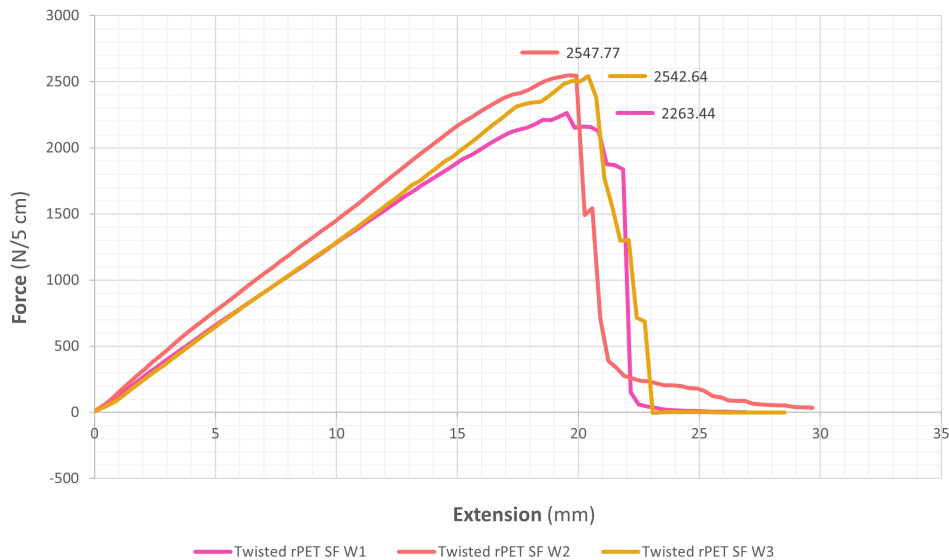| General Info	Weave specifications			Test samples criteria					
Specimen Name	**Weave Pattern**	**Warp density (yarns/cm)**	**Weft density (yarns/cm)**	**Dimensions (cm²)**	**Initial length (cm)**	**Extension (mm)**	**Elongation %**	**Failure Load (N/5cm)**	**Extension Rate (mm/min)**
Twisted rPET W1	Plain weave	10	11	5×24.5	15.0	20.0	13.3	2646.23	100
Twisted rPET W2	Plain weave	10	11	5×24.5	14.5	21.7	15.0	2959.46	100
Twisted rPET W3	Plain weave	10	11	5×24.5	14.6	18.6	12.7	2738.56	100
Twisted rPET SF W1	Plain/twill back-layer	10	16.6	5×25	20.1	19.5	9.7	2263.44	100
Twisted rPET SF W2	Plain/twill back-layer	10	16.6	5×25	18.5	19.9	10.8	2547.77	100
Twisted rPET SF W3	Plain/twill back-layer	10	16.6	5×25	20	20.4	10.2	2542.64	100

Conclusion

In essence, this weave configuration proves promising partly for the low discrepancy between the strength of plain and solar cell-engulfing specimens in combination with the low elongation values, and partly for the strain relief surrounding the SFs provided by the plain woven zones. Nevertheless, there is still a major loss of strength as seen with flat rPET weaves when compared with the maximum theoretical strength in the previous tests which is traced back to the slipping, wrinkling, and ultimately tearing behavior. Another drawback is the high probability for SF wrinkling as the applied load approaches failure load which may compromise the SF efficiency.

Twisted rPET Fabric Composite

The final fabric tests conducted were carried out on a composite fabric woven from twisted rPET yarns and monofilaments to examine the impact monofilaments have over the strength and elongation behaviors. In the warp direction, rPET yarns formed the main yarns and the monofilaments were inserted every three yarns while in the filling direction, only rPET yarns were used. During weaving, achieving equal tensioning between the two yarn types proved difficult. This is mainly due to stiffness difference which made the monofilament yarns consistently elongate, requiring multiple tensioning of the fabric; therefore, the resulting fabric developed loose areas and a curvature along the length. Six handwoven specimens, all in the warp direction, with a plain weave structure were tested. Three of the specimens incorporated PET films with a fabric backing layer. A speckling pattern was also applied to the specimens to allow for strain field measurements. Eventually, the specimens were stretched until failure at 100 mm/min.

Results demonstrated significantly lower failure load for the specimens without SF replicas with an average load of 1622.5 N/5cm. This is also considerably lower than the values from previous twisted rPET fabric tests. Specimens with replicas achieved an average of 2289.4 N/5cm which is 255 N less than that of their counterparts from the previous rPET tests; however, the elongation at break was higher for the former specimens (15%) compared to the latter (10.4%).

Table 5.9: Twisted rPET fabric-composite test results

General Info	Weave specifications			Test samples criteria					
Specimen Name	**Weave Pattern**	**Warp density (yarns/cm)**	**Weft density (yarns/cm)**	**Dimensions* (cm²)**	**Initial length (cm)**	**Extension (mm)**	**Elongation %**	**Failure Load (N/5cm)**	**Extension Rate (mm/min)**
Twisted rPET+MF W1	Plain weave	10	11	5×19	19.2	26.4	13.7	1576.26	100
Twisted rPET+MF W2	Plain weave	10	11	5×19	19.2	26.2	13.7	1535.80	100
Twisted rPET+MF W3	Plain weave	10	11	5×19	19.2	28.4	14.8	1755.41	100
Twisted rPET+MF SF W1	Plain/twill back-layer	10	16.6	5×19.2	19.4	29.2	15.1	2472.97	100
Twisted rPET+MF SF W2	Plain/twill back-layer	10	16.6	5×18.2	18.4	28.5	15.5	2200.29	100
Twisted rPET+MF SF W3	Plain/twill back-layer	10	16.6	5×20.4	20.7	30.1	14.6	2194.79	100

* Length measured is gauge length.
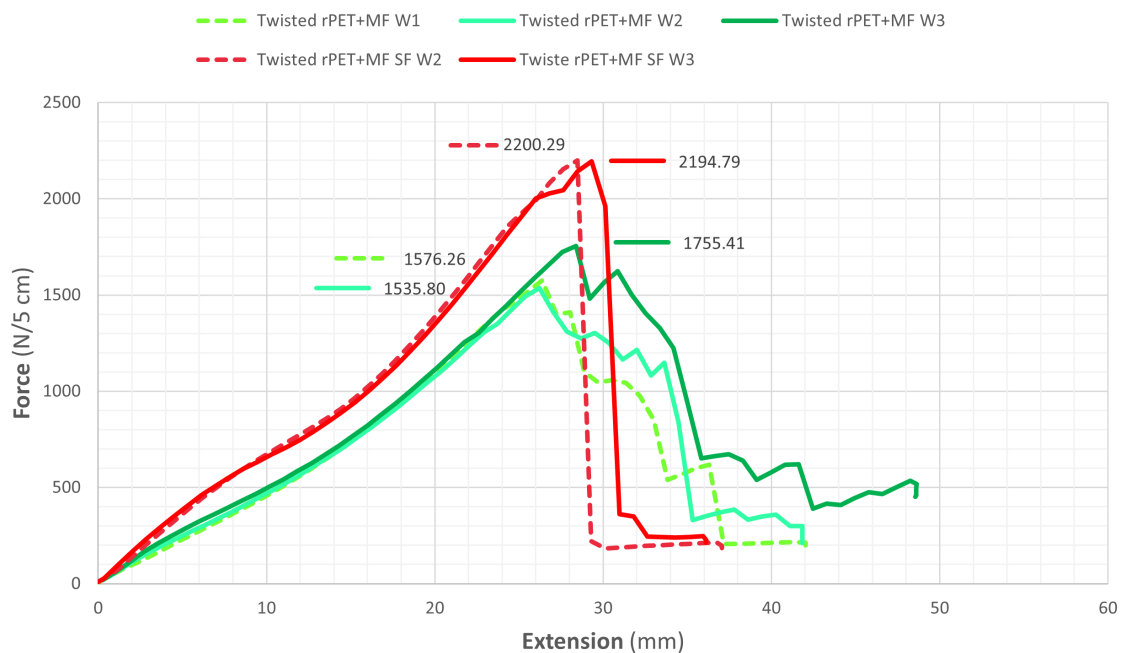
**Figure 5.34:** Load-extension graphs for Twisted rPET+MF SF specimens.

Twisted rPET+MF specimens all showed failure in the middle of the specimen while Twisted rPETMF SF specimens failed at the borders of solar cell segments, except for Twisted rPET+MF SF W1 where failure occurred at the backing fabric behind the SF replica close to the clamp. The strain diagrams at peak load and after failure are given below.

Figure 5.35: Strain field of Twisted rPET fabric composite specimens.
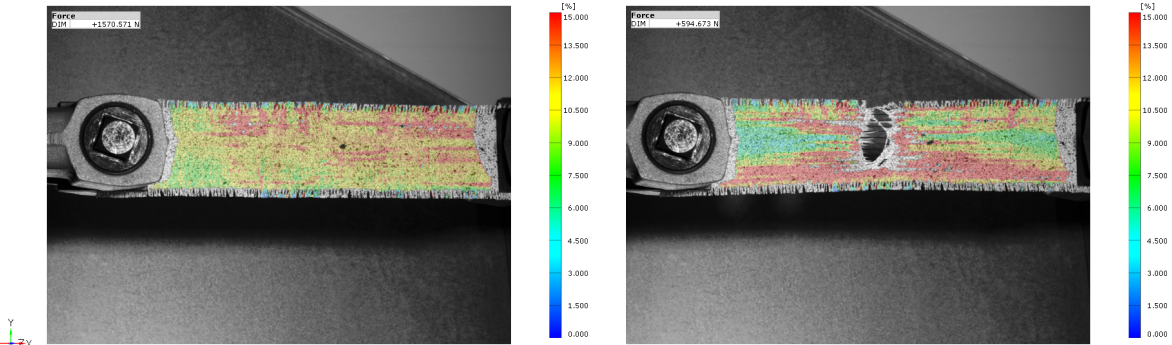
(a) Twisted rPET + MF W1 strain field along the longitudinal direction at maximum load (left) & after failure (right).
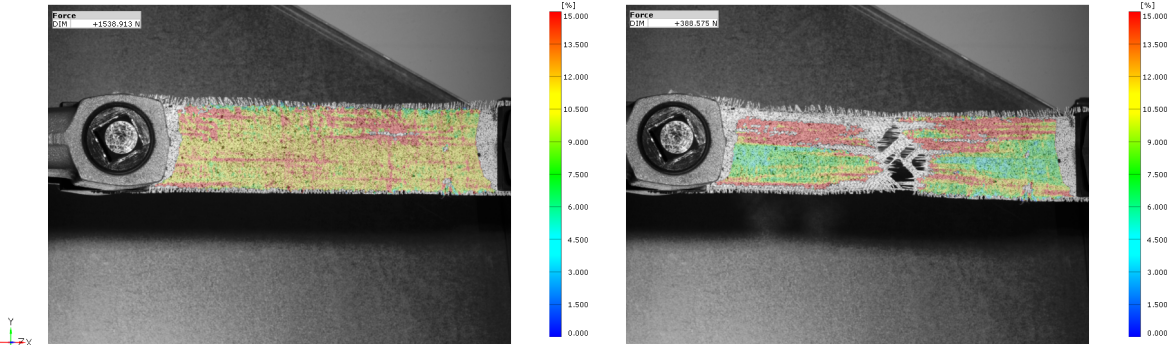
(b) Twisted rPET + MF W2 strain field along the longitudinal direction at maximum load (left) & after failure (right).
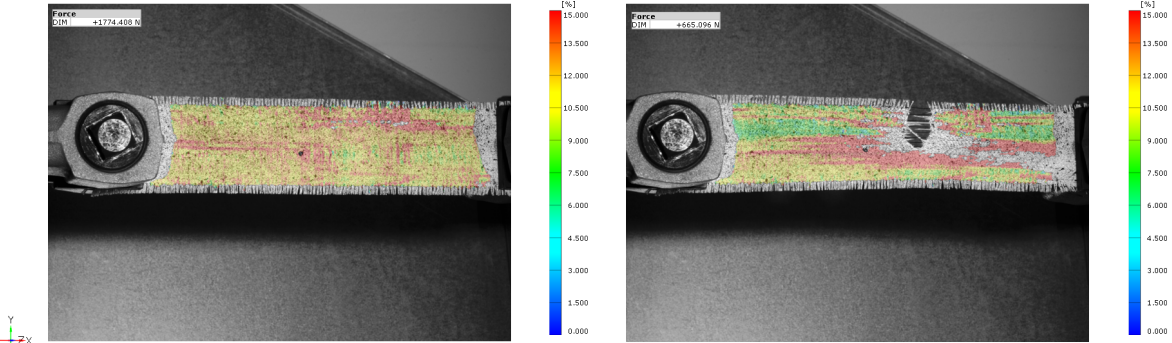
(c) Twisted rPET + MF W3 strain field along the longitudinal direction at maximum load (left) & after failure (right).

Figure 5.36: Strain field of Twisted rPET fabric composite specimens with SF insertions.

(a) Twisted rPET + MF SF W1 strain field along the longitudinal direction at maximum load (left) & after failure (right).
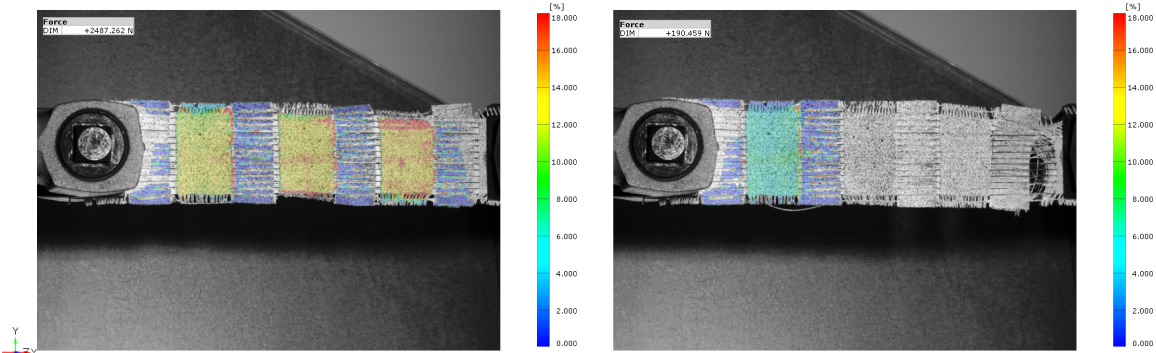

(b) Twisted rPET + MF SF W2 strain field along the longitudinal direction at maximum load (left) & after failure (right).
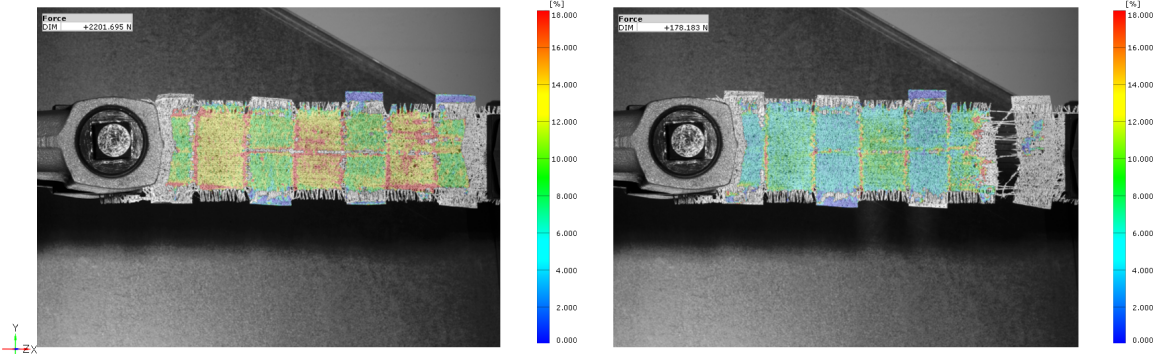

(c) Twisted rPET + MF SF W3 strain field along the longitudinal direction at maximum load (left) & after failure (right).
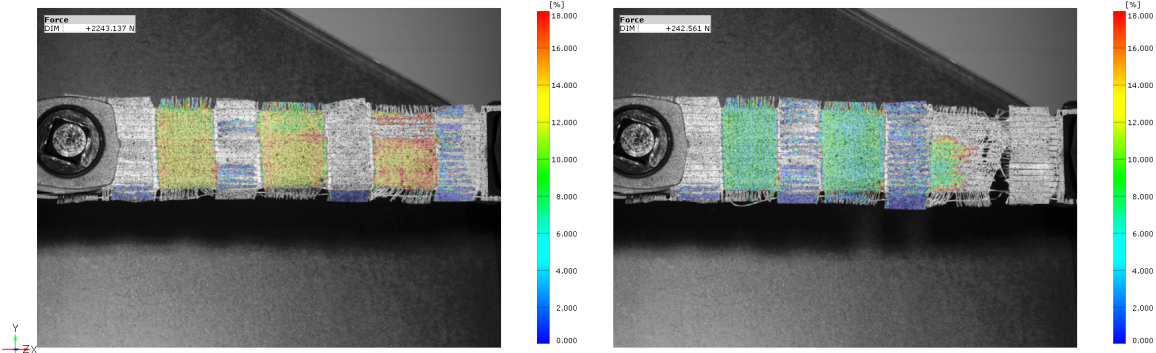
Conclusions

- The lower strength of the Twisted rPET+MF specimens is most probably due to two main reasons: firstly, the different tensioning during weaving created looser areas and caused the fabric to become curved. This meant that during testing some warp yarns were tensioned more than others. Secondly, the frequency of monofilament yarns might have separated the rPET yarns collective behavior when resisting load. In other words, the monofilaments being this close made the rPET yarns bundle in smaller groups such that tearing might occur.

- For the Twisted rPET+MF SF specimens, the failure load was less than that of Twisted rPET SF partly because of the monofilaments present which replaced the stronger rPET yarns and partly because of the uneven tensioning encountered in weaving. The backing-layer fabric behind the PET inserts helped stabilize the fabric and reduce the effect of the uneven tension during weaving which explains the minor reduction in strength compared to Twisted rPET SF specimens.

- In general, it can be concluded that the monofilament yarns largely influence the weaving process, and in turn, causes the loss of strength. Additionally, adding monofilaments to the twisted rPET configuration in the same frequency (i.e., every 3 yarns) reduces the strength of the fabric by 10%, but increases the elongation at failure by 4.6%.

5.2.3. OPV Module Tests

The initial test setup consisted of the Mark-10 uniaxial tensile machine and an LED Panel, having a matching light spectrum with that of the PV module, for the lighting. Logging of the current and voltage was performed by an arduino board. The OPV strips were first soldered with wires at the contact points then mounted onto the test rig using wide clamps where the contacts protruded from the clamps. This limited the shading of the cells. Wider clamps also enabled access to the contact wiring and avoided the clamping of the contacts, hence, avoiding any possible contact failure during loading. The LED panel was placed 35 cm from the PV strip to achieve a constant light coverage over the active area while limiting any temperature effects. Prior to the start of the tensile test, the maximum power point (MPP) was found using a rheostat. The idea is to have this point as the reference point for the current and voltage measurements so that the effect of tensile loading on both values can be examined.
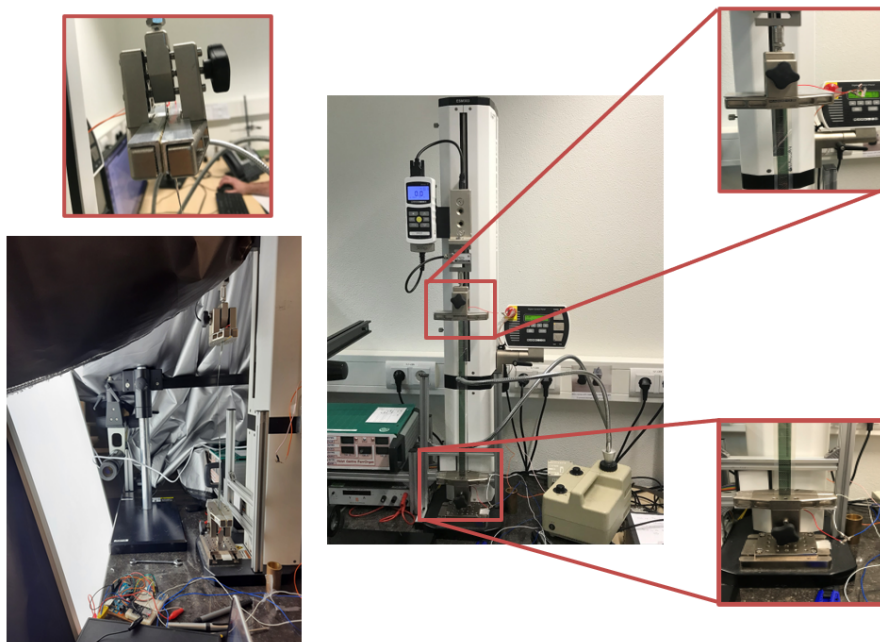

Figure 5.37: Test setup of the 1st OPV module test.

Results showed excessive slippage beyond the 200 N margin thus, mechanical failure was not reached. Different clamps were applied to prevent the slippage but the outcome was the same. Additionally, the current and voltage measured had very low values which could not be used to identify failure trends. This is because artificial light had a much lower irradiance value than that used under standard testing conditions (i.e. 1000 W/m^2) which meant the LED panel could not stimulate the OPV strip enough to see a trend.

The second solar cell test series employed a different setup and test protocol; two construction lamps were used for the light source providing 700 W/m^2 light intensity each. Instron 5566 tensile rig with pneumatic clamps was used for the mechanical testing. Similar to the previous test, wires were soldered to the strips' contacts and connected to the arduino board for electrical measurements; however this time, a potentiometer was added that can be manually adjusted to vary the resistance. By increasing the resistance, the open circuit voltage (V_{OC}) can be obtained, and by decreasing the resistance, the short-circuit current (I_{SC}) can be measured. Somewhere in between lies the maximum power point (MPP) which could also be identified. The approach was to either set the potentiometer at the maximum power point (MPP), such that the impact of the tension can be seen on the V_{MPP} and I_{MPP} values, or at the I_{SC}. The load at electric failure is then identified at the time the current (I_{MPP} or I_{SC}) drops to zero since the solar cells are connected in series, where current is the determining factor for electric failure (refer to section **2.2.3**). In order to mount the specimens into the clamps, two complete cells had to be covered at both ends, resulting in low current and voltage values. This could be mitigated by increasing the light intensity through reducing the distancing between the lamps and the test specimen. Therefore, the electrical-logging approach used depended on how high the V_{MPP} and I_{MPP} could be achieved with a specific light distancing. It should be noted that if the lamps are close to the specimens, the specimen's temperature will rise and this will affect the results.

**Figure 5.38:** Test setup of the 2nd OPV module test.

Tests were performed on five OPV modules at an extension rate of 50 mm/min. Only for the first specimen, the I_{MPP} and V_{MPP} were measured reaching as high as 2.6 mA and 3.24 V at the start of the test. The I_{MPP} was not high enough to allow a good representation of the degradation trend; consequently, the I_{SC} trend was measured for the remaining tests. For the third OPV specimen, the lamps were moved 15 cm closer to the specimen to increase the I_{SC} value further. The temperatures of the specimens were checked at the start and end of each test using an infrared thermometer to ensure a uniform temperature range across all tests. After carrying out the tests, the results from the current-time measurements and the force-extension measurements were correlated using the time stamps to determine the load at electric failure. The results mostly showed a plastic mode of failure where viscous deformation of the PET material took place at the yielding point followed by progressive elongation and a gradual increase in tensile force. All specimens exhibited delaminations between the active material and the PET after the yielding. OPV strip 3 experienced a rapid decline in measured force and the specimen showed excessive necking and out-of-plane buckling at the area closest to the lamp; this clearly indicates that the temperature influenced the mechanical failure due to the shorter distance in between. OPV strip 5, on the other hand, experienced a sudden rupture at 566 N beyond

the yield point which is most likely due to the uneven PET width on both sides of the active material. Furthermore, the electric failure load was found somewhere after the yielding phase at a force larger than 550 N, indicating that the delamination between the active material and the PET is most probably the cause of failure.

The results are summarized in the following table:

Table 5.10: Electo-mechanical test results

Specimen Name	Mechanical data					Electrical data		
	Gauge length (mm)	Extension at yield (mm)	Force at yield (N)	Max. Extension (mm)	Max. Force (N)	Current (mA)	Voltage (v)	Electric Failure Load (N)
OPV strip 01	340	12.1	563.23	80.0	650.46	2.60	3.24	555.77
OPV strip 02	340	11.1	615.99	80.0	666.05	3.11	-	594.87
OPV strip 03	340	9.0	660.87	31.8	561.43	2.80	-	634.51
OPV strip 04	340	11.1	594.20	80.0	644.30	2.69	-	574.87
OPV strip 05	340	11.4	682.13	12.3	566.42	2.69	-	681.30
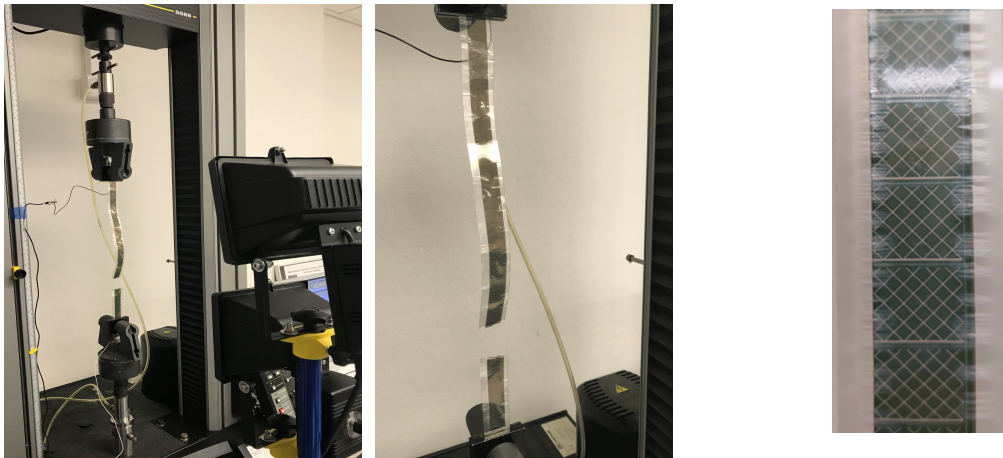
Figure 5.39: Rupture of OPV strip 05.

Figure 5.40: Delamination between encapsulant and active material.
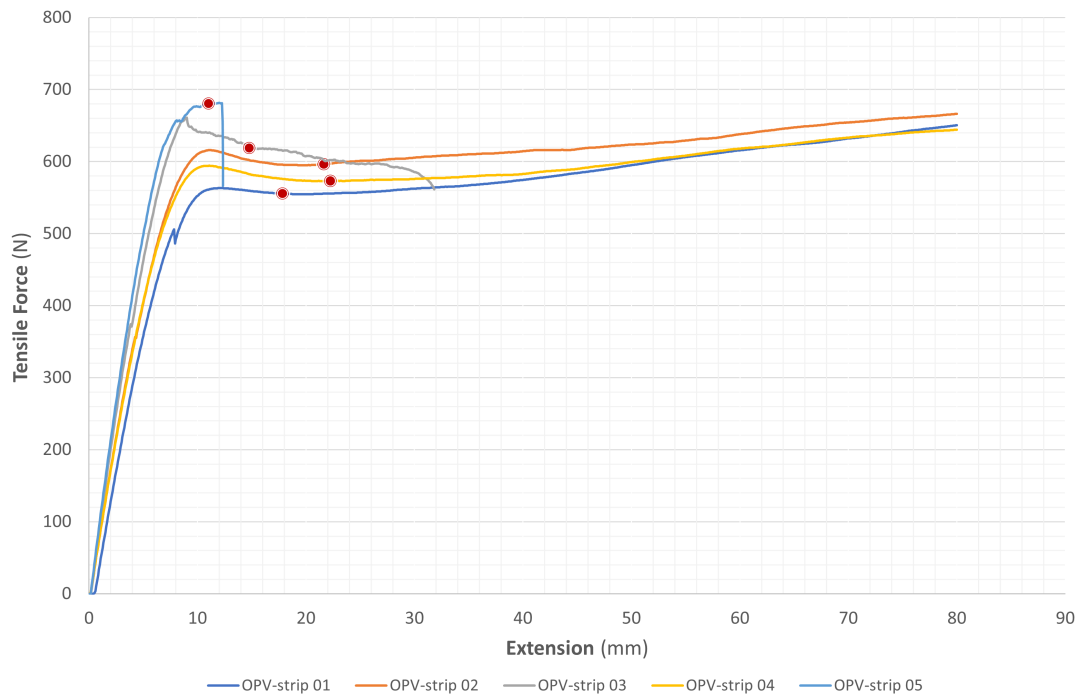
Figure 5.41: OPV specimens tensile behavior; red points indicate points of electric failure.

Conclusions

- Temperature has a high impact on not only the solar cells but also the mechanical failure.

- Large variations in encapsulant dimensions induces rupture failure.

- Electric failure happens after yielding (at ≈ 4.7%) and above 550 N.

- Tensile loading of the OPV module under high temperatures exceeding 65°C results in an excessive out-of-plane deformation in the encapsulant. The unevenness in the encapsulant dimensions was also found to cause rupture failure in a specimen at approximately 670 N.
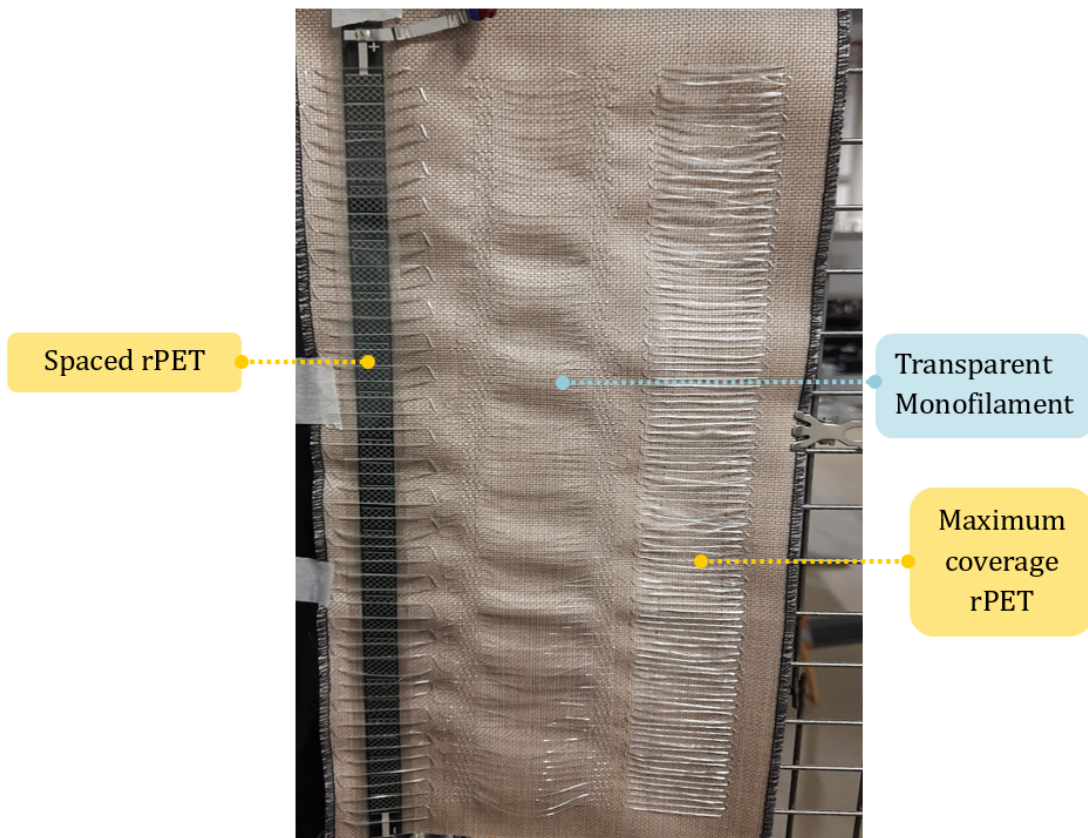
5.2.4. Float Yarn Test

In order to address the shading effect caused by the float yarn type and density, flat rPET yarns and monofilament yarns were used to identify the least impact on the solar cell modules' efficiency. Testing components consisted of a fabric piece with different float yarns, an OPV module, an LED wall solar simulator producing 1 sun of irradiance (1000 W/m^2), and a Keithley 2420 source meter for electrical measurements. The test was carried out by weaving three float segments into a fabric, one segment from transparent monofilament yarns and two others from flat rPET. The density of the monofilament yarns was equal to that of one of the rPET float sections, whereas the density was increased for the other rPET section (as shown in **Figure 5.42**). The fabric was attached to a metal frame and an OPV sample was inserted, first, into the float section with high density rPET yarns. Then, the frame was made to face the LED wall and electrical measurements were taken. This process was repeated using the same OPV sample for the monofilament floats section and for the spaced rPET section, in that order; however, in between the two measurements, the electrical behavior of the plain sample without floats was measured to determine whether photodoping took place.

**Figure 5.42:** Fabric cloth used for the float yarns test.

Figure 5.43: Float yarn test setup showing the solar wall (left) & the metal frame with the specimen attached (right).

Prior to the test start, efficiency measurements were performed on the same OPV sample used in the tests to benchmark the initial behavior. Subsequent test measurements were each performed twice and the average values calculated. The most relevant results are summarized below according to the chronological order of testing:

Table 5.11: Float yarn test results

	Original sample	Max. coverage rPET	Transparent Monofilaments	No Floats	Spaced rPET
Pmax (W)	0.127	0.130	0.146	0.170	0.146
Eff (%)	2.164	2.224	2.495	2.897	2.491
Rseries (Ohms.cm^2)	42547.4	40540.7	36243.4	31828.8	34796.6

It was seen that with maximum rPET coverage, the OPV efficiency slightly increased and the series resistance decreased, when compared to that of the original sample. The efficiency increased again for the monofilament floats by 0.33% followed by a further increase in the intermediate test where no floats were used; the efficiency was measured 0.73% higher than for the original sample. At this point, it becomes clear that the sample underwent photodoping which caused the efficiency to continue increasing and so interfered with the test results.
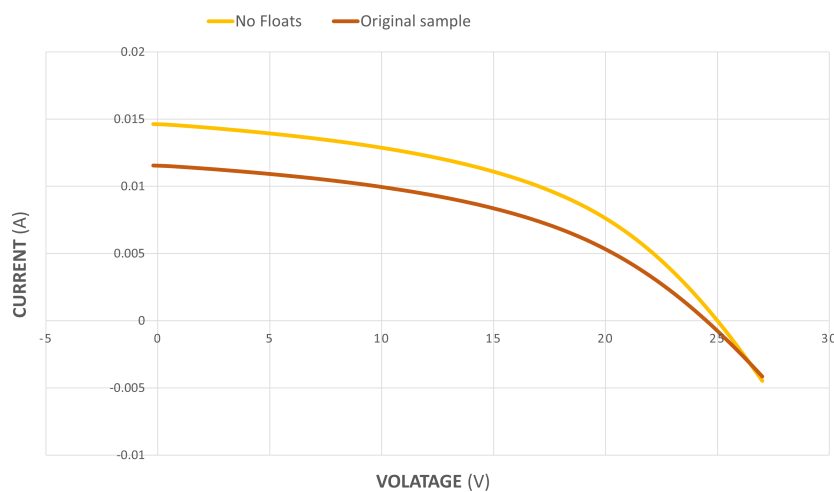
Figure 5.44: I-V curve showing the photodoping effect.
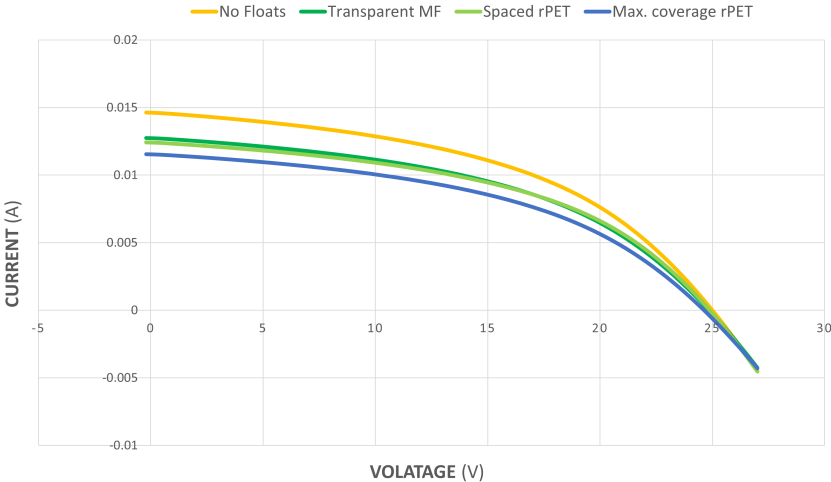
Figure 5.45: I-V curve comparison.

Conclusion

The test results prove inconclusive due to the light-soaking effect the OPV strip experienced; however, it could still be argued that the less dense rPET floats reduce the efficiency by 0.4% given that the efficiency measurement for the less dense rPET yarns was performed directly after the measurement without floats.

6

Conclusions & Recommendations

6.1. General Conclusions

The research presented herein was set out to explore the research question of whether integrating encapsulated-solar film into textiles through the weaving process could yield a load-bearing structural fabric that can generate energy for implementation in the textile architecture domain. The main aim was to construct a modular fabric configuration with a fabric strength of 3000 N/5cm in both weave directions without compromising the OPV module's performance; however, to adequately answer the research question, all three pre-defined objectives pertaining to the strength, active material area coverage, and electrical output need to be considered.

From mono-axial strip tests, results demonstrated that a plain woven fabric consisting of recycled polyester yarns and OPV modules can achieve a tensile strength of 2500 N/5cm in the warp direction without stress transfer to the solar film, and when monofilament yarns were added, the achieved strength dropped to 2200 N/5cm. Therefore, both configurations proved insufficient to meet the 3000 N/5cm strength objective. Similarly, the active area within the OPV module resembles 26.4% of the developed fabric module area (50×50 cm^2) and is capable of producing 6.8 watts of power per 1 m^2 of fabric under STC which prove to be less than the required 50% and the 20 W/m^2 objectives, respectively. It can, therefore, be concluded that a solar structural textile is not achievable with the current configuration; however, by modifying the fabric components and the weaving process, a functional fabric configuration that meets the objectives seems within reach. This research has thus, provided several directions that could help future researchers/textile designers reach the proposed target values.

Furthermore, the following main conclusions pertaining to failure behavior, measurement methods, or design can be extracted based on the test type performed:

I. Uniaxial tensile fabric tests:

A. Failure behaviour

- Fabric composites woven from coated yarns and monofilament yarns exhibit an open mesh structure and a two-step ductile failure behavior in the direction where the two yarns are used. The stiffer PES/TPU yarns fail first at a certain peak load followed by monofilament extension where a second peak load is reached, a failure behavior induced by the difference in yarn stiffnesses. The resulting fabric develops large elongations at the peak loads and proves difficult to equally stress.

- Composite 2/2 twill weaves made of TPU-coated polyester yarns and monofilaments showed equal strengths in the warp and weft directions compared to plain weaves.

- PES/TPU fabrics demonstrated insufficient tensile strength, large elongations, and dimension instability, all of which thwart their field application.

81

- Fabrics woven from rPET yarns attained higher strengths without causing strain in the solar module, reaching a failure load of 2500 N/5cm measured in the warp direction when twisted yarn versions were used.

- Adding monofilament yarns to the rPET fabric reduced its strength directly, by replacing rPET yarns, and indirectly, through the weaving process to 2200 N/5cm. They also increased the elongation at break in the weave direction to which they are added. Fabrics with monofilaments do not reach complete separation at failure due to their large elongation capacity that enables them to elongate once the rPET yarns break.

- From the DIC measurements and visual inspections of the failure patterns, high contact stresses are found to occur at the solar film border in warp specimens ultimately leading to failure at these zones. In the weft direction, failure typically occurs at the ends of the solar film. Both outcomes indicate that the solar film does not strain under loading.

- The local failure zones found at the solar film replicas are responsible for premature strength failure in the fabric.

- Specimens woven on a hand-loom exhibit a lower fabric strength than actually possible, especially when flat fibrous yarns, such as the flat rPET, are used, or when multiple yarns with different stiffness properties are used. This is because of the difficulty in maintaining equal tensioning among yarns and preventing slippage during weaving.

B. Measurement methods

- Using Digital Image Correlation (DIC) to create strain field measurements for PES/TPU fabrics is not suitable as it possesses an open-meshed structure and proves difficult when applying a speckling pattern without having voids, yet it can be used for the denser rPET fabrics while ensuring multiple paint layers fill any apparent voids.

- The current strip tensile testing procedures stipulated in EN ISO 13934-1 cannot be fully used to verify the tensile strength of composite fabrics or fabrics with solar modules; the specimen dimensions specified by the test are insufficient to include a representative fabric test specimen. In case yarns with different stiffness are included in uncoated fabric, a fixed test speed is not sufficient to verify the failure behavior, instead both low and high extension rates must be used.

C. Design suggestions

- For textile architecture applications requiring relatively lower tensile strength values and could accommodate a fabric tensioned only along the warp, such as in facades, the twisted rPET fabric could be used in design using a warp direction strength of 2200 N/5cm, whereas the same fabric with added monofilament yarns could be designed using 1900 N/5cm warp strength; this is assuming appropriate conductive yarns and proper electric connections are used. Appropriate design factors should then be applied.

II. OPV module tensile tests:

A. Failure behaviour & Design suggestions

- Mechanical failure load of the OPV module and its force-elongation behavior are mainly influenced by the encapsulant's material strength, dimensions, and temperature during stretching.

- The solar module can sustain 550 N tensile force and 4.7% straining prior to complete electric failure which suggests that the current OPV modules without flexible interconnects should not be designed to carry load, given the large difference in strength and elongation between the module and the fabric. Additionally, the module's contacts can only be fixated into the fabric as long as the strain and tensile force do not exceed the given limits in the final application.

B. Measurement method

- Electro-mechanical testing performed using standard tensile loading equipment, a high irradiance light source, and an Arduino board is a possible option to determine both the mechanical failure load and electric failure load of an OPV module; nevertheless, this is only valid if the temperature of the sample is controlled and the consistency of the light source's irradiance is guaranteed. The results did not indicate the progressive electric failure trend under loading therefore, the load at which the largest loss in performance occurs was not accurately determined.

6.2. Discussion

Through an extensive investigation of key principles in the fields of textile architecture, flexible photovoltaics, and fabric design, a proposal is presented for a modular fabric design configuration consisting of three yarn types and an OPV module that can support the dual-function of the fabric. The proposed design introduces a novel solar cell-to-fabric integration method that utilizes the weaving process to create woven solar fabrics suitable for load-bearing textile architecture applications. Multiple parameters were identified within the fabric module to generate different structural properties, aesthetic appearances, and allow for scalability. Additionally, the work performed herein presents three testing procedures that can be used to verify a fabric layout that utilizes woven encapsulated OPV cells/modules using the identified module parameters; namely, uniaxial tensile strip tests to determine the tensile strength of the fabric composite, uniaxial tensile tests with electrical performance logging to identify the electric failure load for OPV modules, and electrical performance test to determine the float yarn's density and material with the least shading effect. As a result, the findings constitute a verification scheme for the strength, failure behavior, and electrical performance identification for further design optimizations.

Nevertheless, several limitations can be identified in the undertaken methods and design choices:

- The highest achieved strength results were based on testing only performed on warp specimens which is insufficient for bi-axially tensioned architecture textiles.

- Hand-weaving introduced unequal tension within the test specimens, causing slippage or premature failure; therefore, higher fabric strength could not be achieved.

- Strength tests mainly focused on the main areas providing the fabric's strength and since the electrical connections design is outside of this research's scope, the areas with conductive yarns were not included in strength tests. Although the failure load and behavior of the fabric in those areas are less likely to diverge from the remaining fabric, as implied by the fabric including TPU and monofilament yarns, this test would help examine the strength of the connections.

- The fabric module dimensions and layout were largely influenced by the OPV module's shape and dimensions. Hence, the current fabric is not suited for using solar films of different dimensions.

- Additional verification tests of the wide clamps setup and its impact on the results were not performed.

- For the electro-mechanical tests, clamping of the specimens without covering the solar cells could not be achieved. As a result, the progressive degradation of performance with tension could not be accurately determined. Moreover, temperature measurements using an infrared thermometer also suffered a loss of accuracy as the measurement had to be performed at a distance causing the heat radiating from the lamps to interfere with the results.

- The floats' effect testing procedure did not yield useful results due to the light-soaking effect experienced by the samples.

6.3. Recommendations

Based on the aforementioned conclusions and shortcomings per test type, the following recommendations are proposed for the further development of the structural solar fabric design and the testing methods:

I. Fabric Design

- Since the main failure cause lie in the contact stresses at the borders or corners of the SF, opting for a stronger yarn for the entire fabric to increase the strength would be inefficient (unless higher fabric strength than 3000 N/5cm is desired). Reinforcing the failure zones locally through the weave structure should be a more efficient option.

- Studying the performance of the different weave structures using geometrical or analytical models is also recommended to increase the strength of the fabric and to allow for integrating differently shaped solar modules.

II. Testing & Measurement Methods

A. Uniaxial tensile fabric tests:

- Fabrics with monofilament yarns were shown to be highly susceptible to elongation indicating that the rate of extension applied in the tensile tests will influence the strength results; thus, the effect of both low speed and high speed tensile tests should be checked.

- Testing the strength of rPET fabrics in the weft direction is recommended.

- Twisted rPET fabric composite tests should be repeated using specimens woven in a power loom to eliminate the weakening factors induced by hand weaving and acquire a more plausible strength indication.

- Strength tests must be performed at the electrical connection areas to verify the behavior of both the conductive yarns and the electrical connecting elements.

B. OPV module tensile tests:

- As the accuracy of pinpointing the tensile force corresponding to electric failure in the module depends on the simultaneous measurement of time, more precise testing time stamps could be used.

- A higher sensitivity sensor could be used with the arduino board for more accurate current measurements.

- To prevent the shading of solar cells in the OPV module by the clamps, adjusted clamps will need to be used or the test procedure changed.

- The infrared thermometer used for the temperature measurements could be replaced with an areal field temperature tool for more reliable results.

C. Float yarn shading tests:

- To circumvent the impact photo-doping has on the test, the same specimen should not be continuously used for all the float variations one after the other, but instead, the OPV film's performance should be measured before each insertion iteration to provide a benchmark for assessment.

References

[1]   *Al Bayt Stadium in giant tent completes ahead of World Cup in Qatar*. URL: `https://www.dezeen.com/2021/12/06/al-bayt-stadium-world-cup-qatar-giant-tent/`.

[2]   H Asadi et al. "Investigations into the Long-term Behaviour of Fabrics. VIII International Conference on Textile Composites and Inflatable Structures STRUCTURAL MEMBRANES 2017 IN-VESTIGATIONS INTO THE LONG-TERM BEHAVIOUR OF FABRICS HASTIA ASADI*, JÖRG UHLEMANN*, THOMAS STEGMAIER †, VOLKMAR". In: *VIII International Conference on Textile Composites and Inflatable Structures*. 2017, pp. 217–228. ISBN: 978-84-946909-9-0. URL: `http://www.uni-due.de/imlWebpage:http://http://www.ditf.de/`.

[3]   Hastia Asadi, Jorg Uhlemann, and Natalie Stranghoner. "Uniaxial Strip and Grab Test Methods for Tensile Testing of Architectural Fabrics". In: *Proceedings of the TensiNet Symposium 2019* June (2019).

[4]   Md Asaduzzaman et al. "Effect of Weave Type Variation on Tensile and Tearing Strength of Woven Fabric". In: *Technium: Romanian Journal of Applied Science and Technology* 2.6 (2020), pp. 34–40. DOI: `10.47577/technium.v2i6.1409`. URL: `www.techniumscience.com`.

[5]   Chiara Bedon and Vlatka Rajčić. "Textiles and fabrics for enhanced structural glass facades: Potentials and challenges". In: *Buildings* 9.7 (2019). ISSN: 20755309. DOI: `10.3390/BUILDINGS9070156`. URL: `www.mdpi.com/journal/buildings`.

[6]   B. K. Behera and P. K. Hari. *Woven textile structure: Theory and applications*. 2010, pp. 1–450. ISBN: 9781845695149. DOI: `10.1533/9781845697815`. URL: `www.woodheadpublishing.`.

[7]   H M Behery. "Yarn structural requirements for knitted and woven fabrics". In: *Advances in yarn spinning technology*. Ed. by C Lawrence. Woodhead Publishing, 2010. Chap. 6, pp. 155–189. ISBN: ISBN 978-0-85709-021-8.

[8]   *Best Research-Cell Efficiency Chart | Photovoltaic Research | NREL*. URL: `https://www.nrel.gov/pv/cell-efficiency.html`.

[9]   H Bögner-Balz. *ANALYSIS REPORT: Technical textile fabric property report Poisson's ratio and E-Modulus (Young's modulus)*. Tech. rep. Labor BLUM, June 2013. URL: `www.labor-blum.de`.

[10] H Bögner-Balz. *REPORT ON A BIAXIAL TEST - STAMOID 3739 FR Fabric*. Tech. rep. Labor BLUM, Apr. 2008.

[11] H. Bögner-Balz, R. Blum, and J. Köhnlein. "Structural behaviour of fabrics and coatings for architectural fabric structures". In: *Fabric Structures in Architecture*. Elsevier Inc., Apr. 2015, pp. 123–157. ISBN: 9781782422402. DOI: `10.1016/B978-1-78242-233-4.00004-8`.

[12] *Cells, Modules, Panels and Arrays - FSEC Energy Research Center*. URL: `https://energyresearch.ucf.edu/consumer/solar-technologies/solar-electricity-basics/cells-modules-panels-and-arrays/`.

[13] *Copper Indium Gallium Selenide (CIGS)? - SF Magazine*. URL: `https://www.solarfeeds.com/mag/wiki/copper-indium-gallium-selenide/`.

[14] *Eden Project*. URL: `https://stringfixer.com/nl/Eden_Project`.

[15] Y.E. El Mogahzy. "Types of fabric for textile product design". In: *Engineering Textiles*. Elsevier, 2009, pp. 271–299. DOI: `10.1533/9781845695415.2.271`. URL: `https://linkinghub.elsevier.com/retrieve/pii/B9781845690489500107`.

[16] Eman Eltahan. "Structural parameters affecting tear strength of the fabrics tents". In: *Alexandria Engineering Journal* 57.1 (Mar. 2018), pp. 97–105. ISSN: 11100168. DOI: `10.1016/j.aej.2016.12.005`.

[17] B. Forster and M. Mollaert. *European Design Guide for Tensile Surface Structures*. TensiNet, 2004. ISBN: 908086871x.

[18] K. L. Gandhi. "The fundamentals of weaving technology". In: *Woven Textiles: Principles, Technologies and Applications* (Jan. 2019), pp. 167–270. DOI: `10.1016/B978-0-08-102497-3.00005-2`. URL: `https://doi.org/10.1016/B978-0-08-102497-3.00005-2`.

[19] F. Heinzelmann, T. Bristogianni, and P. Teuffel. "Functional-layered textiles in architecture". In: *Fabric Structures in Architecture*. Elsevier Inc., Apr. 2015, pp. 159–186. ISBN: 9781782422402. DOI: `10.1016/B978-1-78242-233-4.00005-X`.

[20] R. Houtman. "Materials used for architectural fabric structures". In: *Fabric Structures in Architecture*. 2015, pp. 101–121. ISBN: 9781782422402. DOI: `10.1016/B978-1-78242-233-4.00003-6`.

[21] *HOW TO GET WHAT YOU WANT*. URL: `https://www.kobakant.at/DIY/?p=8012`.

[22] Brian P Justusson, David M Spagnuolo, and Jian H Yu. *Assessing the Applicability of Digital Image Correlation (DIC) Technique in Tensile Testing of Fabric Composites*. Tech. rep. 2013.

[23] Jan Knippers et al. *Construction Manual for Polymers + Membranes: Materials, Semi-finished Products, Form Finding, Design*. Ed. by Judith Faltermeier et al. Institut für internationale Architektur-Dokumentation, 2011, pp. 100–107. ISBN: 9783920034416.

[24] Frederik C. Krebs and Markus Hösel. "The Solar Textile Challenge: How It Will Not Work and Where It Might". In: *ChemSusChem* 8.6 (2015), pp. 966–969. ISSN: 1864564X. DOI: `10.1002/cssc.201403377`.

[25] R. Kronenburg. "Introduction: The development of fabric structures in architecture". In: *Fabric Structures in Architecture*. Woodhead Publishing, Jan. 2015, pp. 1–21. ISBN: 9781782422402. DOI: `10.1016/B978-1-78242-233-4.00001-2`.

[26] B. Kumar and J. Hu. "Woven fabric structures and properties". In: *Engineering of High-Performance Textiles*. Woodhead Publishing, Jan. 2017, pp. 133–151. ISBN: 9780081012734. DOI: `10.1016/B978-0-08-101273-4.00004-4`.

[27] Qingxiang Li and Alessandra Zanelli. "A review on fabrication and applications of textile envelope integrated flexible photovoltaic systems". In: *Renewable and Sustainable Energy Reviews* 139 (Apr. 2021). ISSN: 18790690. DOI: `10.1016/j.rser.2020.110678`.

[28] Maryam Mansoori et al. "Adaptive Woden Architecture. Designing a Wood Composite with Shape-Memory Behavior". In: *Digital Wood Design*. Ed. by Fabio Bianconi and Marco Filippucci. Vol. 24. Springer, 2019, pp. 703–717. DOI: `10.1007/978-3-030-03676-8{\_}27`.

[29] Robert R. Mather and John I.B. Wilson. *Fabrication of photovoltaic textiles*. May 2017. DOI: `10.3390/coatings7050063`.

[30] *Members of Tensinet*. URL: `https://www.tensinet.com/index.php/about/members-of-tensinet?view=project&id=4670`.

[31] Athanasios Milionis, Eric Loth, and Ilker S. Bayer. "Recent advances in the mechanical durability of superhydrophobic materials". In: *Advances in Colloid and Interface Science* 229 (Mar. 2016), pp. 57–79. ISSN: 0001-8686. DOI: `10.1016/J.CIS.2015.12.007`.

[32] Mohammad Mobarak Hossain. "A Review on Different Factors of Woven Fabrics' Strength Prediction". In: *Science Research* 4.3 (2016), p. 88. ISSN: 2329-0935. DOI: `10.11648/j.sr.20160403.13`.

[33] J. Monjo-Carrió and J. Tejera. "The use of textile materials for architectural membranes". In: *Fibrous and Composite Materials for Civil Engineering Applications*. Elsevier, 2011, pp. 325–387. DOI: `10.1533/9780857095583.3.325`.

[34] Shilpi Nagpal. *Fibres - Fibre To Fabric*. URL: `https://classnotes.org.in/class-6/science/fibre-to-fabric/fibres/`.

[35] Yasir Nawab, Talha Hamdani, and Khubab Shaker. *Structural Textile Design: Interlacing and Interlooping*. 2017, pp. 47–82. ISBN: 9781315390406.

[36] NEN. *(ISO 13934-1) Textiles-Tensile properties of fabrics-Part 1: Determination of maximum force and elongation at maximum force using the strip method*. Tech. rep. 2013.

[37] *Olympic Basketball Arena | WilkinsonEyre*. URL: `https://www.wilkinsoneyre.com/projects/olympic-basketball-arena`.

[38] *OPV Solar Trees at EXPO 2015 | ASCA®*. URL: `https://en.asca.com/projects/asca-structures-en/opv-solar-trees-at-expo-2015/`.

[39] *Organic Solar Cells - Fraunhofer ISE*. URL: `https://www.ise.fraunhofer.de/en/business-areas/photovoltaics/perovskite-and-organic-photovoltaics/organic-solar-cells-and-modules.html`.

[40] Carol Monticelli Politecnico et al. "Mechanical Robustness investigation of organic photovoltaics for membrane integrated flexible solar cells". In: *Proceedings of the International Association for Shell and Spatial Structures (IASS)*. ECS, 2013. URL: `https://www.researchgate.net/publication/277075307`.

[41] *Pompidou Center, Metz - Shigeru Ban | Arquitectura Viva*. URL: `https://arquitecturaviva.com/works/pompidou-center-metz`.

[42] A G Prodromou and J Chen. "On the relationship between shear angle and wrinkling of textile composite preforms". In: *Composites Part A* 2.3 (1997), pp. 491–503.

[43] Giancarlo C. Righini and Francesco Enrichi. "Solar cells' evolution and perspectives: A short review". In: *Solar Cells and Light Management: Materials, Strategies and Sustainability*. Elsevier, Jan. 2019, pp. 1–32. ISBN: 9780081027622. DOI: `10.1016/B978-0-08-102762-2.00001-X`.

[44] *Ripstop | materials breakdown | UF PRO*. URL: `https://ufpro.com/us/blog/materials-breakdown-ripstop`.

[45] Achala Satharasinghe, Theodore Hughes-Riley, and Tilak Dias. *A review of solar energy harvesting electronic textiles*. Oct. 2020. DOI: `10.3390/s20205938`.

[46] A Schnabel and T Gries. "Production of non-crimp fabrics for composites". In: *Non-crimp fabric composites*. Woodhead Publishing, 2011. Chap. 1, pp. 3–41. URL: `https://doi.org/10.1533/9780857092533.1.3`.

[47] *SEDUS STOLL AG BY LUDLOFF + LUDLOFF ARCHITEKTEN – aasarchitecture*. URL: `https://aasarchitecture.com/2013/02/sedus-stoll-ag-by-ludloff-ludloff-architekten/`.

[48] *Shade in the 'Beverly Hills' of Mexico - Fabric Architecture Magazine*. URL: `https://fabricarchitecturemag.com/2016/12/21/shade-in-the-beverly-hills-of-mexico/`.

[49] R A Shareef and H A S Al-Alwan. "Sustainable textile architecture: history and prospects". In: *IOP Conference Series: Materials Science and Engineering* 1067.1 (Feb. 2021), p. 012046. ISSN: 1757-8981. DOI: `10.1088/1757-899x/1067/1/012046`.

[50] F. Sloan. "Liquid crystal aromatic polyester-arylate (LCP) fibers: Structure, properties, and applications". In: *Structure and Properties of High-Performance Fibers* (2017), pp. 113–140. DOI: `10.1016/B978-0-08-100550-7.00005-X`.

[51] Arno Smets et al. *Solar energy The physics and engineering of photovoltaic conversion, technologies and systems*. UIT Cambridge Ltd., 2016. ISBN: 978 1 906860 75 2.

[52] *Solar Decathlon - Techstyle Haus - pvilion 2014*. URL: `https://www.pvilion.com/2014-solar-decathlon-techstyle-haus/`.

[53] Natalie Stranghöner et al. "Prospect for European Guidance for the Structural Design of Tensile Membrane Structures". In: 2016.

[54] *structural geometry of filament yarns*. URL: `https://www.cfccarbon.com/attachment/structural-geometry-of-filament-yarns.html`.

[55] M. Tausif, T. Cassidy, and I. Butcher. "Yarn and thread manufacturing methods for high-performance apparel". In: *High-Performance Apparel: Materials, Development, and Applications*. Elsevier, Jan. 2017, pp. 33–73. ISBN: 9780081009048. DOI: `10.1016/B978-0-08-100904-8.00003-1`.

[56] *Textile roofing, castle ruins of Thierstein | Kugel Architects, Stuttgart Germany*. URL: `https://www.kugel-architekten.com/content.php?n=1&d=28`.

[57] *The world's first energy-efficient ETFE façade installed using printed Organic Photovoltaic, OPVIUS GmbH, Press release - PresseBox*. URL: `https://www.pressebox.com/pressrelease/opvius-gmbh-kitzingen/The-worlds-first-energy-efficient-ETFE-facade-installed-using-printed-Organic-Photovoltaic/boxid/907556`.

[58]   *Thin-Film*. URL: `https://www.powerfilmsolar.com/technology/thin-film`.

[59]   *Tongeren | The Nomad Concept - lightweight organic architecture in textile following parametric design*. URL: `https://nomadconcept.com/en/projects/public/tongeren/`.

[60]   *Webinar Stability of Perovskite solar cells | TNO*. URL: `https://www.tno.nl/en/about-tno/events/2021/perovskite-solar-cells/`.

[61]   *Westraven - office for rijkswaterstaat by architectenbureau cepezed b.v. - Issuu*. URL: `https://issuu.com/cepezed/docs/l_westraven_eng_issuu`.

[62]   A. Zanelli. "Architectural fabric structures in the refurbishment of archaeological and cultural heritage areas". In: *Fabric Structures in Architecture*. Elsevier Inc., Apr. 2015, pp. 481–527. ISBN: 9781782422402. DOI: `10.1016/B978-1-78242-233-4.00015-2`.

[63]   Alessandra Zanelli, Carol Monticelli, and Salvatore Viscuso. "Closing the loops in textile architecture: Innovative strategies and limits of introducing biopolymers in membrane structures". In: *Research for Development*. Springer, 2020, pp. 263–276. DOI: `10.1007/978-3-030-33256-3{\_}25`.

[64]   *Zenith Music Hall Strasbourg - Textile facade - Canobbio*. URL: `https://www.canobbio.com/en/portfolio/zenith-music-hall-strasbourg/`.